
[All ETDs from UAB](#)

[UAB Theses & Dissertations](#)

2020

Elucidating The Role Of Hedgehog Signaling In Tumor Cell Response To Dna Damage And Microenvironmental Stress

Tshering Dolma Lama-Sherpa
University of Alabama at Birmingham

Follow this and additional works at: <https://digitalcommons.library.uab.edu/etd-collection>

 Part of the [Medical Sciences Commons](#)

Recommended Citation

Lama-Sherpa, Tshering Dolma, "Elucidating The Role Of Hedgehog Signaling In Tumor Cell Response To Dna Damage And Microenvironmental Stress" (2020). *All ETDs from UAB*. 834.
<https://digitalcommons.library.uab.edu/etd-collection/834>

This content has been accepted for inclusion by an authorized administrator of the UAB Digital Commons, and is provided as a free open access item. All inquiries regarding this item or the UAB Digital Commons should be directed to the [UAB Libraries Office of Scholarly Communication](#).

ELUCIDATING THE ROLE OF HEDGEHOG SIGNALING IN TUMOR CELL
RESPONSE TO DNA DAMAGE AND MICROENVIRONMENTAL STRESS

by

TSSHERING D LAMA-SHERPA

LALITA A. SHEVDE-SAMANT, CHAIR
DOUGLAS HURST
RAJEEV SAMANT
EDDY SHIH-HSIN YANG
YANG YANG

A DISSERTATION

Submitted to the graduate faculty of The University of Alabama at Birmingham,
in partial fulfillment of the requirements for the degree of
Doctor of Philosophy

BIRMINGHAM, ALABAMA

2020

Copyright by
TSHERING D LAMA-SHERPA
2020

ELUCIDATING THE ROLE OF HEDGEHOG SIGNALING IN TUMOR CELL
RESPONSE TO DNA DAMAGE AND MICROENVIRONMENTAL STRESS

TSSHERING D LAMA-SHERPA

GRADUATE BIOMEDICAL SCIENCES: CANCER BIOLOGY

ABSTRACT

Hypoxia within solid tumors presents as a barrier to the effectiveness of cancer treatment. Hypoxia has been implicated in cancer cell resistance to standard therapies used in the clinic to treat breast cancer. Additionally, the treatment resistance mechanisms in cancer cells are exacerbated by oncogenic pathways that enable adaptation to the hypoxic microenvironment. Cancer cells often co-opt signaling pathways essential for embryonic development as a defense against cellular attacks. Hedgehog (Hh) signaling pathway is one of such embryonic development pathways that have been implicated in mitigating cancer growth, metastasis, and resistance to therapy. Hh signaling pathway promotes proliferation, tissue remodeling, patterning, differentiation, and vascularization in normal development. However, abnormal engagement of the Hh pathway in cancer fosters tumor initiation and progression. Dysregulated Hh signaling is also associated with breast cancer progression and metastasis.

In this study, we examine the role of Hh signaling in lethal DNA break repair, adaptation to hypoxia, and crafting of tumor hypoxia. We found that the zinc-finger transcription factor GLI1, a terminal effector of the Hh pathway, is essential for the repair of ribosomal DNA (rDNA) double-strand breaks (DSBs). Inhibition of GLI1 impairs the

global non-homologous end joining (NHEJ) DSB repair pathway. Additionally, we found that inhibiting GLI1 impacts RNA polymerase I activity and cellular viability.

We also report that Hh signaling mitigates tumor hypoxia quantified by radiolabeled tracer, [¹⁸F]-fluoromisonidazole (FMISO) positron emission tomography (PET) imaging upon the administration of Vismodegib, a FDA-approved Hh inhibitor *in vivo*. Furthermore, we uncovered the mechanistic role of Hh in enabling hypoxia adaptation through robust activation of HIF signaling in a VHL-dependent manner. In addition to modulating temporal changes in hypoxia, we found that inhibition of Hh signaling leads to decreased pulmonary metastasis.

Thus, we identified the role of Hh signaling in facilitating defense against genotoxic stress and maneuvering the tumor microenvironment in breast cancer to promote tumor progression and metastasis. Our findings provide a novel insight into targeting Hh signaling in breast cancer clinically to mitigate tumor proliferation, hypoxia, and metastasis.

Keywords: Breast cancer, Hedgehog signaling, Double-Strand breaks repair, Hypoxia, Metastasis

DEDICATION

I dedicate this dissertation to my parents, Dawa Jangbu Lama and Jangmu Sherpa.

ACKNOWLEDGMENTS

I would like to thank my mentor Dr. Lalita A Shevde-Samant for her continuous guidance, support, and mentorship. Secondly, I would like to thank Dr. Rajeev Samant, who acted as both co-mentor and committee member and provided expertise and helpful feedback. Additionally, I would like to acknowledge my committee members: Dr. Eddy Yang, Dr. Douglas Hurst, and Dr. Yang Yang for their valuable suggestions that help guide my projects. I am also grateful for the past and present Samant lab members: Victor Lin, Brandon Metge, Sarah Kammerud, Mateus Mota, Dominique Hinshaw, Hebaallah Alsheikh, Shannon Meier, Amr Elhamamsy, Atul Kumar, and Sushma Pinninti.

TABLE OF CONTENTS

	<i>Page</i>
ABSTRACT.....	iii
DEDICATION.....	v
ACKNOWLEDGMENTS.....	vi
LIST OF TABLES.....	ix
LIST OF FIGURES.....	x
LIST OF ABBREVIATIONS.....	xiii
INTRODUCTION.....	1
Breast cancer.....	1
Breast cancer pathology and risk factors.....	1
Molecular subtypes of breast cancer.....	2
Tumor microenvironment.....	5
Fibroblasts.....	6
Endothelial cells.....	7
Pericytes.....	8
Lymphocytes.....	8
Dendritic cells.....	10
Macrophages.....	10
Hypoxia.....	11
Treatment for triple-negative breast cancer.....	12
Surgery.....	12
Radiotherapy.....	13
Chemotherapy.....	14
Hedgehog signaling pathway in TNBC.....	15
Hedgehog signaling in DNA repair.....	16
Hedgehog signaling in hypoxia.....	17
HEDGEHOG SIGNALING IN CARCINOGENESIS.....	21

AN EMERGING REGULATORY ROLE FOR THE TUMOR MICROENVIRONMENT IN THE DNA DAMAGE RESPONSE TO DOUBLE-STRAND BREAKS.....	37
HEDGEHOG SIGNALING ENABLES REPAIR OF RIBOSOMAL DNA DOUBLE-STRAND BREAKS	72
QUANTITATIVE AND MOLECULAR ANALYSIS OF INHIBITION OF HEDGEHOG SIGNALING PATHWAY ON HYPOXIA IN PRECLINICAL MODEL OF TNBC	113
DISCUSSION AND FUTURE DIRECTIONS	145
Hedgehog signaling in DSB repair	145
Hedgehog signaling in crafting hypoxic microenvironment and adaptation to hypoxia.....	149
Interaction between hypoxia and DDR	152
Alterations in DDR in hypoxia	153
Alteration in immune cell function in hypoxia.....	153
LIST OF REFERENCES	158
APPENDICES	
IACUC APPROVAL FORMS	174

LIST OF TABLES

<i>Table</i>	<i>Page</i>
HEDGEHOG SIGNALING IN CARCINOGENESIS	
1	Examples of potential predictive biomarkers for the Hh signaling pathway35
2	Examples of ongoing trials of Hh inhibitors in cancer36
AN EMERGING REGULATORY ROLE FOR THE TUMOR MICROENVIRONMENT IN THE DNA DAMAGE RESPONSE TO DOUBLE-STRAND BREAKS	
1	Different DSB repair pathway proteins and their associated inhibitors70
2	Current clinical trials targeting DNA DSB repair pathway proteins as mono- and combination therapy agents71
HEDGEHOG SIGNALING ENABLES REPAIR OF RIBOSOMAL DNA DOUBLE- STRAND BREAKS	
1	Sequences of primer pairs used in this study. F and R designate the forward and reverse primers, respectively.....110

LIST OF FIGURES

Figures *Page*

INTRODUCTION

- 1 TME stimulus determine distinct macrophage phenotypes19
- 2 Hypoxia response pathway determine cellular adaptation to hypoxia.....20

HEDGEHOG SIGNALING IN CARCINOGENESIS

- 1 Schematic of the classical, canonical vertebrate Hh signaling pathway.....34

AN EMERGING REGULATORY ROLE FOR THE TUMOR MICROENVIRONMENT IN THE DNA DAMAGE RESPONSE TO DOUBLE-STRAND BREAKS

- 1 DSBs-inducing agents used for the treatment of cancer67
- 2 Cellular DSBs are repaired mainly through HR and NHEJ; both mechanisms
involve distinct repair proteins.....68
- 3 The solid tumor microenvironment comprising hypoxia, inflammation,
and immune cells impact DSB repair pathways in cancer cells.69

HEDGEHOG SIGNALING ENABLES REPAIR OF RIBOSOMAL DNA DOUBLE- STRAND BREAKS

- 1 Ionizing radiation induces GLI1 binding to novel sequences in rDNA.....102
- 2 Inhibition of Hh/GLI signaling delays ionizing radiation-induced DSB
repair in TNBC cells103
- 3 Hh inhibition impairs NHEJ and delays repair of rDNA DSBs104

4	Inhibiting Hh/GLI signaling impairs re-activation of Pol I activity following irradiation-induced DSBs.....	106
5	Ionizing radiation induces GLI1 binding to novel sequences in rDNA.....	107
6	Inhibition of Hh/GLI signaling delays ionizing radiation-induced DSB repair in TNBC cells	108
7	Hh inhibition impairs NHEJ and delays repair of rDNA DSBs..	109
8	Inhibiting Hh/GLI signaling impairs re-activation of Pol I activity following irradiation-induced DSBs.....	110

QUANTITATIVE IMAGING AND MOLECULAR ANALYSIS OFFER INSIGHTS
INTO THE ROLE OF HEDGEHOG SIGNALING IN AUGMENTING TUMOR
HYPOXIA

1	Inhibiting Hh signaling by Vismodegib mitigates tumor hypoxia in TNBC mice mode.....	137
2	Vismodegib alters the tumor microenvironment and decreases lung metastasis in TNBC mice model.....	138
3	Hypoxia activates the Hh Pathway in TNBC cell lines	139
4	Inhibition of Hh signaling impairs cellular hypoxia response in hypoxic conditions	140
5	Inhibition of Hh signaling pathway decreases HIF-1 α transcription factor stability in VHL-dependent mechanism.	141
6	Inhibition of Hh signaling pathway decreases tumor hypoxia <i>in vivo</i>	142
7	Inhibition of Hh signaling disrupts collagen fiber alignment..	143
8	Inhibition of Hh signaling pathway decreases HIF-1 α transcription factor stability.	144

DISCUSSION AND FUTURE DIRECTIONS

1	Alteration of RAD51 in I-SceI transfected NHEJ and HR GFP reporter cells.....	146
---	---	-----

2	Inhibiting Hh signaling increases sensitivity to IR-induced DSBs in aggressive mammary tumor line 4T1.	148
3	Inhibition of Hh signaling decreases metabolic reliance on OXPHOS with a reciprocal increase in glycolysis in M2 macrophages.	156

LIST OF ABBREVIATIONS

AFM	Atomic Force Microscopy
ALCAM	Activated Leukocyte Cell Adhesion Molecule
ALK	ALK Receptor Tyrosine Kinase
ATR	ATR Serine/Threonine Kinase
AURKA	Aurora Kinase A
AURKB	Aurora Kinase B
BCS	Breast Conserving Surgery
BER	Base Excision Repair
BL1/2	Basal-Like 1 and 2
BRCA	Breast Cancer 1/2 Gene
BRCA1/2	Breast And Ovarian Cancer Susceptibility Protein 1
BUB1	BUB1 Mitotic Checkpoint Serine/Threonine Kinase
CAFs	Cancer-Associated Fibroblasts
CCL2	C-C Motif Ligand 2
CD4	CD4 Molecule
CD8	CD8 Molecule
CHEK1	Checkpoint Kinase 1
CXCL12	C-X-C Motif Chemokine 12
CXCL12	C-X-C Motif Chemokine Ligand 12

DAMP	Damage-Associated Molecular Patterns
DCIS	Ductal Carcinoma in Situ
DCs	Dendritic Cells
DDR	DNA Damage Repair
DHCR24	24-Dehydrocholesterol Reductase
DSB	Double-Strand Break
EGF	Epidermal Growth Factor
EGFR	Epidermal Growth Factor Receptor
EMT	Epithelial Mesenchymal Transition
EPAS1	Endothelial PAS Domain Protein 1
ER	Estrogen
FDA	Food and Drug Administration
FEN1	Flap Endonuclease
FGF	Fibroblast Growth Factors
FKBP5	FKBP Prolyl Isomerase 5
FOXA1	Forkhead Box A1
Gab1	GRB2 Associated Binding Protein 1
GM-CSF	Granulocyte-Macrophage Colony Stimulating Factor
HER2	Human Epidermal Growth Factor Receptor 2
Hh	Hedgehog
HIFs	Hypoxia Inducible Factors
HRE	Hypoxia Response Element
IBC	Inflammatory Breast Cancer

ICI	Immune Checkpoint Inhibitors
IDC	Invasive Ductal Carcinoma
IFN γ	Interferon Gamma
IFN γ	Interferon gamma
IGF	Insulin Like Growth Factor
IGF1R	Insulin Like Growth Factor 1 Receptor
IL	Interleukin
IL-2	Interleukin 2
ILC	Invasive Lobular Carcinoma
IM	Immunomodulatory
IM	Immunomodulatory
LAR	Luminal Androgen Receptor
LAR	luminal androgen receptor
LIG1	DNA Ligase 1
LPS	Lipopolysaccharide
M	Mesenchymal
MCSF	Macrophage Colony-Stimulating Factor
MDC1	Mediator Of DNA Damage Checkpoint 1
MET	MET Proto-Oncogene, Receptor Tyrosine Kinase
MHC	Major Histocompatibility Complex
MMP	Matrix Metalloproteinases
MMR	Mismatch Repair
MSL	Mesenchymal Stem-Like

mTOR	Mechanistic Target Of Rapamycin Kinase
mTOR	Mechanistic Target Of Rapamycin Kinase
MVD	Microvessel Density
MYC	MYC Proto-Oncogene, BHLH Transcription Factor
NBS1	Nijmegen Breakage Syndrome 1
NER	Nucleotide Excision Repair
NF- κ B	Nuclear Factor Kappa B
NGF	Nerve Growth Factor
PAMP	Pathogen-Associated Molecular Patterns
PARP	Poly Adenosine Diphosphate-Ribose Polymerase
PD-1	Programmed Death
PD-L1	Programmed Death Ligand
PDGF	Platelet-Derived Growth Factors
PDGF	platelet-derived growth factor
PHD	Proline Hydroxylase
PI3K	Phosphatidylinositol-4,5-bisphosphate 3-kinase
PIK3CA	Catalytic Subunit Alpha
pO ₂	Pressure of Oxygen
PR	Progesterone
RAD51	RAD51 Recombinase
RAD51C	RAD51 Paralog C
RANK	Receptor Activator Of Nuclear Factor Kappa B
RANKL	Receptor activator of Nuclear factor- κ B (RANK) Ligand

rDNA	Ribosomal DNA
ROS	Reactive Oxygen Species
SEER	Surveillance, Epidemiology, and End Results
SHG	Second Harmonics Generation
src	SRC Proto-Oncogene, Non-Receptor Tyrosine Kinase
SSB	Single-Strand Break
TCR	T Cell Receptor
TGF- β	Transforming Growth Factor Beta
TGF β 1	Transforming Growth Factor Beta 1
T _H 1	T Helper
TME	Tumor Microenvironment
TNBC	Triple-Negative Breast Cancer
TP53	Tumor Protein P53
T _{regs}	Regulatory T Cells
UNG	Uracil DNA Glycosylase
VEGF	Vascular Endothelial Growth Factor
VEGFR2	Vascular Endothelial Growth Factor Receptor 2
VHL	Von Hippel Lindau
XRCC3	X-Ray Repair Cross Complementing 3
γ -H2AX	γ Gamma H2A.X Variant Histone

INTRODUCTION

Breast Cancer

Breast cancer is the most common cancer among women in the US and worldwide. In 2020, it is predicted that about 276,480 new cases of invasive breast cancer will be diagnosed in women in the US (1). This number only adds to a growing population of women who are living with and managing the condition. Although, increased public awareness on preventive measures and screenings have helped lower the death rates over the last decade, an estimated 42,170 women will die breast cancer in 2020 (1, 2). Breast cancer is currently ranked as the second leading cause of cancer-related death among women, second only to lung cancer. The complexity in treating the breast cancer originates from its heterogeneous nature both within the tumor cells (intra-heterogeneity) and across the tumor population (inter-heterogeneity) (3, 4). Additionally, the tumor microenvironment also affects cancer and stromal cells' behavior adding to the intricacies of the disease (5-7). A better understanding of breast cancer progression and ability to design therapeutic targets with consideration to these influences would be critical to improve survival.

Breast cancer Pathology and risk factors

Breast cancer is an abnormal growth of cells in the mammary tissue. The cellular changes most commonly occur in the epithelial cells lining ductal and lobular regions of the breast (8). Breast cancer is broadly subdivided into four types based on the

pathological assessment; ductal carcinoma in situ (DCIS), Invasive ductal carcinoma (IDC), Invasive lobular carcinoma (ILC), and Inflammatory breast cancer (IBC) (9). Almost 81% of the breast cancers that are diagnosed are classified as invasive where the cancerous cells have already invaded through the walls of the ducts or glands into the surrounding tissue (1). Early detection and treatment drastically improve the survival rates of breast cancer patient. The relative survival rates for breast cancer patient with metastasis is only 27% compared to 99% for a localized tumor (10). There are several risk factors that are associated with breast cancer, these include age, race or ethnicity, family history, genetic predisposition, earlier menstruation and later menopause, radiotherapy to the chest wall, exercise, diet, alcohol and tobacco consumption, never having children, increased breast tissue density, lack of physical exercise, and hormone replacement therapy (11-14). Of specific relevance to our geographical location, there are discrepancies in the incidence and death rates of breast cancer based on race. African American women have a decreased incidence of breast cancer but have increased death rate in comparison to Caucasian women. This racial disparity is attributed to later stage diagnosis due to decreased access to care, higher obesity, inherited genetic mutations, and other health conditions (15, 16).

Molecular subtypes of breast cancer

The molecular subtypes of breast cancer are based on the gene expression profile of the tumor population. There are four main molecular subtypes of breast cancer: luminal A, luminal B, Her2 enriched, and basal like/ triple-negative (17, 18). Luminal breast cancer occurs in the luminal epithelium cells that lines mammary ducts. Luminal A is the most common subtype and are less aggressive than the other subtypes. It is

characterized by their estrogen (ER) positive receptor status and low proliferation rate. Luminal B is characterized by their progesterone (PR) positive receptor status and high proliferation rate. Luminal B breast cancer have worse prognosis compared to luminal A. Luminal breast cancer is responsive to hormonal therapies like tamoxifen and aromatase inhibitors. These inhibitors block ER receptor signaling reducing breast cancer cell growth and production of estrogen and androgens (18, 19).

Human epidermal growth factor receptor 2 (HER2)-enriched molecular subtype of breast cancer is characterized by the lack of ER and PR, but an increased expression of HER2. HER2 subtype presents with higher histologic grade and has higher mutations in TP53 and PIK3CA genes (20, 21). It responds better to chemotherapy in comparison to luminal subtypes. HER2-enriched subtypes can be treated by HER2 receptor targeted therapies that include trastuzumab (anti-HER2 monoclonal antibody), lapatinib (anti-HER2 tyrosine kinase inhibitor), pertuzamab (monoclonal antibody that blocks dimerization of HER2 and HER3) (21).

The basal-like/ Triple-negative breast cancer (TNBC) subtype is characterized by high expression of proliferation-related genes commonly associated with basal and myoepithelial cells. TNBC is associated with BRCA1/2 mutations, high relapse rates, and poor overall survival rate (22, 23). Additionally, it is more common in African American women compared to Caucasian women (1, 24). Only 10-15% of all breast cancer are TNBC subtype, but it affects younger women, has higher histological grade, an increased probability to metastasize (23). TNBCs are negative for ER and PR expression, and do not have amplification of HER2 receptors; therefore, endocrine therapies or anti-HER2 targeted treatments are not effective in TNBC (25). Although, TNBC patients respond

better to chemotherapy compared to other subtypes, it has high rate of recurrence and resistance. Importantly, among all subtypes TNBC patients have the lowest overall survival rate in the first 3 to 5 years after initial diagnosis (22, 25).

TNBC is highly heterogenic and is further classified into six different subtypes based on gene expression profiling and unique mutational analysis. These subtypes include: basal-like 1 and 2 (BL1/2), immunomodulatory (IM), mesenchymal (M), mesenchymal stem-like (MSL), and luminal androgen receptor (LAR) (26). About 78.6% of TNBC have overlap with the basal-like subset of TNBC based on the PAM50 gene expression profile (22). The unique molecular signatures can possibly explain the varied response to therapy in TNBC patients. BL1, in particular, shows high Ki-67 expression while BL2 present with higher expression of growth factor signaling, glycolysis, and gluconeogenesis. Both, BL1 and BL2 have higher expression of DNA damage-response and cell cycle genes and therefore, respond better to DNA damaging agents such as cisplatin. M subtypes presents with overexpression of proliferation related genes, whereas MSL subtypes are enriched in genes related to mesenchymal stem cells. MSL also display increased expression of genes involved in angiogenesis and growth. M and MSL subtypes both overlap in the expression of genes involved in epithelial-mesenchymal transition, chemoresistance, tumor matrix remodeling, cellular differentiation, and motility. M and MSL subtype respond better to Phosphatidylinositol-4,5-Bisphosphate 3-Kinase (PI3K)/ Mechanistic Target Of Rapamycin Kinase (mTOR) inhibitors such as NCP-BEZ235 and abl/src tyrosine kinase inhibitors such as dasatinib. The IM subtype of TNBC presents with a characteristic increase in genes related to immune signaling with higher expression of T cell-associated genes, cytokine signaling, antigen processing and

presentation. However, IM subtype of TNBC is speculated to be the result of stromal cell contamination and possibly high tumor lymphocyte infiltration in the tumor. The presence of tumor infiltrating cells was found to be a good prognostic marker and increase in lymphocytes was associated with reduced mortality and recurrence (27). Immune modulation in the TNBC tumor microenvironment can possibly yield as better therapeutic target. Among all the subtypes of TNBC, LAR shows the most differential gene expression. LAR subtype are enriched in genes related to steroid synthesis, hormone signaling, androgen/estrogen metabolism, and androgen receptors (26). Since LAR subtype is composed of androgen receptor-driven tumors, receptor antagonists like flutamide are used in clinic (28). Apart from targeting the tumor cells itself, it is critical to understand how the tumor cells control the microenvironment for their own benefit. Tumor microenvironment can significantly influence how tumors respond to therapy.

Tumor Microenvironment (TME)

Tumors are heterogeneous and comprises a vast array of cells. It encompasses several cell types that include immune cells, fibroblasts, leukocytes, adipocytes, myoepithelial, and endothelial cells. Additionally, soluble factors like enzymes, cytokines, hormones, growth factors, and extracellular matrix make up the non-cellular components of the TME (29, 30). During normal mammary gland development and differentiation, epithelial cells are in constant crosstalk with the stromal entities in the TME. This cellular crosstalk prevents neoplastic transformation by regulating paracrine signaling between epithelial and stromal cells (31). TME has been attributed to play an important role in the subsequent transition from invasive to metastatic carcinoma during which, infiltration of fibroblasts, leukocytes, and increased angiogenesis is seen. The

abnormal TME might also play an important role in breach of the ductal basement membrane observed during breast tumor progression (29, 31, 32). To better understand cancer progression, we need to focus on the composition of the breast TME and aberrant signaling in the tumor stroma that is also simultaneously influenced by the physical and chemical environment.

Fibroblasts. Tumor itself is considered as a wound that never heals and fibroblasts might have a critical role in its progression (33). Fibroblasts are involved in the wound healing process and maintenance of ECM. During wound healing, fibroblasts migrate toward the wound site and differentiate into myofibroblasts that express factors necessary for ECM remodeling (34). Myofibroblasts, also called cancer-associated fibroblasts (CAFs), are one of the most abundant cell type in the breast cancer stroma and are defined by expression of α -smooth muscle actin. (35). The origin of CAFs is disputed, although they might be derived from multiple sources: endothelial cells, epithelial cells, smooth muscle cells, or mesenchymal stem cells (36). CAFs secrete a plethora of chemokines, growth factors ECM proteins that lead to enhanced tumor growth, dissemination, and metastasis (35). CAFs foster an immune-suppressive microenvironment through secretion of Transforming growth factor beta (TGF- β), Vascular Endothelial Growth Factor (VEGF), and C-X-C Motif Chemokine Ligand 12 (CXCL12) that promote epithelial mesenchymal transition (EMT), angiogenesis, and chemoattraction (30, 37, 38). The Nuclear Factor Kappa B (NF- κ B) developmental signaling pathway, was found to be critical in inflammation mediated by CAFs. Inhibition of NF- κ B led to diminished macrophage recruitment, vascularization, and tumor growth in a mouse model of squamous cell carcinoma (38). The use of 3D models that recapitulate blood brain barrier implicated

CAFs in supporting breast cancer metastasis to brain through enhanced vascular permeability (39) . In fact, high presence of myofibroblasts in breast IDC tissue was linked to shorter overall survival and relapse-free survival in patients (40). Therefore, understanding CAFs and their dynamic changes in tumor would be important for developing novel targets in breast cancer.

Endothelial cells. The vascular endothelium covers the interior walls of blood vessels forming a barrier between blood cells and adjacent tissues (41). Endothelial cells are quiescent unless recruited in tissue in response to injury or hypoxia leading to rapid vessel growth called angiogenesis . During tumor progression, soluble factors in the TME stimulate endothelial cells and their associated pericytes through production of growth factors like VEGF, fibroblast growth factors (FGF), platelet-derived growth factors (PDGF) (42). Hypoxic tumor cells, CAF, and macrophages release blood vessel stimulating and inhibiting factors (43). Pro-angiogenic factor binding to the receptors on endothelial cells induce their activation and lead to morphological changes in blood vessels evident as enlargement of vessel diameter, degradation of basement membrane, and recruitment of pericytes (44, 45). At the growing front, endothelial cells secrete matrix metalloproteinases (MMP) to facilitate degradation of ECM and migrate along the ECM with the help of cell surface molecules like integrins. The new blood vessels adhere to each other, form lumen-containing vessels that are further stabilized by recruitment of pericytes and smooth muscle cells (44, 46). Multitude of pro-angiogenic factors have been discovered; of all of them, VEGF is the most well studied. VEGF inhibitors inhibit VEGF binding to the receptors. VEGF inhibitors are currently being tested alone or in combination in clinic but with limitations due to vascular toxicities during treatment (45).

Among the various strategies to assess angiogenesis in tumor, microvessel density (MVD) is a preferred method (47). MVD are usually evaluated using immunostaining against CD31 as an endothelial cell marker and isolectin B4 to identify neovascular structures within tumor (47-49).

Pericytes. Pericytes are stromal cells that are integral to vasculature formation. Pericytes wrap around endothelial cells and communicate to endothelial cells through paracrine and juxtacrine signaling (50). Pericytes and endothelial cells are separated by basement membrane, but can contract through the holes in the basement membrane. PDGF-B, TGF- β , VEGF, and angiopoietin signaling govern the cellular communication between endothelial cells and pericytes for recruitment in the angiogenic sprouts (36, 50).

Activated pericytes allow for endothelial cell proliferation, enhanced matrix deposition alteration, leaky endothelial cell junctions, angiogenesis, and increased metastasis (51). Studies in invasive breast cancer note that low pericyte coverage in addition to high met receptor tyrosine kinase expression in cancer cells correlated with a poor prognosis for patients indicating that pericytes prevent neoplastic transformation and metastasis (52). However, targeting pericytes by blocking its proliferation and survival depleted lymphoma growth indicating pericytes may have distinct, non-overlapping roles depending on tumor types (53).

Lymphocytes. Majority of the lymphocytes that infiltrate the breast TME are T lymphocytes (54). Various T cell sub-populations infiltrate the TME, although, their distribution differs between tumor types (55). T cells are derived from common lymphoid

progenitor cells that originate in the bone marrow and are defined by the expression of T cell receptor (TCR). They mature, differentiate, and commit to different lineages in the thymus. T cells are classically subdivided into CD8⁺ cytotoxic lymphocytes or CD4⁺ helper cells. CD8 and CD4⁺ T cell TCRs recognize antigens presented by major histocompatibility complex (MHC) I or MHCII respectively (56). Naïve T cells that are CD3⁺CD4⁺ and CD3⁺CD8⁺ cells can further differentiate into effector T cells after stimulation by antigen, co-stimulatory molecules, and cytokines in the secondary lymphoid organs. Regulatory T cells (T_{regs}) are CD3⁺CD4⁺ effector T cells express cytokines like IL-10 and TGFβ in the TME and are immunosuppressive (57). T_{reg} are associated with bad prognosis in breast cancer (57, 58). T_{reg} express receptor activator of nuclear factor-κB (RANK) ligand (RANKL) that activates RANK signaling in mammary carcinoma cells and increases pulmonary metastasis (59). T helper cells are CD3⁺CD4⁺ effector T cells express IL-2 and Interferon gamma (IFN-γ) and support cellular immunity. T helper cells are subdivided into T_{H1}, T_{H2}, and T_{H17}. T_{H1}, T_{H2} express IL-4, IL-5, and IL-13 and support humoral immunity, and T_{H17} produce IL-17A, IL-17F, IL-21, and IL-22 and support anti-inflammatory environment during pathogen invasion. Cytotoxic T cells are CD3⁺CD8⁺ effector T cells that produce perforin and granzymes and target cancer cells for apoptosis through antigen binding. Cytotoxic T cell infiltration is associated with antitumor activity and longer survival in breast cancer patients independent of tumor grade, tumor size, lymph node stage, vascular invasion and HER2 status(60). Although, T lymphocyte infiltration is predictive of good prognosis, immune checkpoint expression on T lymphocytes like programmed death (PD-1) expression and programmed death ligand (PD-L1) expression in tumor cells can modulate the immune

response (61). Therefore, immune checkpoint inhibitors (ICI) are garnering significant interest as immunotherapy (62).

Dendritic cells. Dendritic cells (DCs) activate naïve T cells and induce effector T cell differentiation in the secondary or tertiary lymphoid organs by antigen presentation (30). DCs regulate the adaptive immune responses by capturing, processing , and presenting antigens from tumor cells. Maturation of DCs allow them to migrate and cross present antigens to T cells. Antigen presentation is determined by detection by the recognition of pathogen-associated molecular patterns (PAMP) or damage-associated molecular patterns (DAMP) (30, 63). Cytokines such as IL-10, prostaglandin E2, and VEGF can affect DC maturation in the TME (64). Tumor associated DCs are mostly immature and unable to elicit a T cell response. Instead, they produce pro-angiogenic factors like VEGF and stimulate endothelial cell migration leading to tumor progression (65).

Macrophages. Macrophages constitute up to 50% of the mass of a solid breast tumor microenvironment and are the frontline cells of innate immunity (66). They provide defense against external attacks by releasing pro-inflammatory cytokines and recruiting T and B lymphocytes to the site of inflammation (54, 66). They originate in the blood monocytes and get recruited at the tumor sites by chemoattractants like chemokine C-C motif ligand 2 (CCL2) expressed by stromal and tumor cells (67). Macrophages can be polarized depending on the pro-inflammatory or anti-inflammatory stimuli they receive in their surrounding TME (**Figure 1**). Macrophages can be sub-divided according to their cytokine expression pattern and cellular properties into two main groups, the M1 and M2

macrophages (68). M1 macrophages express cytokines like IL-1, IL-6, and TNF, whereas M2 macrophages express IL-4, IL-10, IL-13, and TGF β (69). M1 macrophages, release reactive oxygen and nitrogen species and have a pro-inflammatory role. In contrast, M2 macrophages promote angiogenesis, matrix remodeling, and consequently, tumor growth (66, 70). M2 macrophages has also been implicated in facilitating metastases in breast cancer (71).

Hypoxia. As a tumor progresses, the increase in cellular density and decreased apoptosis drive the tumor to a hypoxic state (72). The need for higher oxygen consumption coupled by the remoteness from the nearest blood vessel reduces oxygen availability and creates an oxygen gradient (73, 74). To overcome hypoxia, cancer cells induce survival tactics involving the upregulation of hypoxia inducible factors (HIFs) which activate expression of several genes that ultimately results in increased angiogenesis, metabolic reprogramming, survival and metastasis (74, 75). Studies with direct measurement of partial pressure of oxygen (pO₂) in human breast cancers found a marked decrease in median pO₂ compared to normal breast tissue (76). Oxygen availability in normoxic conditions regulates the HIF-1 α transcription factor by post-translation modifications through hydroxylation at its two proline sites by O₂ activated proline hydroxylase (PHD). Among the four isoforms of PHD, PHD2 is the main hydroxylase responsible for HIF-1 α hydroxylation(77). Hydroxylated HIF- α is then ubiquitinated by an E3 ligase called Von Hippel Lindau protein (VHL) leading to its degradation by 26S proteasome (78, 79). In contrast, lack of O₂ in hypoxic condition inactivates hydroxylation reactions leading to rapid accumulation of HIF-1 α and HIF-2 α which can heterodimerize with HIF-1 β and

bind to the hypoxia response element (HRE) sequence in its target genes (72) (**Figure 2**). There are thousands of target genes of HIF proteins and they are pre-dominantly involved in regulation of angiogenesis, metabolic reprogramming, drug resistance, and survival (73, 74).

The TME plays a critical role in tumor progression and metastasis, it ultimately governs how tumors respond to therapies. It is critical that treatment modalities are designed effectively to target the tumor-promoting crosstalk and interaction of tumor cells with stromal cells, immune cells, and the physiological changes in the TME.

Treatments for TNBC

Breast cancer treatment is primarily based on multiple factors including the type and stage of cancer (1, 80). Breast cancer treatment regimens include surgery, chemotherapy, radiation, and endocrine therapy (81). Among the breast cancer subtype, TNBC tends to occur more frequently in premenopausal women than older women. TNBC subtype patients are more likely to present with *BRCA1* or *BRCA2* mutation and show poor disease-free and overall survival compared to other subtypes (82). Therefore, there is a need for more effective therapeutic options for TNBC. Since, TNBC is a heterogeneous tumor, there is no one-size-fits-all treatment method available for it. Rather, TNBC patients are treated based on the tumor size and whether the tumors have metastasized to distant organs (83).

Surgery. In the early-stage of TNBC, mastectomy can be done and it involves the removal of the breast and nearby lymph nodes to avoid the spread of the cancer. Alternatively, breast conserving surgery (BCS) (also called lumpectomy) plus

radiotherapy is also done when the tumor is small. In BCS the surgeon removes the lump from the breast and nearby lymph nodes. Meta-analysis study comparing the treatment outcomes in TNBC patients show that BCS plus radiotherapy treated patients achieved better locoregional control and favorable overall survival rates compared to mastectomy (84). Women with advanced TNBC undergo radiation and/or chemotherapy with or without surgery (1, 80). Secondary analysis of TNBC patients with stages II or III show that their chances of qualifying for BCS increases after neoadjuvant systemic therapy (85).

Radiotherapy. Radiotherapy is a high energy radiation given to TNBC patients with locoregional tumor following mastectomy and lumpectomy. Studies show that mastectomy without radiotherapy leads to increased risk of locoregional recurrence of tumor compared to those treated with lumpectomy and adjuvant radiation therapy (86). Similarly, another study investigated whether there is survival advantage of adjuvant radiotherapy using Surveillance, Epidemiology, and End Results (SEER) database and found that radiotherapy after surgery is beneficial to TNBC patients in terms of overall survival (87). However, Khalifa et al., did not find significant difference between TNBC patients that were administered irradiation versus those who omitted it after surgery in terms of survival outcomes (88). In another study, pro-inflammatory tumor after radiotherapy was used as a novel biomarker to predict recurrence, metastasis, and mortality in TNBC patients. IR-induced DSBs increases PD-L1 expression in an ATM/ATR/CHK1-dependent manner and engage activation of STAT1/STAT3 (89). Radiation increased neo-antigen expression and enhanced immunogenicity when

combined with anti-PD-1 and anti-CTLA-4 therapy (90). This study indicates that radiotherapy might help activate the immune system and possibly predict the overall outcome in TNBC (91).

Chemotherapy. There are several chemotherapies that are recommended by the National Comprehensive Cancer Network as a guideline for treatment of TNBC. Chemotherapies are given to patients to lower the chance of cancer growth and spread. Chemotherapies such as anthracycline (Adriamycin or doxorubicin) and cyclophosphamide (with or without fluorouracil) followed by taxane (paclitaxel or docetaxel) are given to TNBC patients as a first line therapy (83). Clinical trials with capecitabine, eribulin, ixabepilone, and platinum drugs like carboplatin or cisplatin have also shown clinical efficacy in metastatic TNBC patients in a second or later line treatment setting (83). Some TNBC patients do respond to chemotherapy and have good survival chances; however, some patients relapse with chemo-resistant tumor and eventually die from the disease (92). A genomic analysis study of TNBC patients segregated according to their chemosensitivity and chemoresistance found that mutations in the androgen receptor/ FOXA1 pathway were predictive of TNBC patients that benefited from chemotherapy. Additionally, BRCA-deficient TNBC show higher clonal mutation and are associated with higher immune activation and reasonably higher chemosensitivity (93). Mostly chemotherapy drugs are given to the patients as a monotherapy or in some cases in combination, depending on its toxicity to the patient. In metastatic TNBC patients, taxanes-based combination are better than anthracycline-based combinations in relation to progression-free survival and response rate (94). Atezolizumab, a selective PD-L1 inhibitor, in

combination with nab-paclitaxel was recently shown to have improved progression-free survival in advanced or metastatic TNBC (95). Based on this trial, the combination has achieved accelerated approval by the US Food and Drug Administration (FDA) in patients with high tumor PD-L1 expression (83, 95).

In addition to these therapies, novel targeted therapies are currently under investigation for AKT, poly (adenosine diphosphate[ADP]-ribose) polymerase (PARP), antibody drug conjugates, and immune checkpoint inhibitors in TNBC. These clinical trials have stringent patient selection criteria and outcomes from these trials cannot be generalized for all TNBC patients (83, 96-98).

Hh signaling pathway in TNBC

During embryonic development the mammary epithelium undergoes massive morphological changes that require active signal exchange between epithelial cells and mesenchymal cells (99, 100). Activation of key developmental signaling pathway such as Wntless (WNT), Notch, Hippo, TGF- β , and Hh signaling is important to regulate morphogenesis changes and cellular fate (100). Developmental signaling pathways are inactive in adult tissue, but in several cancers including TNBC, these pathways are re-activated. Hh signaling is one of such developmental signaling pathway implicated in cellular pathogenesis, proliferation, differentiation, angiogenesis, and multidrug resistance (discussed in more details in page 23). Hh signaling promotes TNBC tumor growth, invasion, metastasis, and recurrence (99, 101).

Hh in DNA damage repair. Chemotherapy and radiotherapy treatments in TNBC culminate in DNA damage through induction of genotoxic stress. DNA damage can lead to chromosomal loss and rearrangements, exacerbation of existing gene deletions, or cell death. With the advent of PARP inhibitors like olaparib and talazoparib, that are effective in BRCA mutated breast cancer, there is a renewed interest in challenging the DNA damage repair (DDR) mechanisms in cancer (102). Interestingly, Hh signaling is involved in the DDR process and presents as an important therapeutic target to overcome chemo- and radiotherapy resistance in the treatment of cancer (103).

Hh inhibition interferes single-strand break (SSB) repair process such as Nucleotide Excision Repair (NER), Base Excision Repair (BER), and Mismatch Repair (MMR) (103). Inhibition of Hh signaling by small molecule inhibitor GANT61 directly binds GLI1/2 leading to downregulation of NER-related genes like ERCC1 and XPD, in cisplatin-resistant ovarian cancer cells (104). Consequently, abrogating Hh signaling increased chemosensitivity in the cancer cells in an NER-dependent manner. Similarly, inhibition of Hh signaling down-regulated expression of MMR-related genes MSH6 and EXO1 and induced cell cycle arrest in human colon cancer cells, and in pancreatic ductal adenocarcinoma cells diminished MMR activity by repressing the MLH1 promoter activity (105, 106). Additionally, GANT61 downregulates BER by diminishing transcription of BER-related genes like 5'Flap endonuclease (FEN1), uracil DNA glycosylase (UNG), DNA ligase I (LIG1) and KIAA0101 in human colon cancer cell (103, 105). Hh inhibition also impairs the BER gene XRCC1, which is upregulated in ovarian cancer resistant to cisplatin (104). Hh signaling plays a critical role in SSBs repair pathway in cancer cells.

Hh is also implicated in the double-strand break (DSB) repair pathway. Hh inhibition by GANT61 led to a decrease in homologous recombination-related genes like RAD51C (XRCC3), RAD54B, RAD51, and HELLS in human colon cancer (105). GANT61 in human colon carcinoma HT29 cells also induced DNA DSBs evident by an increase in surrogate marker γ -H2AX nuclear foci and ATM-dependent activation of Mediator Of DNA Damage Checkpoint 1 (MDC1) and Nijmegen Breakage Syndrome 1 (NBS1)(107). Furthermore, Zhang et al., confirmed that GANT61 increased colon cancer cell death by transcriptional regulation of CDT1, which is one of the DNA licensing factors (108). We have recently shown that Hh signaling is essential for rDNA DSBs and its inhibition impacts the non-homologous end joining repair pathway (109).

Hh in hypoxic TME. Hypoxic microenvironment presents as a challenge to effective chemo-and radio-therapy treatment. In hypoxic conditions, ionizing radiation is 50% less effective compared to normal oxygen conditions since oxygen is needed to form free radicals that create DNA lesions (110, 111). Likewise, chemotherapy is less effective in hypoxic conditions due to lower efficacy of drugs in the absence of oxygen (112). Therefore, there is a need for evaluating mechanisms that govern the cellular adaptation in hypoxic microenvironment.

Among various cellular alterations that hypoxia induces or exacerbates, Hh signaling is one of them. Biklsma et al., reported that hypoxia induces Hh activity mediated by HIF-1 α in ischemic adult tissue and inhibition of HIF-1 α decreased Hh activity (113). Similarly, hypoxia mediated activation of Hh signaling is also reported in pancreatic cancer (114). Supporting this study, Spivak-Kroizman et al., showed that

hypoxia increased HIF-1 α levels in pancreatic cancer cells and the paracrine signaling between cancer cells and fibroblasts mediated by Sonic Hh ligand led to increased desmoplasia (115, 116). Sonic Hh ligand mediated Hh signaling also regulates hypoxia in myocardial cell and cholangiocarcinoma and serves a protective role in hypoxia response (117, 118). Currently, a mechanistic study of the role of Hh signaling in hypoxia adaptation in breast cancer is understudied.

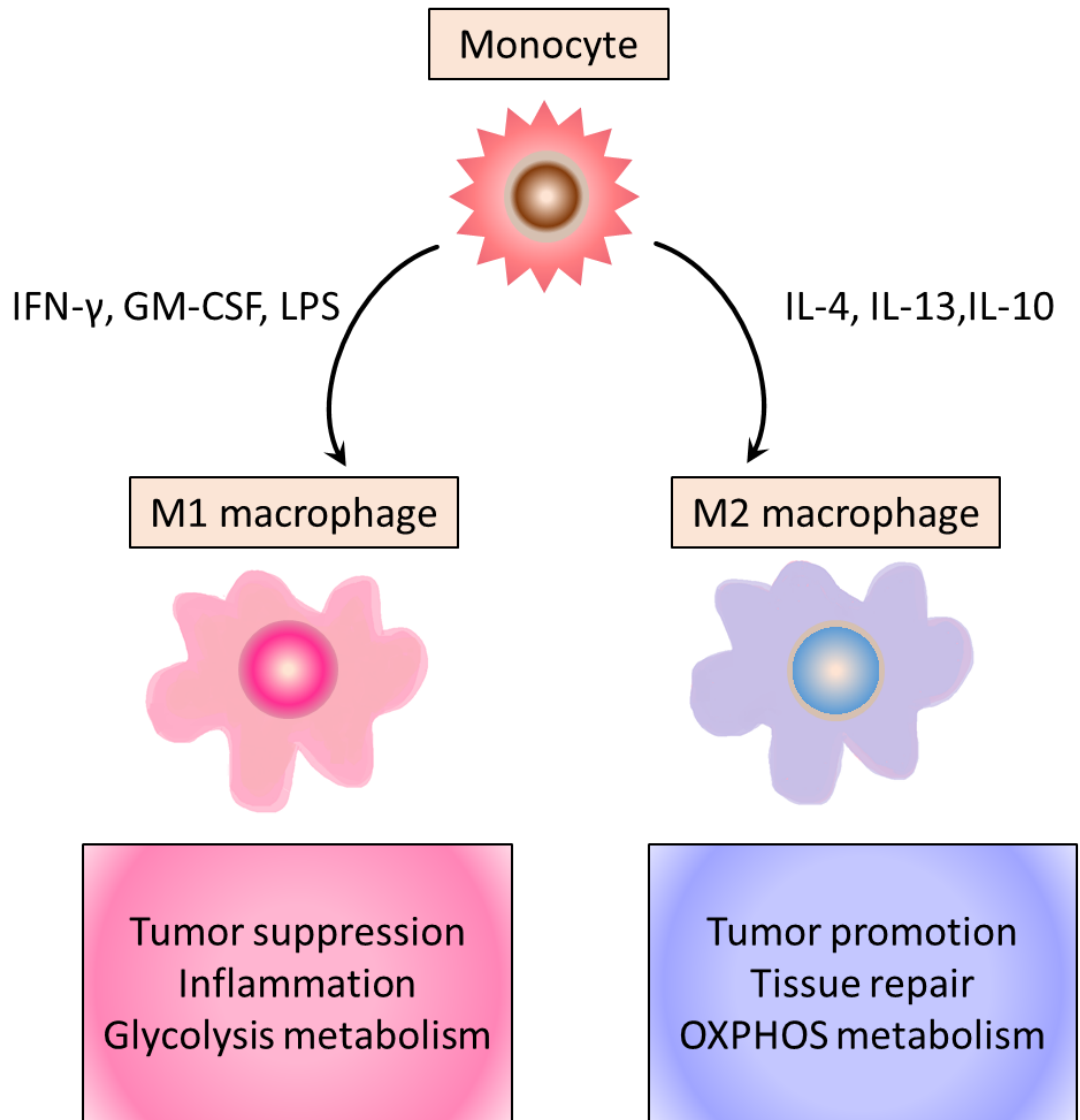


Figure1. TME stimulus determine distinct macrophage phenotypes. Monocytes can be polarized depending on the pro-inflammatory and anti-inflammatory stimuli they receive in their surrounding and are typically divided into two main groups, the M1 and M2 macrophages. IFN- γ , Granulocyte-Macrophage Colony Stimulating Factor (GM-CSF), and Lipopolysaccharide (LPS) polarize the monocytes towards tumor suppressing, inflammation promoting M1 macrophages. Alternatively, Interleukins (IL4, IL-13, IL-10) polarization monocytes to an immunosuppressive, anti-inflammatory M2 macrophages.

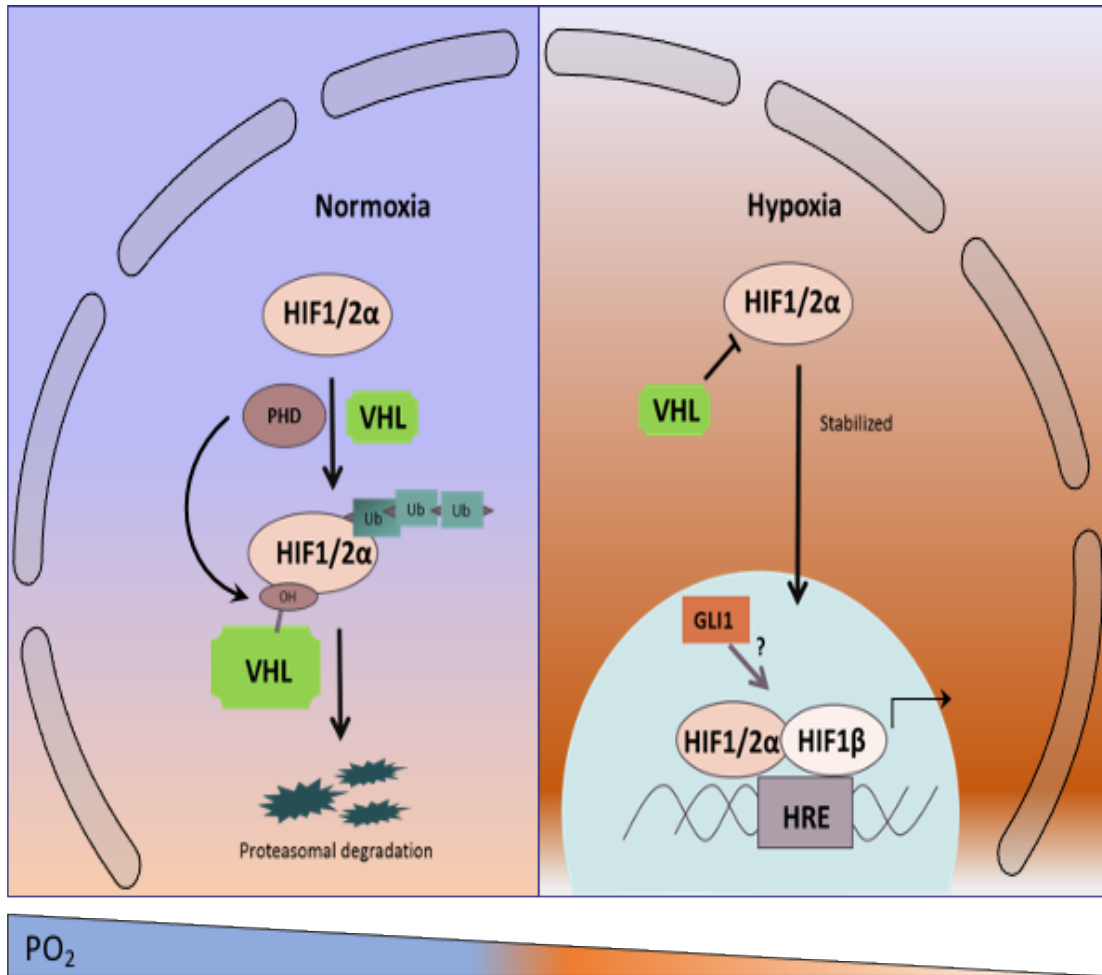


Figure 2. Hypoxia response pathway determine cellular adaptation to hypoxia. In normoxia, HIF1/2 α is targeted for proteasome degradation due to combined action of PHD and VHL. PHD hydroxylates HIF1/2 α in the presence of oxygen and VHL recognizes hydroxylated HIF1/2 α and poly-ubiquitinates it leading to 26S proteasome degradation. However, in hypoxic condition, PHD is inactive and thus, HIF1/2 α is stabilized. Stable HIF1/2 α translocate into the nucleus where it forms heterodimer with HIF1 β leading to transcription activation of genes that are important in angiogenesis, metastasis, metabolic reprogramming, pH regulation, drug resistance, and survival.

HEDGEHOG SIGNALING IN CARCINOGENESIS

by

TSSHERING D LAMA-SHERPA*, VICTOR TG LIN*, AND LALITA A. SHEVDE

Published in Springer eBook

Copyright

2019

by

Springer Nature

Used by permission

Format adapted for dissertation

Abstract

The Hedgehog (Hh) pathway mediates normal patterning during embryogenesis and contributes to tissue homeostasis after development is complete. Aberrant activation of Hh signaling has been implicated in a wide variety of malignancies and is involved in multiple cellular processes important in carcinogenesis and tumor progression. Strikingly, mutations that constitutively activate the Hh pathway cause the nevoid basal cell carcinoma (BCC) syndrome (NBCCS), which is a heritable cancer predisposition syndrome that greatly increases the risk of developing BCCs and medulloblastomas. Preclinical data have demonstrated that Hh inhibition is an attractive target in cancer, but the translation of this research to the clinic has been a challenge. Despite a number of negative clinical trials, Hh-directed therapies are proven to be effective in cancers reliant on this pathway, and future trials must be designed to properly select for patients with Hh-driven tumors to increase the likelihood of a positive result. Here, we review the mechanisms underlying the pathway and different strategies used to inhibit Hh signaling. We also discuss the role that the Hh pathway plays in carcinogenesis and carefully examine available trial data to understand why clinical applications have lagged behind preclinical successes. Finally, we address the future of Hh-directed therapies and factors that will be critical to effectively expanding their use in the treatment of cancer patients.

Keywords: Hedgehog, GLI, PTCH, SMOH, Carcinogenesis, Development, Precision oncology, Basal cell carcinoma (BCC), Medulloblastoma

Introduction

Hedgehog (Hh) signaling serves a central role in embryogenesis and tissue homeostasis. The Hh pathway was initially defined in *Drosophila*, where it was shown to play an important part in polarity and patterning of body segments in larval development. The name of the pathway derives from the characteristic short and hairy appearance of Hh-mutated *Drosophila* larvae, which resemble hedgehogs. While the signaling pathway in invertebrates is distinct from the mammalian one, they both consist of complex networks of proteins that ultimately drive the nuclear translocation of zinc finger transcription factors, promoting expression of specific target genes. Vertebrate Hh signaling is evolutionarily conserved and promotes tissue remodeling, patterning, differentiation, and vascularization. In development, Hh signaling is precisely controlled and normal patterning relies on differences in ligand concentration and duration of exposure. However, abnormal engagement of the Hh pathway has also been implicated in tumor initiation and progression. Cancer is known to recapitulate normal development, and neoplastic cells co-opt ontogenic pathways such as Hh signaling in order to promote growth, metastasis, and resistance to therapy [1]. Aberrant activation of Hh signaling has been demonstrated in a wide variety of malignancies, including basal cell carcinoma (BCC), medulloblastoma, breast cancer, pancreatic ductal adenocarcinoma, glioma, rhabdomyosarcoma, ovarian cancer, and hepatocellular carcinoma, underlining its importance in cancer biology. Accordingly, there has been great interest in targeting Hh signaling to treat cancer. Here, we introduce our current understanding of the Hh pathway, discuss its role in carcinogenesis, and examine the current state and future potential of Hh-directed therapies in the clinic.

An Overview of Hedgehog Signaling

Much of our current understanding of the Hh signaling pathway stems originally from studies in *Drosophila*. While there are evolutionarily conserved elements, key differences exist between the invertebrate and mammalian Hh pathways. For instance, in contrast to the invertebrate Hh pathway, the primary cilium plays an important role in the mammalian Hh pathway [2]. These specifics are beyond the scope of this text, which will focus only on vertebrate signaling (Figure 1) and its relevance to human disease.

The classical, ligand-initiated Hh pathway is activated by the binding of Hh ligands—sonic hedgehog (SHH), desert hedgehog (DHH), and indian hedgehog (IHH)—to the transmembrane protein receptor Patched (PTCH). PTCH spans the membrane twelve times and, in the absence of Hh ligand, constitutively represses vesicle-bound Smoothed (SMOH), a G-protein-coupled signal transduction molecule. PTCH forms a co-receptor complex with cell adhesion molecule (CAM)-related/downregulated by oncogenes (CDO), brother of CDO (BOC), and growth arrest-specific 1 (GAS1). Ligand binding to this multimolecular co-receptor complex leads to the internalization of PTCH and consequently relieves its inhibitory effect on SMOH, which is then able to translocate to the primary cilium. This ultimately starts a signaling cascade that results in the release of glioma-associated oncogene (GLI) transcription factors from a repressor complex that includes suppressor of fused (SUFU), kinesin family member 7 (KIF7), protein kinase A (PKA), glycogen synthase kinase 3 β (GSK3 β), and casein kinase 1 (CK1). GLI transcription factors are then free to translocate to the nucleus where they promote target genes. In the absence of Hh ligand binding, this macromolecular complex is sequestered at the microtubules of the primary cilium [3]. The Hh pathway can also be activated in a

non-classical, Hh ligand-independent manner. Signaling mediated by tumor-associated cytokines such as osteopontin (OPN), transforming growth factor β (TGF- β), platelet-derived growth factor (PDGF), and stromal-derived factor 1 (SDF-1) via their respective receptors can potentiate GLI activity independent of Hh ligands and SMOH [4].

Canonical, GLI-mediated Hh signaling requires GLI-initiated transcription of different genes, particularly those involved in cellular differentiation, stem cell maintenance, and tissue development. There are three GLI family members: GLI1, GLI2, and GLI3. Full-length GLI proteins act as transcriptional activators of downstream targets, and truncation via proteasomal processing changes their function from activation to repression. GLI2 and GLI3 carry a repressor domain in the N-terminus that GLI1 lacks, and thus GLI1 is thought to function only as a transactivator. Conversion of GLI2 or GLI3 from full-length activator to truncated transcriptional repressor involves phosphorylation catalyzed by PKA, GSK3 β , and CK1, followed by ubiquitination by the Skp/Cullin/F-box (SCF)- β TrCP E3 ligase, resulting in proteasomal processing to remove the C-terminal transactivator domain [5]. Hh signaling can also proceed via the GLI-independent, non-canonical pathways, with or without direct SMOH involvement. SMOH-independent non-canonical Hh signaling leads to cell proliferation and survival, whereas SMOH-dependent signaling modulates intracellular Ca²⁺ balance and the actin cytoskeleton through activation of the Rac small GTPase [4].

Given the complex nature of Hh signaling, it is unsurprising that a variety of inhibitors have been developed to study these pathways. Some agents act at the level of Hh ligands, such as the small-molecule inhibitor robotnikinin and 5E1, a monoclonal antibody directed against SHH. SMOH inhibitors represent the largest class of Hh

inhibitors. These include cyclopamine, a natural compound derived from wild corn lilies, and its synthetic small-molecule derivatives, such as vismodegib and sonidegib (formerly known as erismodegib). Finally, there are direct GLI antagonists, which include GLI antagonists 58 and 61 (GANT-58 and -61) and Hh pathway inhibitor 1 (HPI-1). In addition to the agents listed above, several drugs approved for other indications have also been identified as Hh inhibitors. These include the antifungal itraconazole, which inhibits SMOH through a site distinct from the cyclopamine derivatives, and arsenic trioxide, an agent used to induce differentiation in acute promyelocytic leukemia (APL) that has also been shown to inhibit Hh signaling at the level of GLI [6].

Hedgehog Signaling in Carcinogenesis

The most compelling demonstration of the importance of Hh signaling in carcinogenesis is the nevoid basal cell carcinoma syndrome (NBCCS), also known as basal cell nevus syndrome (BCNS) or Gorlin syndrome. This is an inherited cancer predisposition disorder that typically results from loss of function mutations in PTCH1, the gene encoding PTCH. In the absence of PTCH function, tonic repression of SMOH is relieved, and ligand-independent downstream signaling proceeds unabated. Patients with NBCCS are particularly susceptible to developing BCCs and medulloblastomas. As discussed in more detail later, targeting Hh signaling in these two tumor types has yielded the most encouraging clinical results.

Subsequently, multiple unrelated groups of patients meeting clinical criteria for NBCCS, but who lacked the expected mutation in PTCH1, underwent exome sequencing of lymphocyte DNA in an effort to identify other causative mutations. In this fashion,

mutations in SUFU were also determined to cause NBCCS [7]. As SUFU acts to negatively regulate GLI function, loss of function mutations in SUFU would be predicted to similarly result in constitutive Hh pathway activation autonomous of ligand binding. However, because SUFU acts downstream of SMOH, it is expected tumors arising in SUFU-related NBCCS would be refractory to SMOH inhibitors, unlike PTCH-related NBCCS.

Aside from BCC and certain medulloblastomas, Hh signaling has also been implicated in a wide variety of cancers, including glioma, lymphoma, multiple myeloma, and carcinomas of the breast, colon, ovaries, pancreas, and prostate. The possible routes of activation are equally varied. In addition to mutations of proteins that result in ligand-independent pathway activation as described above, aberrant Hh signaling can also result from the overexpression of Hh ligands, either by the cancer cells themselves in an autocrine loop or from the surrounding stroma via paracrine signaling. Finally, nonclassical activation can arise from dysregulation of other pathways involved in carcinogenesis, including K-Ras, NF- κ B, mTOR/S6K, and c-Jun [4].

Functionally, inappropriate Hh activation has been linked to multiple hallmarks of cancer [3]. It has been shown to drive cell proliferation through upregulation of Myc and cyclin D1, and immortalizes cancer cells by upregulating human telomerase reverse transcriptase (hTERT). Hh signaling can also allow cancer cells to resist apoptosis by upregulating the antiapoptotic protein B-cell lymphoma 2 (Bcl-2) and downregulating Bcl-2-associated death promoter (BAD). The Hh pathway potentially mediates immune evasion as well, with evidence suggesting that Hh inhibition enhances antigen presentation by increasing the expression of major histocompatibility complex (MHC)

class I proteins in cancer cells and enhancing the number of tumor infiltrating lymphocytes (TILs). Finally, Hh activation can drive tumor invasion and metastasis by triggering the epithelial-to-mesenchymal transition (EMT), while stimulating angiogenesis through expression of vascular endothelial growth factor (VEGF) and fibroblast growth factor (FGF). It can also predispose to osseous metastases by preparing the metastatic niche through the expression of osteoclast-promoting cytokines, including receptor activator of NF- κ B ligand (RANKL) and OPN.

Targeting Hedgehog in the Clinic

While there is a wide variety of Hh inhibitors used in scientific studies, the clinically-relevant armamentarium is limited. At present, SMOH inhibitors are the only class of agents specifically targeting Hh signaling that are available for use in the clinic. There are two FDA-approved drugs on the market, vismodegib and sonidegib. Currently, the only labeled indication for Hh-directed therapy is in non-resectable BCC. The ideal treatment of BCC is with local therapies: resection with adjuvant radiation therapy if there are any positive surgical margins that cannot be re-excised. However, on the basis of the ERIVANCE, STEVIE, and BOLT trials, SMOH inhibitors are now an option in cases where local therapies are not possible, either because of unresectable lesions or metastasis. Recent clinical trial data also indicate SMOH inhibitors can reduce the frequency of recurrent BCCs in patients with NBCCS [8].

Although there is an abundance of data in the preclinical setting demonstrating the importance of Hh signaling in a variety of different cancer types, clinical trials assessing the addition of SMOH inhibitors to standard treatment in advanced colon cancer, small

cell lung cancer, and pancreatic cancer have all yielded negative results. Clinical trials have also been negative for the use of SMOH inhibitors in the maintenance setting for ovarian cancer in second or third complete remission [9] and for unselected recurrent medulloblastomas [10]. However, while these last two clinical trials yielded negative results, they do illustrate important concepts critical for the future success of Hh-directed therapy in cancer treatment.

In the CONSORT trial, the intention was to use vismodegib maintenance to disrupt tumor-stroma interactions to prolong the progression free interval in ovarian cancer in complete remission after prior relapse. However, the expression of Hh ligands—SHH and IHH, as measured by quantitative RT-PCR—was lower in comparison to prior studies of banked ovarian cancer tissue, suggesting that the eligibility criteria for this trial may have selected out the population likely to benefit from this targeted treatment approach [9]. In the PBTC-025B and PBTC-032 studies, patients with recurrent medulloblastoma were treated with vismodegib. When patients were stratified into SHH-driven and non-SHH-driven tumors by IHC, it was clear that the responses were confined to the SHH-driven tumors, as would be expected.

Interestingly, further analysis indicated that SHH-driven tumors that had concurrent strong diffuse staining of p53, which is associated with dominant-negative mutations of the p53 DNA-binding domain, were also insensitive to vismodegib [10]. Taken in combination, these data suggest that careful selection of patients will be a primary determinant for the clinical success of Hh-directed therapy, not only to identify those with tumors driven by the Hh pathway, but also potentially to stratify their likelihood of response based on other factors, such as p53 status.

The Future of Hedgehog-targeted Therapies

Going forward, the viability of Hh targeting as a cancer treatment strategy hinges on several critical factors. First and foremost is the development of other Hh inhibitors. As described above, Hh signaling is comprised of a collection of complex pathways that can be either dependent on or independent of Hh ligands, SMOH, and GLI. While a diverse collection of inhibitors is available in the laboratory setting, only SMOH-dependent pathways can be targeted in the clinic. Because of this significant limitation, there are two major challenges to overcome. First, mutations of SMOH that abrogate binding to cyclopamine-derived SMOH inhibitors have already been identified and render all currently available agents ineffective. Secondly, SMOH inhibitors will not be useful in cases where GLI is activated independent of SMOH. Development of direct GLI inhibitors in particular will help to bridge the gap that currently exists between the laboratory and the clinic. Alternatively, to bypass the long development cycle required for new drugs, another approach has been to evaluate drugs already approved for other indications that also function as Hh inhibitors. While preclinical testing suggests that itraconazole and arsenic trioxide can both be used to target Hh signaling and to bypass resistance mutations, these findings require confirmation in ongoing clinical trials before they can be used to treat patients [6].

Based on the available evidence, the future success of Hh-directed therapies will clearly be dependent on the appropriate selection of patients. Thus, another priority going forward must be the identification of candidates most likely to benefit from Hh-targeted therapies. Accordingly, the development and validation of biomarkers for Hh-driven cancers is of paramount importance (Table 1).

As the capability to profile cancers in the clinic using advanced molecular testing and liquid biopsies becomes more prevalent, it is also critical to determine the utility of Hh-directed therapy in tumors determined to be driven by Hh (Table 2). Because of this, ongoing large-scale precision oncology trials, such as NCI-MATCH and ASCO's TAPUR may hold the key. These studies will screen large numbers of patients for Hh-driven cancers based on the specific tumor genomic profile and funnel these patients to Hh-directed therapies, unlike prior trials which were either unselected or too small to have a significant cohort of Hh-driven cancers. They may also help to identify other malignancies in which a role for Hh signaling has not yet been demonstrated. With the recent tumor agnostic approval of the immune checkpoint inhibitor pembrolizumab, there are likely to be more drug approvals based on specific tumor biology irrespective of cancer type. While Hh-targeted therapy is currently only approved for BCC, the hope is that these large-scale precision oncology trials will eventually justify a similar expansion of the role of Hh inhibitors.

Summary

A large body of evidence has demonstrated the importance of Hh signaling in a diverse range of cellular processes involved in carcinogenesis and tumor progression. Numerous preclinical studies have shown that inhibition of Hh signaling is an effective strategy to target cancer cells. Unfortunately, with a few notable exceptions, preclinical successes have not yet translated to clinical efficacy. However, this seems likely to be the sequelae of suboptimal patient selection and a limited arsenal of Hh inhibitors available for use in human subjects. With recent improvements in technology that allow the

heretofore unprecedented ability to rapidly and cost-efficiently analyze the genomic profiles of individual tumors, more precise identification of patients likely to benefit from Hh-targeted therapy will soon be possible. Furthermore, as new agents targeting different elements of the Hh pathway become available, advanced molecular testing may also help guide treatment choices, allowing clinical oncologists to stratify patients into subpopulations likely to benefit from specific inhibitors. While the enthusiasm for Hh-directed therapies has been somewhat dampened due to a number of negative clinical trials to date, with continuing technological advances in precision oncology, there is now reason for renewed optimism.

References

1. Lin VTG, Pruitt HC, Samant RS, Shevde LA. Developing Cures: Targeting Ontogenesis in Cancer. *Trends Cancer*. 2017;3(2):126-36.
2. Briscoe J, Therond PP. The mechanisms of Hedgehog signalling and its roles in development and disease. *Nat Rev Mol Cell Biol*. 2013;14(7):416-29.
3. Hanna A, Shevde LA. Hedgehog signaling: modulation of cancer properties and tumor microenvironment. *Mol Cancer*. 2016;15:24.
4. Shevde LA, Samant RS. Nonclassical hedgehog-GLI signaling and its clinical implications. *Int J Cancer*. 2014;135(1):1-6.
5. Pan Y, Wang B. A novel protein-processing domain in Gli2 and Gli3 differentially blocks complete protein degradation by the proteasome. *J Biol Chem*. 2007;282(15):10846-52.
6. Kim J, Aftab BT, Tang JY, Kim D, Lee AH, Rezaee M, et al. Itraconazole and arsenic trioxide inhibit Hedgehog pathway activation and tumor growth associated with acquired resistance to smoothed antagonists. *Cancer Cell*. 2013;23(1):23-34.
7. Smith MJ, Beetz C, Williams SG, Bhaskar SS, O'Sullivan J, Anderson B, et al. Germline mutations in SUFU cause Gorlin syndrome-associated childhood medulloblastoma and redefine the risk associated with PTCH1 mutations. *J Clin Oncol*. 2014;32(36):4155-61.
8. Tang JY, Ally MS, Chanana AM, Mackay-Wiggan JM, Aszterbaum M, Lindgren JA, et al. Inhibition of the hedgehog pathway in patients with basal-cell nevus syndrome: final results from the multicentre, randomised, double-blind, placebo-controlled, phase 2 trial. *Lancet Oncol*. 2016;17(12):1720-31.
9. Kaye SB, Fehrenbacher L, Holloway R, Amit A, Karlan B, Slomovitz B, et al. A phase II, randomized, placebo-controlled study of vismodegib as maintenance therapy in patients with ovarian cancer in second or third complete remission. *Clin Cancer Res*. 2012;18(23):6509-18.
10. Robinson GW, Orr BA, Wu G, Gururangan S, Lin T, Qaddoumi I, et al. Vismodegib Exerts Targeted Efficacy Against Recurrent Sonic Hedgehog-Subgroup Medulloblastoma: Results From Phase II Pediatric Brain Tumor Consortium Studies PBTC-025B and PBTC-032. *J Clin Oncol*. 2015;33(24):2646-54.
11. Ellison DW, Dalton J, Kocak M, Nicholson SL, Fraga C, Neale G, et al. Medulloblastoma: clinicopathological correlates of SHH, WNT, and non-SHH/WNT molecular subgroups. *Acta Neuropathol*. 2011;121(3):381-96.

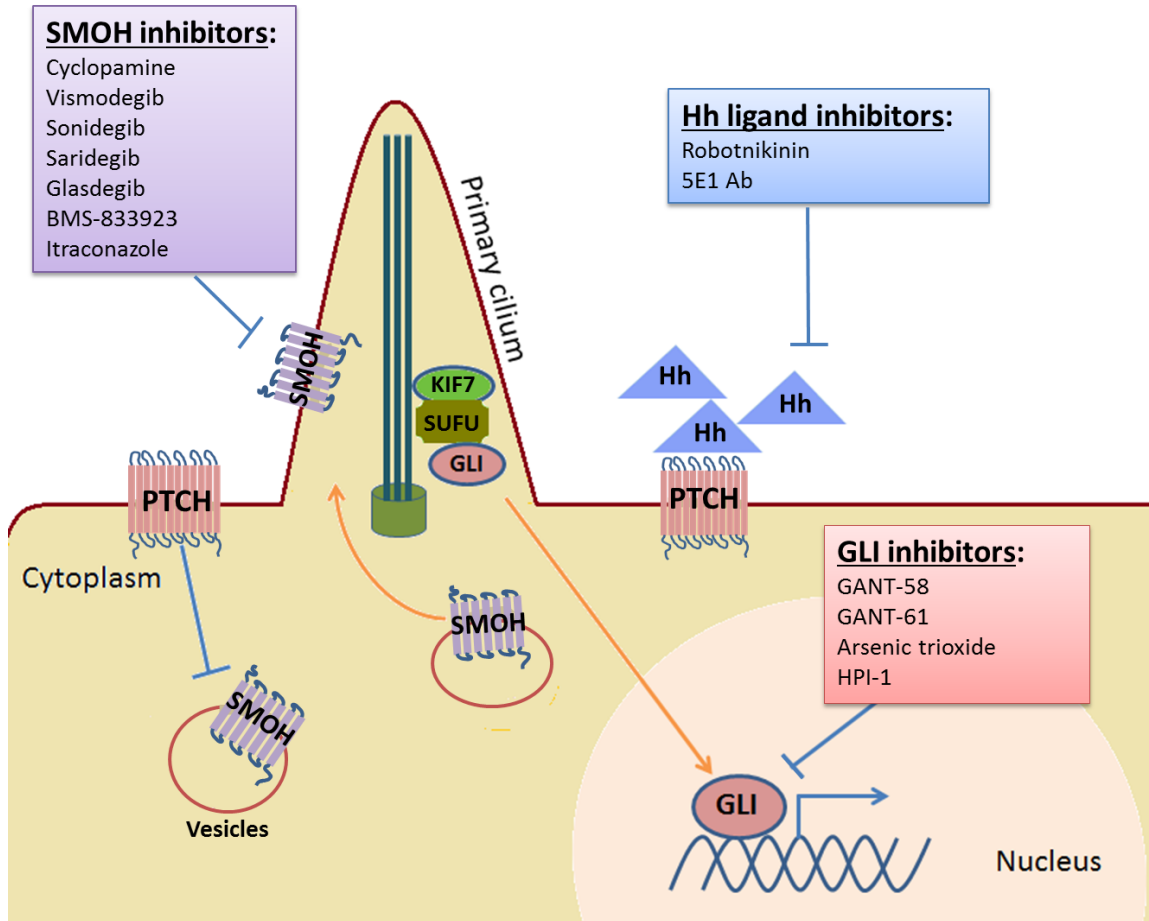


Figure 1: Schematic of the classical, canonical vertebrate Hh signaling pathway. In the absence of Hh ligand, PTCH represses SMOH, which is sequestered in vesicles. After binding of Hh ligand to PTCH, SMOH translocates to the primary cilium. This releases GLI from a repressor complex that includes SUFU and KIF7. GLI is then able to translocate to the nucleus and function as a transcriptional activator of target genes. Inhibitors of this pathway can work at the level of Hh ligands, SMOH, and GLI.

Hh Signaling Pathway	Cancer Type	Affected Biomarker	Method of Detection	Target	Active Drugs/Company
Loss of PTCH1 function	BCC	PTCH1	Not routinely tested	SMOH	Vismodegib (Erivedge®) Genentech/Roche Sonidegib (Odomzo®) Novartis [1]
Loss of PTCH1 function	NBCCS	PTCH1	Molecular genetic testing	SMOH	Vismodegib (Erivedge®) Genentech/Roche [8]
Loss of SUFU function	NBCCS	SUFU	Molecular genetic testing	SUFU	None [7]
<i>PTCH1</i> deletion	medulloblastoma	GAB1*	IHC	SMOH	Vismodegib (Erivedge®) Genentech/Roche [10]
<i>PTCH1</i> deletion	medulloblastoma	PTCH1	FISH	SMOH	Vismodegib (Erivedge®) Genentech/Roche [10]
<i>SHH/IHH</i> amplification	ovarian cancer	SHH/IHH	qRT-PCR	SHH/IHH	None [9]
<i>PTCH1</i> deletion or inactivating mutations	Advanced solid tumors	PTCH1	NGS	SMOH	Vismodegib (Erivedge®) Genentech/Roche (currently being evaluated in active clinical trials, such as ASCO TAPUR)

Table 1: Examples of potential predictive biomarkers for the Hh signaling pathway.

Hh Inhibitor	Disease	ClinicalTrials.gov Identifier	Biomarker-Selected?
arsenic trioxide and itraconazole	basal cell carcinoma	NCT02699723	No
glasdegib	AML	NCT01841333	No
glasdegib	AML	NCT02038777	No
glasdegib	myelofibrosis	NCT02226172	No
glasdegib	MDS and AML	NCT02367456	No
sonidegib	multiple myeloma	NCT02086552	No
vismodegib	medulloblastoma	NCT01601184	Yes
vismodegib	medulloblastoma	NCT01878617	Yes
vismodegib	AML	NCT02073838	No
vismodegib	advanced solid tumors	NCT02091141	Yes
vismodegib	advanced solid tumors	NCT02465060 (NCI-MATCH)	Yes
vismodegib	meningioma	NCT02523014	No
vismodegib	myelofibrosis	NCT02593760	No
vismodegib	advanced solid tumors	NCT02693535 (ASCO's TAPUR)	Yes
vismodegib	triple-negative breast cancer	NCT02694224	No
vismodegib	urothelial carcinoma	NCT02788201	Yes
vismodegib	advanced solid tumors	NCT02925234	Yes
vismodegib	advanced gastric adenocarcinoma	NCT03052478	Yes
vismodegib	glioblastoma	NCT03158389	Yes
vismodegib	advanced solid tumors	NCT03297606	Yes

Table 2: Examples of ongoing trials of Hh inhibitors in cancer.

AN EMERGING REGULATORY ROLE FOR THE TUMOR MICROENVIRONMENT
IN THE DNA DAMAGE RESPONSE TO DOUBLE-STRAND BREAKS

by

TSSHERING D LAMA-SHERPA AND LALITA A. SHEVDE

Mol Cancer Res. 2020 Feb; 18(2): 185–193.

Copyright

2020

by

Lama-Sherpa et al.

Open access license, no permission required

Format adapted for dissertation

Abstract

Radiation, alkylating agents, and platinum-based chemotherapy treatments eliminate cancer cells through the induction of excessive DNA damage. The resultant DNA damage challenges the cancer cell's DNA repair capacity. Among the different types of DNA damage induced in cells, double-strand breaks (DSBs) are the most lethal if left unrepaired. Unrepaired DSBs in tumor cells exacerbate existing gene deletions, chromosome losses and rearrangements, and aberrant features that characteristically enable tumor progression, metastasis, and drug resistance. Tumor microenvironmental factors like hypoxia, inflammation, cellular metabolism, and the immune system profoundly influence DSB repair mechanisms. Here, we put into context the role of the microenvironment in governing DSB repair mechanisms. Implications: This minireview presents an important consideration for therapies that specifically target sustenance of cancer cells by the tumor microenvironment and highlights key considerations to overcome resistance to DNA damage-inducing therapies.

Keywords: DNA double-strand break repair, tumor microenvironment, inflammation, hypoxia, immune checkpoints, cellular metabolism.

Introduction

DNA repair during carcinogenesis

Genomic stability is essential to guarantee the inheritance of correct genetic information. Nevertheless, endogenous or exogenous environmental factors can act as DNA-damaging agents leading to genetic alterations (1). Endogenous factors include byproducts of cell metabolism, while exogenous agents encompass ionizing radiation, ultraviolet light (UV), and chemotherapeutic drugs (1). Integrity of DNA is vitally important as mutations can lead to carcinogenesis (2). Since the resolution of DNA lesions is critical to cell survival, repair processes are in place to protect DNA integrity (2). These repair processes involve the activation of the cell cycle checkpoints (CHK1, CHK2, p53, p21) to stall the cell cycle, removal of mutagenic lesions in DNA, and cell death through apoptosis or senescence if repair fails (1). The goal is to avoid erroneous information being passed to the progeny and to potentially interrupt neoplastic transformations.

Genomic instability is a characteristic of most cancers. This is supported by the observation that tumor cells often have unchecked proliferation, chromosomal translocations, and aneuploidy as a consequence of mutagenic lesions in DNA (2). Furthermore, mutations in DNA repair genes form the basis of many hereditary cancers underscoring their importance in oncogenesis (3-5). Xeroderma pigmentosum (XP) is a hereditary disease caused by a defect in nucleotide excision repair (NER) and predisposes individuals to skin cancer (3). Likewise, germline mutations in the DNA repair gene ataxia telangiectasia mutated (ATM), can lead to increased sensitivity towards ionizing radiation, humoral and cellular immunodeficiency, and pre-disposition to cancer (3).

Individuals with AT have ~60-180 times increased risk of developing cancer that primarily includes lymphomas and leukemia (3). The pre-disposition to cancer is most likely associated to impaired DNA damage repair given ATM's role in DNA damage repair and cell cycle progression (3, 4). Germline mutations in BRCA genes, which are involved in homologous recombination, predispose the individual to breast and ovarian cancer. Approximately 5–7% of all hereditary breast cancers have BRCA gene mutations (5).

Complementing surgery, current treatment modalities in cancer include strategies such as ionizing radiation, alkylating agents, and platinum-based chemotherapy all of which induce excessive DNA damage (1). The ensuing DNA damage warrants effective DNA repair capacity, which may be limited in tumor cells. Compared to normal cells, cancer cells have a higher accumulation of DNA damage and build-up of replicative stress due to faulty cell cycle checkpoint activation (1, 2). In a normal cell, such mutational burden would mean cell death. However, cancer cells utilize mutagenic repair pathways to their advantage and escape death (2). Since cancer cells already have a higher mutational load, targeting their repair capacity provides a therapeutic window where the cytotoxicity of anticancer agents can be boosted. Based on the nature of the DNA lesion, single- or double-strand breaks, the cell invokes specific mechanisms to repair the damage. Summarized below are a variety of repair mechanisms that are employed by cells depending on the type of DNA lesion.

Major single-strand DNA break (SSB) repair pathways

SSBs are highly common in cells and are efficiently repaired through specific SSB repair processes (6). NER removes lesions that could potentially lead to helix

distortion, particularly those induced by UV. In eukaryotes, it involves the removal of a 24–32 nucleotide stretch of DNA directed by endonuclease activity and restoration by DNA polymerase activity (6). Base excision repair (BER) recognizes DNA bases damaged by oxidation, deamination, and alkylation. DNA glycosylase initiates BER by recognizing and removing damaged bases, which are processed by the APE-1 endonuclease and later restored through DNA polymerase and a ligase (7). Mismatch repair (MMR) recognizes incorrectly paired bases, and recruits repair proteins to damaged sites. Exonuclease 1 (EXO1) removes the mismatch, then polymerase δ fills the gap and seals the nick through DNA ligase I (LIG1) (8). The direct repair mechanism reverses oxidative lesions created by methylating agents. This is a single-step process mediated by the enzymatic activity of methylguanine methyltransferase (MGMT) that removes the alkyl group from the oxidative lesion in DNA. Following repair, MGMT undergoes rapid self-degradation (6). Unrepaired SSB in proliferating cells can lead to the collapse of DNA replication forks and might even result in the formation of DSBs (1).

Cellular kinase processes in DSBs repair

Immediate response to genotoxic stresses leading to DSBs is carried out by the damage-sensing MRN (MRE11-RAD50-NBS1) complex. The MRN complex plays a key role in activating ATM, a DNA-damage signaling kinase (9). ATM responds to DNA damage throughout the cell cycle and is mainly responsible for phosphorylation of the histone H2A variant H2AX at serine 139 to generate phosphorylated H2AX (γ -H2AX). γ -H2AX formation at sites of DSBs makes it a surrogate marker for DSBs (10, 11). Other phosphatidylinositol-3-OH-kinase-like family members including DNA-PKcs (the

catalytic subunit of DNA-dependent protein kinase) and ataxia telangiectasia and Rad3-related (ATR) also have redundant functions in phosphorylating H2AX. ATM also phosphorylates checkpoint kinase 2 (CHK2) (12). ATM-CHK2 signaling is important to ensure activation of DSB repair through the accumulation of DNA repair proteins and chromatin-remodeling complexes (9, 11).

Major DSB DNA break repair pathways

DSBs are created by genotoxic agents commonly used in the treatment of cancer. For example, radiotherapy, radiomimetics, bifunctional alkylators, topoisomerase inhibitors, and replication inhibitors can all lead to DSBs (Fig 1). DSBs caused by these agents can be resolved through the following DSB repair pathways.

Homologous recombination (HR). depends on a homologous sister chromatid DNA strand for repair and hence requires cell cycle progression into the S/G2 phase (Fig 2). An early step of DSB repair involves recruitment of the MRN nuclease. DNA end resection is coordinated by MRN proteins resulting in single strand 3' overhangs (reviewed in (13)). The MRN complex aids in the recruitment of p53 binding protein 1 (53BP1) and BRCA1. BRCA1 and C-terminal binding protein-Interacting Protein (CtIP) promote DNA end resection leading to HR (14). During the G1 phase of cell cycle, replication timing regulatory factor 1 (RIF1) is recruited to DSBs by 53BP1 (15, 16). Together, 53BP1 and RIF1 antagonize HR by inhibiting accumulation of BRCA1 at damage sites favoring non-homologous end joining (NHEJ). However, during the G2 phase of cell cycle, RIF1 accumulation is antagonized by BRCA1, leading to a switch to HR (15, 16).

Replication protein A (RPA) protects the single strands and facilitates the recruitment of HR proteins like BRCA1, BRCA2, partner and localizer of BRCA2 (PALB2), RAD51, X-ray repair cross-complementing protein 2 (XRCC2), and XRCC3. During the recombination process, the 3' overhangs invade the sister chromatid to form a heteroduplex (13). End processing is completed by excision repair cross-complementing group 1 (ERCC1), and DNA end gaps are filled by DNA polymerase. This is a high-fidelity repair mechanism and does not generate mutations during the repair process (13, 17).

Non-Homologous End Joining (NHEJ) . is the other major pathways that repairs DSBs in mammalian cells. NHEJ involves rapid end-ligation of broken DNA ends regardless of the stage of the cell cycle (Fig 2). NHEJ in mammalian cells requires the Ku70/80 heterodimer, DNA-PKcs, XRCC4 (X-ray repair cross-complementing protein 4), DNA ligase IV (LIG4), Artemis, and XRCC4-like factor (XLF) (reviewed in (18)). The broken DNA ends are tethered by the Ku70/80 heterodimer. DNA-PKcs is recruited to the repair site forming the DNA-PK complex. DNA-PKcs can be auto-phosphorylated or phosphorylated by ATM (19). The DNA-PK complex phosphorylates H2AX, XRCC4, DNA ligase IV (LIG4), and XLF. The end ligation process through NHEJ needs DNA end-processing and activity of DNA polymerases mu and lambda, which can be error-prone (18). Ligation also needs the DNA ends to be altered, and such alteration can include removal of damaged nucleotides, and addition or removal of undamaged nucleotides. While NHEJ is a predominant DNA DSB repair pathway in mammalian cells following radiation, this repair process can lead to chromosomal rearrangements (18, 20).

Alternative NHEJ. pathways were first discovered in Ku70-deficient yeast cells. Compared to classical NHEJ, alternative NHEJ is 20-fold less efficient (21, 22). The microhomology-mediated end joining (MMEJ) repair pathway exists as a backup when NHEJ repair proteins like DNA-PKcs and Ku70/80 are compromised and HR is limited. This alternative NHEJ pathway is reliant on micro-homologous regions of 5-25 base pairs. Unlike the canonical NHEJ pathway, MMEJ always results in losses of sequence (22). Therefore, this pathway leads to excessive genomic deletions and chromosomal translocations.

DSB repair proteins serve important functions in cancer cell survival. Even a single DSB has the ability to cause cell death if left unrepaired. In several tumor types like breast cancer, lung cancer, leukemia, and lymphoma, a high proportion of DSB repair genes are overexpressed when compared with other DNA repair pathways (23). As such, it is imperative to understand how DSB repair can be inhibited in tumor cells, so that current cancer therapies can be more effective. The tumor cells' response to DNA damage is governed by the integration of complex cellular and environmental cues. Therefore, in the ensuing sections of this review, we will put into context the impact of microenvironmental factors in directing DSB repair pathways.

Microenvironment and DSB DNA repair

Hypoxia and DSB repair

Hypoxia is characterized as a low oxygen condition prevalent in the tumor microenvironment. The oxygen availability in hypoxic regions is diminished due to rapid tumor proliferation and poor vasculature (24). Most advanced solid tumors, including

those of the breast, head and neck, pancreatic, lung, brain, prostate, and cervix, have hypoxic regions. The presence of hypoxia clinically correlates with poor prognosis in patients (25). The HIF-1 α transcription factor is upregulated in response to hypoxia; this activates expression of several target genes that collectively orchestrate increased angiogenesis, metabolic reprogramming, and survival (26). In normoxic conditions, oxygen-activated proline hydroxylase (PHD) regulates HIF-1 α through post-translational modifications. PHD hydroxylates HIF-1 α at its two proline sites and marks it for degradation. Hydroxylated HIF-1 α is then ubiquitinated by an E3 ligase, called von Hippel Lindau protein (VHL), leading to its degradation by the 26S proteasome (24). In contrast, lack of oxygen in hypoxic conditions inactivates hydroxylation reactions leading to rapid accumulation of HIF-1 α and HIF-2 α which can heterodimerize with HIF-1 β and bind to the hypoxia response element (HRE) sequence in target genes (27).

The hypoxic tumor microenvironment confers tumor cells with resistance to chemo- and radiotherapy (28). In hypoxic conditions, tumor cells are less prone to ionizing radiation-induced damage than in normal conditions. Hall et al. compared doses needed for sensitizing mammalian cells under hypoxic versus normoxic conditions and found that it takes a dose of 1 Gy to sensitize 99% cells under normoxic conditions; however, only 50% of hypoxic cells are sensitized at the same dose (29). Ionizing radiation creates DNA damage through a process that involves free radical formation. These free radicals create a variety of DNA lesions. In hypoxia, low oxygen levels compromise the generation of reactive oxygen species (ROS), and tumor cells are therefore more resistant to radiation therapy (30). Similarly, chemotherapeutic drugs are

less effective in hypoxic conditions due to their low efficacy in the absence of oxygen (28).

Hypoxia drives genetic instability through the impairment of DSB repair via transcriptional, translational, and epigenetic regulation of several important repair proteins like DNA-PKcs, Ku70/80, BRCA1, and RAD51 (31). Hypoxia regulates DSB repair and has distinct effects depending on the chronic (longer than 24hr) versus acute (shorter than 24hr) state of hypoxia. In response to acute hypoxia, ATM-CHK2 signaling is activated and leads to increased cell survival (32). In addition, DSB repair proteins are involved in HIF-1 α stability. Under hypoxia, activated ATM phosphorylates HIF-1 α at serine 696, stabilizing HIF-1 α (33). BRCA1 and DNA-PKcs both interact with HIF-1 α and regulate its stability as well (34, 35). Studies in prostate cancer using NHEJ and HR reporter plasmids to assess DSB repair show that chronic hypoxia engages NHEJ and restricts HR (36). Hypoxia induces p130 dephosphorylation and nuclear localization leading to activation of HIF-independent stress signaling that facilitates formation of the repressive E2F4/p130 complex. The E2F4/p130 complex binds to the E2F site in the proximal promoter of RAD51 and BRCA1, leading to decreased expression of their transcripts (37, 38). Hypoxia-mediated downregulation of RAD51 expression is also observed in vivo (38). There are, however, conflicting reports on the functional involvement of NHEJ in hypoxia. Meng et al. reported that hypoxia elicits downregulation of both, HR and NHEJ-related RNA expression in prostate cancer (39). Another set of reports complement these observations. Tsuchimoto et al. report that DNA-PKcs activity and RNA expression are inhibited under hypoxia (40). Also, Lara et al. reported that expression of Ku70/80 are downregulated in the hypoxic regions of

cervical tumors from patients (41). This is confounded by evidence from Um et al. that DNA-PKcs and Ku70/80 protein expression are upregulated under hypoxia and lead to increased stabilization of HIF-1 α (35). Similarly, Bouquet et al. found that DNA-PKcs is activated under hypoxia and stabilizes HIF-1 α but does not activate and recruit the XRCC4–DNA-ligase-IV complex (42). While it is likely that cellular responses of DNA repair to hypoxia are context-dependent, it is evident that hypoxia contributes significantly towards cellular choices of DSBs repair through modulating HR and NHEJ repair proteins, thereby making cells less sensitive to DNA damage.

Crosstalk between DSB DNA damage response and immune cells

Studies evaluating links between DNA damage response and innate immunity discovered possible crosstalk mainly via the stimulator of interferon genes (STING) pathway. Cyclic GMP-AMP synthase (cGAS) detects cytosolic double-stranded DNA (dsDNA) leading to the synthesis of cyclic GMP-AMP, a secondary messenger that binds to the adaptor protein STING (43). The STING protein is activated and shuttled from the endoplasmic reticulum to the perinuclear endosome where it phosphorylates TANK-binding kinase 1 (TBK1). TBK1 then activates interferon regulatory factor 3 (IRF-3) and nuclear factor kappa B (NF- κ B) required for expression of type I interferon, subsequently enhancing a pro-inflammatory innate immune response (43, 44).

Eliciting anti-tumor response by innate immune cells requires cross-presentation of tumor antigens. Woo et al. demonstrate that the STING pathway has an important role in activating dendritic cells (DCs), interferon beta (IFN- β) expression, and priming of CD8⁺ T cells in vivo (45). STING-deficient mice fail to reject immunogenic tumors

compared to wild type mice due to a defect in induction of critical factors including IL-12, CXCL9, CD86, and CD40 in CD8 α ⁺ DCs (45). STING activation in DCs enables antigen presentation by major histocompatibility complex class I (MHC I) necessary for T cell activation (Fig 3) (43, 46).

It is unclear how DCs uptake tumor-derived DNA, but increased genomic instability through DSB damage may increase fragmented DNA for uptake by DCs. Chromosomal instability aids in the production of cytosolic dsDNA and facilitates metastasis in a cGAS-STING dependent manner (47). DSB-inducing agents like etoposide and DSB repair deficiency (BRCA- and ATM-deficient tumor cell lines) reportedly increase activation of type I signaling responses in a STING-dependent manner (48-50). Additionally, activation of the STING pathway in DCs is essential for irradiation-induced anti-tumor effects. In DCs, STING is important for IFN-induction following radiation (51). Recently, DSB-induced micronuclei have also been reported to stimulate cGAS-mediated STING activation during mitotic progression (52, 53). cGAS binds to γ -H2AX-positive micronuclei formed by rupture of the nuclear membrane following irradiation (53).

Although cytoplasmic cGAS has been well-characterized to have a role in DNA sensing in immune and tumor cells, a recent study shows that nuclear cGAS promotes tumor growth in vivo (54). Nuclear cGAS localizes at sites of DSBs after DNA damage, co-localizes with γ -H2AX, and interacts with poly ADP-ribose polymerase (PARP). cGAS interaction with PARP inhibits HR through downregulation of RAD51 and RPA2 (54). cGAS-STING pathway activation also has a supporting role in tumor growth and

metastasis (47, 55, 56). Hence, it is important to cautiously optimize treatment conditions to target the tumor while activating the innate immune response.

Apart from cGAS, several other DSB repair proteins also are described as DNA sensors. Cytoplasmic DNA-PK and MRE11 act as sensors and activate type I IFNs in fibroblasts and in bone marrow-derived DCs, respectively (57, 58). Ku70 functions as a cytosolic DNA sensor but activates type III IFN through IRF-1 and IRF-7 (59). In DCs, RAD50 interacts with the innate immune adapter CARD9. The introduction of viral DNA or dsDNA leads to the formation of a RAD50, CARD9, and dsDNA complex that induces NF- κ B signaling for IL-1 β production (60). These studies indicate that DNA damage repair proteins are not limited to preserving DNA integrity in the nuclear compartment, but also have important cytoplasmic functions that intersect with innate immune cell responses.

Inflammatory microenvironment and DSB repair

Inflammation plays a major role in protecting against invading pathogens and in the tissue repair process; however, prolonged inflammation can have an adverse effect if left unchecked. The persistence of chronic inflammation in the tumor microenvironment promotes tumor growth through the recruitment of macrophages and unregulated tissue repair (Fig 3) (61). Macrophages in the tumor microenvironment release pro-inflammatory cytokines and aid in genomic instability through the production of ROS and reactive nitrogen species (RNS) (62). ROS generation in itself does not lead to DSBs, but ROS-induced DNA damage can create DSBs (63). ROS-induced DNA damage in transcriptionally active sites creates DNA-RNA hybrids called R-loops and

needs transcription-coupled HR to resolve them (63, 64). Additionally, RNS and superoxide have been found to induce HR at a chromosomally integrated direct repeat in mammalian cells (65). Interestingly, RNS-induced DSBs mediate innate immune function in macrophages (66). ROS AND RNS activate ATM and DNA-PKcs by inducing DSB, which consequently promote inflammasome activation in macrophages and immune response by NK cells (66). Initiation of the DNA damage response in the activated macrophages requires type I IFN signaling culminating in the production of IL-1 β and IL-18 (66). In addition to activated macrophages, physiological DSBs such as VDJ recombination in developing lymphocytes serve an important function with respect to maturation, migration, and homing of immune cells (67).

The NF- κ B transcription factor, the master regulator of inflammation, promotes HR through interaction with CtIP-BRCA1 complexes resulting in BRCA1 stabilization (68). DSBs can lead to ATM-mediated NF- κ B activation (69). ATM-mediated signaling can potentially activate NF- κ B-mediated cytokine expression (IL-6, IL-8, etc.) and modulate functions of immune cells (70). Several cytokines like transforming growth factor beta (TGF- β), interleukin-6 (IL-6), and tumor necrosis factor (TNF) also activate ATM kinase (reviewed in (71)). In fact, TGF- β offers protective effects on cellular survival against γ -radiation-induced DSBs through eliciting NHEJ repair (72).

Additionally, increased γ -H2AX has been observed in various stages of lung cancer development during multistep progression in an inflammation-mediated rat lung cancer model (73). Similarly, mice that were exposed to cerulein, an inducer of pancreatic inflammation, demonstrated increased cell proliferation and elevated γ -H2AX levels. An increase in HR DSB repair was observed in inflammation-induced DNA

damage (74). These findings suggest that inflammation promotes genomic instability synergistically with replication stress-induced DNA damage.

DSB and immune checkpoint regulation

Recent studies have found that DSBs in cancer cells induce immune receptor ligand expression that can stimulate innate immune cells. Natural killer group 2D (NKG2D) receptor recognizes ligands on cancerous and infected cells (75). Expression of the NKG2D ligand makes tumor cells susceptible to surveillance by immune cells. NKG2D ligands can activate NK cells, CD8⁺ T cells, and $\gamma\delta$ T cells and are rarely expressed in normal cells. NKG2D is induced when cells undergo viral infection, replicative and genotoxic stress, or malignant transformation (76). Genotoxic agents stimulate NKG2D ligand expression on mice and human tumor cell lines (77). Another activating receptor involved in NK-cell-mediated tumor cell killing is DNAX accessory molecule-1 (DNAM-1), expressed on the majority of T cells, NK cells, and macrophages following DNA damage. Both NKG2D and DNAM-1 ligands are also expressed on multiple myeloma cells in an ATM/ATR-dependent manner under conditions of genotoxic stress (77, 78). Pharmacological inhibition of ATM, ATR, or CHK1 reduced NKG2D ligand expression on myeloma cells (78). Taken together, this evidence suggests that DSBs in cancer cells enhance expression of NKG2D ligand that serves to stimulate the innate immune response.

Furthermore, genotoxic stress like ionizing radiation increases programmed death-ligand (PD-L1) expression on tumor cells. Elevated PD-L1 expression in tumor cells corresponds with better responses to anti-PD-1 and anti-CTLA-4 therapy through

immune system activation (79). This is supported by IHC staining in lung squamous cell carcinoma that shows a positive correlation between γ -H2AX and PD-L1 expression (80), indicating a possible link between DSBs and PD-L1 expression. Combining ionizing radiation with anti-CTLA4 therapy improved survival in patients with metastatic melanoma (79). Blockade of the PD-1/PD-L1 interaction using anti-PD-1 rescued T cell activity and delayed tumor growth in mice (79). Sato et al. have recently reported a novel link between DSBs and upregulation of PD-L1 expression in cancer cells. DSBs upregulate PD-L1 expression in an ATM/ATR/CHK1-dependent manner and engage activation of STAT1/STAT3, leading to IRF1 mediated upregulation of PD-L1 (81). Similarly, BRCA1/2-mutated high grade serous ovarian cancer was associated with higher association with neoantigen loads, increased CD3+ and CD8+ tumor-infiltrating lymphocytes, and PD-L1 expression (82). Also, metastatic melanoma patients harboring BRCA2 mutations showed higher genomic mutational loads than those with wild type BRCA2-wildtype. Patients with loss-of-function BRCA2 mutations showed improved survival in response to anti-PD-1 therapy (83). Overall, the use of immune checkpoint inhibitors in combination with agents that impair DSB repair may present an effective approach to treat cancers that have failed anti-PD-1 monotherapy.

Cellular metabolites and DSB repair pathway

Although not directly microenvironment-derived, cellular adaptation to the microenvironment leads to the production of distinct metabolites in tumor cells. Emerging studies show that such metabolites play a critical role in DNA repair (84). Hypoxia and mutant isocitrate dehydrogenase (IDH) can lead to the production of the oncometabolite 2-hydroxyglutarate (2-HG) (85). Sulkowski et al. reported that IDH1/2-

mutant cells are deficient in HR due to 2-HG-mediated inhibition of α -ketoglutarate-dependent dioxygenases (85). ATP-citrate lyase (ACLY), which regulates the availability of acetyl-CoA, increases nuclear acetyl-CoA localization and subsequently histone acetylation to favor HR. Histone acetylation at DSB sites promote BRCA1 recruitment and inhibits 53BP1 recruitment, thus, promoting HR-mediated DNA repair (86, 87). Interestingly, irradiation-mediated DNA damage activates DNA-PK-dependent phosphorylation of chromatin-associated fumarase, further enhancing fumarate production and DNA-PK complex at sites of DSB, resulting in increased NHEJ repair (88). Similarly following irradiation, N-acetyl-glucosamine and O-GlcNAcylation promotes histone methylation by enhancer of zeste homolog 2 (EZH2) (89). This post-translational modification by EZH2 enhances H3K27 trimethylation, an important determinant in NHEJ repair (89, 90). Pyruvate kinase M2, a master regulator of metabolic reprogramming, also promotes HR through phosphorylation of CtIP in glioblastoma (91). Irradiation induces CtIP phosphorylation and nuclear localization in an ATM-dependent manner (91). Currently, the field of cellular metabolism and how it affects cellular DNA repair is expanding. Understanding the interplay between microenvironment-induced metabolites and DNA repair defects would provide an important context for improving treatment efficacy.

Crosstalk between tumor microenvironment and SSB

Apart from the DSB repair pathway, SSB repair pathways are also impacted by the tumor microenvironment. We will briefly summarize the topic, although several reviews highlight the impact of the tumor microenvironment on SSB. Hypoxia has a

long-term effect on MMR through downregulating both mRNA and protein levels of MLH1 and MSH2 (reviewed in (31)). NER capacity is decreased in chronic hypoxia; however, the inhibitory effect of hypoxia on NER is not conclusive (31). During inflammation, oxidative stress impairs MMR by downregulating the expression of MutS homolog 6 (MSH6) (92). Additionally, in conditions of chronic inflammation, ROS can downregulate BER by activating the inflammasome (64). Colorectal cancer patients with MMR deficiency show greater infiltration of T cells and higher microsatellite instability indicating a robust crosstalk between MMR and immune cells (93). In fact, tumor with high microsatellite instability is a strong indicator of responsiveness to anti-PD1/PD-L1 immunotherapy (94)

Targeting DSB repair pathways in cancer

PARP is an ADP-ribosylating enzyme that is involved in BER and alternative NHEJ (95). Inhibition of PARP increases DSBs, which are normally repaired by HR. In BRCA-mutant cancers, PARP inhibitors (Table 1) lead to increased apoptosis due to synthetic lethality (95). Phase 3 clinical trials of PARP inhibitor monotherapy with olaparib or talazoparib, showed an improved progression-free survival compared to standard chemotherapy in germline BRCA-mutated and HER2-negative advanced breast cancer patients (96, 97). Based on these results, olaparib and talazoparib are now FDA-approved for the treatment of advanced germline BRCA-mutated breast cancer. Similarly, olaparib, rucaparib, and niraparib are currently FDA-approved for the treatment of advanced BRCA-mutated and platinum-sensitive ovarian cancer (95, 98, 99). The benefit of PARP inhibitors as monotherapy in BRCA1/2 mutant prostate cancer

is currently being investigated in clinical trials (100). As yet, there is no reliable indicator to determine the benefit of PARP inhibition beyond BRCA mutations, but other DNA repair defects remain an active area of investigation (100, 101). However, combination therapy is likely to yield a better response (102).

Several clinical trials are currently assessing the use of DSB repair protein inhibitors in combination with immunotherapy, DNA damaging agents, topoisomerase inhibitors, and chemotherapy (Table 2). Clinical strategies to target ATM, ATR, and CHK in combination with PARP inhibitors are in clinical trials (NCT02588105, NCT03022409, and NCT03057145). Also, the efficacy of DNA-PKcs inhibitors in combination with radiotherapy is being tested in the clinic (NCT02516813). PARP inhibitors in combination with PD-1 inhibitors (NCT03522246), and topoisomerase inhibitors (NCT00588991) are also in trials. ATR inhibitors are also being tested in combination with PD-1 inhibitors and chemotherapy (NCT02264678).

Dinaciclib targets cyclin-dependent kinases upstream of HR and blocks phosphorylation of BRCA1 and EXO1. This activity of dinaciclib is the likely reason that it sensitizes tumor cells to the PARP inhibitor veliparib in a preclinical model of multiple myeloma (103). The efficacy of using dinaciclib with veliparib is currently being tested in the clinic in advanced cancers (NCT01434316). Similarly, preclinical studies showed that hypoxia compromises HR by downregulating BRCA and RAD51 (36, 37). A phase 1/2 trial of cediranib, a pan-vascular endothelial growth factor (VEGF) 1-3 inhibitor regulated by HIF-1 α , in combination with olaparib in patients with platinum-sensitive ovarian cancer, has already shown improved progression-free survival compared to olaparib alone (99, 104). Cediranib is also currently in a clinical study in combination

with olaparib in prostate cancer (NCT02893917). In addition to the FDA-approved drugs, small molecule inhibitors of CHK1/2, WEE1, ATM, ATR, and DNA-PKcs have shown promising results in preclinical studies (reviewed in (105)). Overall, preclinical evidence suggests that immune checkpoint inhibition synergizes with PARP inhibitor treatment in HR-deficient tumors; clinical trials investigating this hypothesis are ongoing.

Conclusions

Genome integrity and maintenance through repair pathways are paramount for normal cellular function. Cancer cells with mutations in one or more of these DNA repair pathways are dependent on the remainder of the functional repair pathways. Current therapies seek to target these functional DNA repair pathways in cancer for synthetic lethality. BRCA mutations are abundant in different cancers; hence, DSB repair pathways may present as viable therapeutic targets. In the clinics, the success of PARP inhibitors for BRCA1/2-mutated ovarian cancer has opened doors for exploring different strategies that combine PARP inhibitors with conventional therapies for durable responses. The role of the tumor microenvironment is an important consideration in developing therapeutics that target DNA repair-deficient cancer cells. Chronic hypoxia, inflammation, and checkpoint activation all play critical roles in facilitating these repair choices. Another developing area of research is exploring the effects of mechanical forces, stroma, and stromal cells in the tumor microenvironment. Tumor cells experience physical stress and are in a constant crosstalk with the stromal cells and stroma; thus, it is essential to identify the nature of DNA damage and repair evoked by these factors. As such, new

insights into the relationship between tumor microenvironment and DNA damage repair present a critical area of investigation to treat cancer effectively.

Acknowledgements

We want to thank Dr. Victor Lin for his helpful comments on the review. We would like to acknowledge funding from the Department of Defense (W81XWH-14-1-0516 and W81XWH-18-1-0036), NCI R01CA169202, The Breast Cancer Research Foundation of Alabama (BCRFA), support from UAB Comprehensive Cancer Center P30CA013148 grant, and AMC21 funds to L.A.S. The authors declare no conflict of interest.

References

1. Ciccia A, Elledge SJ. The DNA damage response: making it safe to play with knives. *Molecular cell*. 2010;40:179-204.
2. Lee JK, Choi YL, Kwon M, Park PJ. Mechanisms and Consequences of Cancer Genome Instability: Lessons from Genome Sequencing Studies. *Annual review of pathology*. 2016;11:283-312.
3. Thoms KM, Kuschal C, Emmert S. Lessons learned from DNA repair defective syndromes. *Experimental dermatology*. 2007;16:532-44.
4. Choi M, Kipps T, Kurzrock R. ATM Mutations in Cancer: Therapeutic Implications. *Molecular cancer therapeutics*. 2016;15:1781-91.
5. Walsh CS. Two decades beyond BRCA1/2: Homologous recombination, hereditary cancer risk and a target for ovarian cancer therapy. *Gynecologic oncology*. 2015;137:343-50.
6. Abbotts R, Wilson DM, 3rd. Coordination of DNA single strand break repair. *Free radical biology & medicine*. 2017;107:228-44.
7. Beard WA, Horton JK, Prasad R, Wilson SH. Eukaryotic Base Excision Repair: New Approaches Shine Light on Mechanism. *Annual review of biochemistry*. 2019;88:137-62.
8. Kunkel TA, Erie DA. Eukaryotic Mismatch Repair in Relation to DNA Replication. *Annual review of genetics*. 2015;49:291-313.
9. Syed A, Tainer JA. The MRE11-RAD50-NBS1 Complex Conducts the Orchestration of Damage Signaling and Outcomes to Stress in DNA Replication and Repair. *Annual review of biochemistry*. 2018;87:263-94.
10. Georgoulis A, Vorgias CE, Chrousos GP, Rogakou EP. Genome Instability and γ H2AX. *International journal of molecular sciences*. 2017;18.
11. Bakkenist CJ, Kastan MB. DNA damage activates ATM through intermolecular autophosphorylation and dimer dissociation. *Nature*. 2003;421:499.
12. Awasthi P, Foiani M, Kumar A. ATM and ATR signaling at a glance. *Journal of cell science*. 2016;129:1285.
13. Wright WD, Shah SS, Heyer WD. Homologous recombination and the repair of DNA double-strand breaks. *The Journal of biological chemistry*. 2018;293:10524-35.

14. Saha J, Davis AJ. Unsolved mystery: the role of BRCA1 in DNA end-joining. *Journal of radiation research*. 2016;57 Suppl 1:i18-i24.
15. Chapman JR, Barral P, Vannier JB, Borel V, Steger M, Tomas-Loba A, et al. RIF1 is essential for 53BP1-dependent nonhomologous end joining and suppression of DNA double-strand break resection. *Molecular cell*. 2013;49:858-71.
16. Escribano-Diaz C, Orthwein A, Fradet-Turcotte A, Xing M, Young JT, Tkac J, et al. A cell cycle-dependent regulatory circuit composed of 53BP1-RIF1 and BRCA1-CtIP controls DNA repair pathway choice. *Molecular cell*. 2013;49:872-83.
17. Sartori AA, Lukas C, Coates J, Mistrik M, Fu S, Bartek J, et al. Human CtIP promotes DNA end resection. *Nature*. 2007;450:509-14.
18. Chang HHY, Pannunzio NR, Adachi N, Lieber MR. Non-homologous DNA end joining and alternative pathways to double-strand break repair. *Nature reviews Molecular cell biology*. 2017;18:495-506.
19. Liu M, Hu W. Functional role of ATM in the cellular response to DNA damage. *Frontiers of Chemical Science and Engineering*. 2011;5:179-87.
20. Kakarougkas A, Jeggo PA. DNA DSB repair pathway choice: an orchestrated handover mechanism. *The British journal of radiology*. 2014;87:20130685.
21. Boulton SJ, Jackson SP. *Saccharomyces cerevisiae* Ku70 potentiates illegitimate DNA double-strand break repair and serves as a barrier to error-prone DNA repair pathways. *The EMBO journal*. 1996;15:5093-103.
22. Seol JH, Shim EY, Lee SE. Microhomology-mediated end joining: Good, bad and ugly. *Mutation research*. 2018;809:81-7.
23. Schaefer MH, Serrano L. Cell type-specific properties and environment shape tissue specificity of cancer genes. *Scientific reports*. 2016;6:20707.
24. Semenza GL. Hypoxia-inducible factor 1: master regulator of O₂ homeostasis. *Current opinion in genetics & development*. 1998;8:588-94.
25. Dhani N, Fyles A, Hedley D, Milosevic M. The clinical significance of hypoxia in human cancers. *Seminars in nuclear medicine*. 2015;45:110-21.
26. Benita Y, Kikuchi H, Smith AD, Zhang MQ, Chung DC, Xavier RJ. An integrative genomics approach identifies Hypoxia Inducible Factor-1 (HIF-1)-target genes that form the core response to hypoxia. *Nucleic acids research*. 2009;37:4587-602.
27. Jaakkola P, Mole DR, Tian YM, Wilson MI, Gielbert J, Gaskell SJ, et al. Targeting of HIF- α to the von Hippel-Lindau ubiquitylation complex by O₂-regulated prolyl hydroxylation. *Science (New York, NY)*. 2001;292:468-72.

28. Graham K, Unger E. Overcoming tumor hypoxia as a barrier to radiotherapy, chemotherapy and immunotherapy in cancer treatment. *International journal of nanomedicine*. 2018;13:6049-58.
29. Gray LH, Conger AD, Ebert M, Hornsey S, Scott OC. The concentration of oxygen dissolved in tissues at the time of irradiation as a factor in radiotherapy. *The British journal of radiology*. 1953;26:638-48.
30. Overgaard J. Hypoxic radiosensitization: adored and ignored. *Journal of clinical oncology : official journal of the American Society of Clinical Oncology*. 2007;25:4066-74.
31. Scanlon SE, Glazer PM. Multifaceted control of DNA repair pathways by the hypoxic tumor microenvironment. *DNA repair*. 2015;32:180-9.
32. Gibson SL, Bindra RS, Glazer PM. Hypoxia-induced phosphorylation of Chk2 in an ataxia telangiectasia mutated-dependent manner. *Cancer research*. 2005;65:10734-41.
33. Cam H, Easton JB, High A, Houghton PJ. mTORC1 signaling under hypoxic conditions is controlled by ATM-dependent phosphorylation of HIF-1alpha. *Molecular cell*. 2010;40:509-20.
34. Kang HJ, Kim HJ, Rih JK, Mattson TL, Kim KW, Cho CH, et al. BRCA1 plays a role in the hypoxic response by regulating HIF-1alpha stability and by modulating vascular endothelial growth factor expression. *The Journal of biological chemistry*. 2006;281:13047-56.
35. Um JH, Kang CD, Bae JH, Shin GG, Kim DW, Kim DW, et al. Association of DNA-dependent protein kinase with hypoxia inducible factor-1 and its implication in resistance to anticancer drugs in hypoxic tumor cells. *Experimental & Molecular Medicine*. 2004;36:233.
36. Bindra RS, Schaffer PJ, Meng A, Woo J, Maseide K, Roth ME, et al. Down-regulation of Rad51 and decreased homologous recombination in hypoxic cancer cells. *Molecular and cellular biology*. 2004;24:8504-18.
37. Bindra RS, Gibson SL, Meng A, Westermark U, Jasin M, Pierce AJ, et al. Hypoxia-induced down-regulation of BRCA1 expression by E2Fs. *Cancer research*. 2005;65:11597-604.
38. Bindra RS, Schaffer PJ, Meng A, Woo J, Maseide K, Roth ME, et al. Alterations in DNA repair gene expression under hypoxia: elucidating the mechanisms of hypoxia-induced genetic instability. *Annals of the New York Academy of Sciences*. 2005;1059:184-95.

39. Meng AX, Jalali F, Cuddihy A, Chan N, Bindra RS, Glazer PM, et al. Hypoxia down-regulates DNA double strand break repair gene expression in prostate cancer cells. *Radiotherapy and oncology : journal of the European Society for Therapeutic Radiology and Oncology*. 2005;76:168-76.
40. Tsuchimoto T, Sakata K, Someya M, Yamamoto H, Hirayama R, Matsumoto Y, et al. Gene expression associated with DNA-dependent protein kinase activity under normoxia, hypoxia, and reoxygenation. *Journal of radiation research*. 2011;52:464-71.
41. Lara PC, Lloret M, Clavo B, Apolinario RM, Bordon E, Rey A, et al. Hypoxia downregulates Ku70/80 expression in cervical carcinoma tumors. *Radiotherapy and oncology : journal of the European Society for Therapeutic Radiology and Oncology*. 2008;89:222-6.
42. Bouquet F, Ousset M, Biard D, Fallone F, Dauvillier S, Frit P, et al. A DNA-dependent stress response involving DNA-PK occurs in hypoxic cells and contributes to cellular adaptation to hypoxia. *Journal of cell science*. 2011;124:1943-51.
43. Chen Q, Sun L, Chen ZJ. Regulation and function of the cGAS-STING pathway of cytosolic DNA sensing. *Nature immunology*. 2016;17:1142-9.
44. Ishikawa H, Barber GN. STING is an endoplasmic reticulum adaptor that facilitates innate immune signalling. *Nature*. 2008;455:674-8.
45. Woo SR, Fuertes MB, Corrales L, Spranger S, Furdyna MJ, Leung MY, et al. STING-dependent cytosolic DNA sensing mediates innate immune recognition of immunogenic tumors. *Immunity*. 2014;41:830-42.
46. Yoneyama M, Suhara W, Fukuhara Y, Fukuda M, Nishida E, Fujita T. Direct triggering of the type I interferon system by virus infection: activation of a transcription factor complex containing IRF-3 and CBP/p300. *The EMBO journal*. 1998;17:1087-95.
47. Bakhom SF, Ngo B, Laughney AM, Cavallo JA, Murphy CJ, Ly P, et al. Chromosomal instability drives metastasis through a cytosolic DNA response. *Nature*. 2018;553:467-72.
48. Brzostek-Racine S, Gordon C, Van Scoy S, Reich NC. The DNA damage response induces IFN. *Journal of immunology (Baltimore, Md : 1950)*. 2011;187:5336-45.
49. Hartlova A, Erttmann SF, Raffi FA, Schmalz AM, Resch U, Anugula S, et al. DNA damage primes the type I interferon system via the cytosolic DNA sensor STING to promote anti-microbial innate immunity. *Immunity*. 2015;42:332-43.
50. Parkes EE, Walker SM, Taggart LE, McCabe N, Knight LA, Wilkinson R, et al. Activation of STING-Dependent Innate Immune Signaling By S-Phase-Specific DNA Damage in Breast Cancer. *Journal of the National Cancer Institute*. 2017;109.

51. Deng L, Liang H, Xu M, Yang X, Burnette B, Arina A, et al. STING-Dependent Cytosolic DNA Sensing Promotes Radiation-Induced Type I Interferon-Dependent Antitumor Immunity in Immunogenic Tumors. *Immunity*. 2014;41:843-52.
52. Harding SM, Benci JL, Irianto J, Discher DE, Minn AJ, Greenberg RA. Mitotic progression following DNA damage enables pattern recognition within micronuclei. *Nature*. 2017;548:466-70.
53. Mackenzie KJ, Carroll P, Martin CA, Murina O, Fluteau A, Simpson DJ, et al. cGAS surveillance of micronuclei links genome instability to innate immunity. *Nature*. 2017;548:461-5.
54. Liu H, Zhang H, Wu X, Ma D, Wu J, Wang L, et al. Nuclear cGAS suppresses DNA repair and promotes tumorigenesis. *Nature*. 2018;563:131-6.
55. Lemos H, Mohamed E, Huang L, Ou R, Pacholczyk G, Arbab AS, et al. STING Promotes the Growth of Tumors Characterized by Low Antigenicity via IDO Activation. *Cancer research*. 2016;76:2076-81.
56. Chen Q, Boire A, Jin X, Valiente M, Er EE, Lopez-Soto A, et al. Carcinoma-astrocyte gap junctions promote brain metastasis by cGAMP transfer. *Nature*. 2016;533:493-8.
57. Karpova AY, Trost M, Murray JM, Cantley LC, Howley PM. Interferon regulatory factor-3 is an in vivo target of DNA-PK. *Proceedings of the National Academy of Sciences of the United States of America*. 2002;99:2818-23.
58. Kondo T, Kobayashi J, Saitoh T, Maruyama K, Ishii KJ, Barber GN, et al. DNA damage sensor MRE11 recognizes cytosolic double-stranded DNA and induces type I interferon by regulating STING trafficking. *Proceedings of the National Academy of Sciences of the United States of America*. 2013;110:2969-74.
59. Zhang X, Brann TW, Zhou M, Yang J, Oguariri RM, Lidie KB, et al. Cutting edge: Ku70 is a novel cytosolic DNA sensor that induces type III rather than type I IFN. *Journal of immunology (Baltimore, Md : 1950)*. 2011;186:4541-5.
60. Roth S, Rottach A, Lotz-Havla AS, Laux V, Muschaweckh A, Gersting SW, et al. Rad50-CARD9 interactions link cytosolic DNA sensing to IL-1beta production. *Nature immunology*. 2014;15:538-45.
61. Hamidzadeh K, Christensen SM, Dalby E, Chandrasekaran P, Mosser DM. Macrophages and the Recovery from Acute and Chronic Inflammation. *Annual Review of Physiology*. 2017;79:567-92.

62. Tan HY, Wang N, Li S, Hong M, Wang X, Feng Y. The Reactive Oxygen Species in Macrophage Polarization: Reflecting Its Dual Role in Progression and Treatment of Human Diseases. *Oxidative medicine and cellular longevity*. 2016;2016:2795090.
63. Teng Y, Yadav T, Duan M, Tan J, Xiang Y, Gao B, et al. ROS-induced R loops trigger a transcription-coupled but BRCA1/2-independent homologous recombination pathway through CSB. *Nature communications*. 2018;9:4115.
64. Srinivas US, Tan BWQ, Vellayappan BA, Jeyasekharan AD. ROS and the DNA damage response in cancer. *Redox biology*. 2018:101084.
65. Kiziltepe T, Yan A, Dong M, Jonnalagadda VS, Dedon PC, Engelward BP. Delineation of the chemical pathways underlying nitric oxide-induced homologous recombination in mammalian cells. *Chemistry & biology*. 2005;12:357-69.
66. Morales AJ, Carrero JA, Hung PJ, Tubbs AT, Andrews JM, Edelson BT, et al. A type I IFN-dependent DNA damage response regulates the genetic program and inflammasome activation in macrophages. *eLife*. 2017;6.
67. Bredemeyer AL, Helmink BA, Innes CL, Calderon B, McGinnis LM, Mahowald GK, et al. DNA double-strand breaks activate a multi-functional genetic program in developing lymphocytes. *Nature*. 2008;456:819-23.
68. Volcic M, Karl S, Baumann B, Salles D, Daniel P, Fulda S, et al. NF-kappaB regulates DNA double-strand break repair in conjunction with BRCA1-CtIP complexes. *Nucleic acids research*. 2012;40:181-95.
69. Wu ZH, Shi Y, Tibbetts RS, Miyamoto S. Molecular linkage between the kinase ATM and NF-kappaB signaling in response to genotoxic stimuli. *Science (New York, NY)*. 2006;311:1141-6.
70. Liu T, Zhang L, Joo D, Sun SC. NF-κB signaling in inflammation. *Signal transduction and targeted therapy*. 2017;2.
71. Centurione L, Aiello FB. DNA Repair and Cytokines: TGF-beta, IL-6, and Thrombopoietin as Different Biomarkers of Radioresistance. *Front Oncol*. 2016;6:175.
72. Kim MR, Lee J, An YS, Jin YB, Park IC, Chung E, et al. TGFbeta1 protects cells from gamma-IR by enhancing the activity of the NHEJ repair pathway. *Molecular cancer research : MCR*. 2015;13:319-29.
73. Blanco D, Vicent S, Fraga MF, Fernandez-Garcia I, Freire J, Lujambio A, et al. Molecular analysis of a multistep lung cancer model induced by chronic inflammation reveals epigenetic regulation of p16 and activation of the DNA damage response pathway. *Neoplasia (New York, NY)*. 2007;9:840-52.

74. Kiraly O, Gong G, Olipitz W, Muthupalani S, Engelward BP. Inflammation-induced cell proliferation potentiates DNA damage-induced mutations in vivo. *PLoS genetics*. 2015;11:e1004901.
75. Duan S, Guo W, Xu Z, He Y, Liang C, Mo Y, et al. Natural killer group 2D receptor and its ligands in cancer immune escape. *Molecular cancer*. 2019;18:29.
76. Cerboni C, Fionda C, Soriani A, Zingoni A, Doria M, Cippitelli M, et al. The DNA Damage Response: A Common Pathway in the Regulation of NKG2D and DNAM-1 Ligand Expression in Normal, Infected, and Cancer Cells. *Frontiers in immunology*. 2014;4:508.
77. Gasser S, Orsulic S, Brown EJ, Raulet DH. The DNA damage pathway regulates innate immune system ligands of the NKG2D receptor. *Nature*. 2005;436:1186-90.
78. Soriani A, Zingoni A, Cerboni C, Iannitto ML, Ricciardi MR, Di Gialleonardo V, et al. ATM-ATR-dependent up-regulation of DNAM-1 and NKG2D ligands on multiple myeloma cells by therapeutic agents results in enhanced NK-cell susceptibility and is associated with a senescent phenotype. *Blood*. 2009;113:3503-11.
79. Twyman-Saint Victor C, Rech AJ, Maity A, Rengan R, Pauken KE, Stelekati E, et al. Radiation and dual checkpoint blockade activate non-redundant immune mechanisms in cancer. *Nature*. 2015;520:373-7.
80. Osoegawa A, Hiraishi H, Hashimoto T, Takumi Y, Abe M, Takeuchi H, et al. The Positive Relationship Between gammaH2AX and PD-L1 Expression in Lung Squamous Cell Carcinoma. *In vivo (Athens, Greece)*. 2018;32:171-7.
81. Sato H, Niimi A, Yasuhara T, Permata TBM, Hagiwara Y, Isono M, et al. DNA double-strand break repair pathway regulates PD-L1 expression in cancer cells. *Nature communications*. 2017;8:1751.
82. Strickland KC, Howitt BE, Shukla SA, Rodig S, Ritterhouse LL, Liu JF, et al. Association and prognostic significance of BRCA1/2-mutation status with neoantigen load, number of tumor-infiltrating lymphocytes and expression of PD-1/PD-L1 in high grade serous ovarian cancer. *Oncotarget*. 2016;7:13587-98.
83. Hugo W, Zaretsky JM, Sun L, Song C, Moreno BH, Hu-Lieskovan S, et al. Genomic and Transcriptomic Features of Response to Anti-PD-1 Therapy in Metastatic Melanoma. *Cell*. 2017;168:542.
84. Turgeon M-O, Perry NJS, Pouligiannis G. DNA Damage, Repair, and Cancer Metabolism. *Frontiers in Oncology*. 2018;8.
85. Sulkowski PL, Corso CD, Robinson ND, Scanlon SE, Purshouse KR, Bai H, et al. 2-Hydroxyglutarate produced by neomorphic IDH mutations suppresses homologous

recombination and induces PARP inhibitor sensitivity. *Science Translational Medicine*. 2017;9:eaal2463.

86. Sivanand S, Rhoades S, Jiang Q, Lee JV, Benci J, Zhang J, et al. Nuclear Acetyl-CoA Production by ACLY Promotes Homologous Recombination. *Molecular cell*. 2017;67:252-65.e6.

87. Wellen KE, Hatzivassiliou G, Sachdeva UM, Bui TV, Cross JR, Thompson CB. ATP-citrate lyase links cellular metabolism to histone acetylation. *Science (New York, NY)*. 2009;324:1076-80.

88. Jiang Y, Qian X, Shen J, Wang Y, Li X, Liu R, et al. Local generation of fumarate promotes DNA repair through inhibition of histone H3 demethylation. *Nature cell biology*. 2015;17:1158-68.

89. Efimova EV, Takahashi S, Shamsi NA, Wu D, Labay E, Ulanovskaya OA, et al. Linking Cancer Metabolism to DNA Repair and Accelerated Senescence. *Molecular cancer research : MCR*. 2016;14:173-84.

90. Zhang Y, Chang JF, Sun J, Chen L, Yang XM, Tang HY, et al. Histone H3K27 methylation modulates the dynamics of FANCD2 on chromatin to facilitate NHEJ and genome stability. *Journal of cell science*. 2018;131.

91. Sizemore ST, Zhang M, Cho JH, Sizemore GM, Hurwitz B, Kaur B, et al. Pyruvate kinase M2 regulates homologous recombination-mediated DNA double-strand break repair. *Cell research*. 2018;28:1090-102.

92. Chang CL, Marra G, Chauhan DP, Ha HT, Chang DK, Ricciardiello L, et al. Oxidative stress inactivates the human DNA mismatch repair system. *American journal of physiology Cell physiology*. 2002;283:C148-54.

93. Kelderman S, Schumacher TN, Kvistborg P. Mismatch Repair-Deficient Cancers Are Targets for Anti-PD-1 Therapy. *Cancer cell*. 2015;28:11-3.

94. Zhao P, Li L, Jiang X, Li Q. Mismatch repair deficiency/microsatellite instability-high as a predictor for anti-PD-1/PD-L1 immunotherapy efficacy. *Journal of hematology & oncology*. 2019;12:54.

95. Murata S, Zhang C, Finch N, Zhang K, Campo L, Breuer EK. Predictors and Modulators of Synthetic Lethality: An Update on PARP Inhibitors and Personalized Medicine. *BioMed research international*. 2016;2016:2346585.

96. Robson M, Im SA, Senkus E, Xu B, Domchek SM, Masuda N, et al. Olaparib for Metastatic Breast Cancer in Patients with a Germline BRCA Mutation. *The New England journal of medicine*. 2017;377:523-33.

97. Litton JK, Rugo HS, Ettl J, Hurvitz SA, Goncalves A, Lee KH, et al. Talazoparib in Patients with Advanced Breast Cancer and a Germline BRCA Mutation. *The New England journal of medicine*. 2018;379:753-63.
98. Bixel K, Hays JL. Olaparib in the management of ovarian cancer. *Pharmacogenomics and personalized medicine*. 2015;8:127-35.
99. Liu JF, Barry WT, Birrer M, Lee JM, Buckanovich RJ, Fleming GF, et al. Combination cediranib and olaparib versus olaparib alone for women with recurrent platinum-sensitive ovarian cancer: a randomised phase 2 study. *The Lancet Oncology*. 2014;15:1207-14.
100. Mateo J, Carreira S, Sandhu S, Miranda S, Mossop H, Perez-Lopez R, et al. DNA-Repair Defects and Olaparib in Metastatic Prostate Cancer. *The New England journal of medicine*. 2015;373:1697-708.
101. Mateo J, Porta N, McGovern UB, Elliott T, Jones RJ, Syndikus I, et al. TOPARP-B: A phase II randomized trial of the poly(ADP)-ribose polymerase (PARP) inhibitor olaparib for metastatic castration resistant prostate cancers (mCRPC) with DNA damage repair (DDR) alterations. *Journal of Clinical Oncology*. 2019;37:5005-.
102. Li A, Yi M, Qin S, Chu Q, Luo S, Wu K. Prospects for combining immune checkpoint blockade with PARP inhibition. *Journal of hematology & oncology*. 2019;12:98.
103. Alagpulinsa DA, Ayyadevara S, Yaccoby S, Shmookler Reis RJ. A Cyclin-Dependent Kinase Inhibitor, Dinaciclib, Impairs Homologous Recombination and Sensitizes Multiple Myeloma Cells to PARP Inhibition. *Molecular cancer therapeutics*. 2016;15:241-50.
104. Kaufman B, Shapira-Frommer R, Schmutzler RK, Audeh MW, Friedlander M, Balmana J, et al. Olaparib monotherapy in patients with advanced cancer and a germline BRCA1/2 mutation. *Journal of clinical oncology : official journal of the American Society of Clinical Oncology*. 2015;33:244-50.
105. Ronco C, Martin AR, Demange L, Benhida R. ATM, ATR, CHK1, CHK2 and WEE1 inhibitors in cancer and cancer stem cells. *MedChemComm*. 2017;8:295-319.

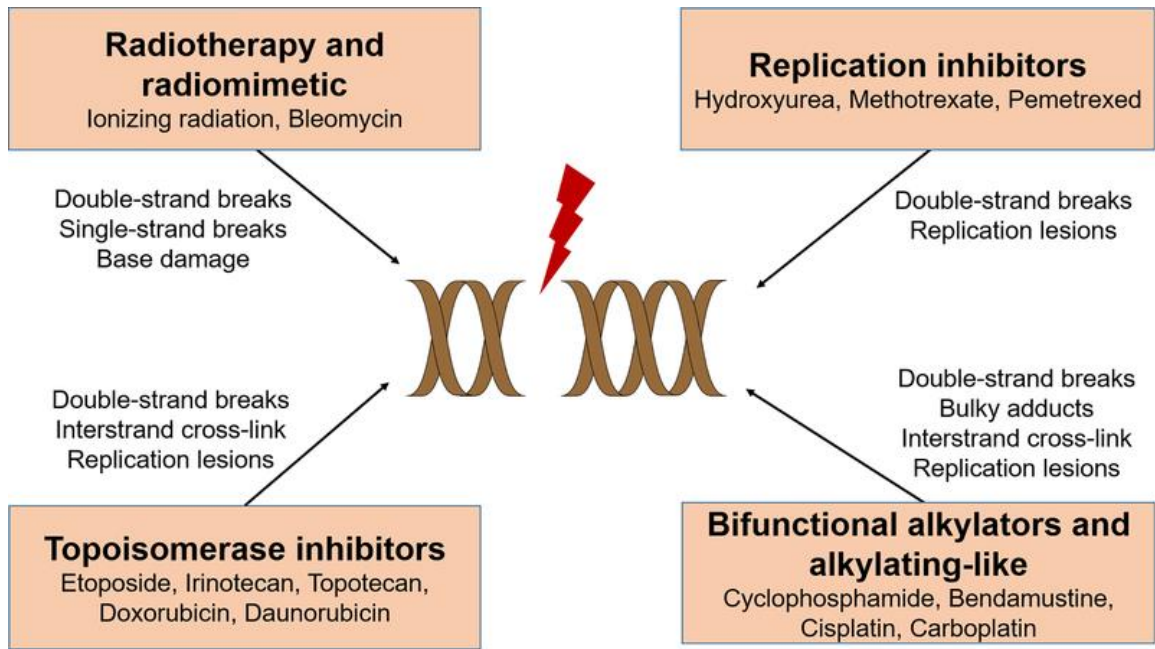


Figure 1. DSBs-inducing agents used for the treatment of cancer.

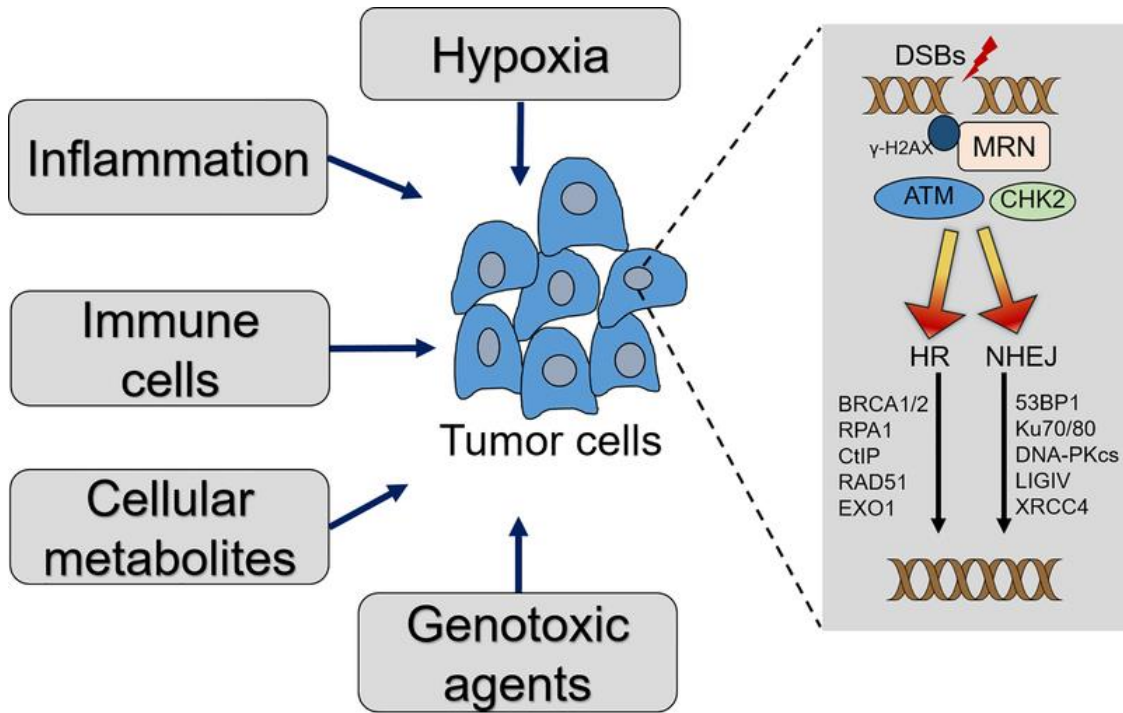


Figure 2. Cellular DSBs are repaired mainly through HR and NHEJ; both mechanisms involve distinct repair proteins. Tumor microenvironment factors like hypoxia, inflammation, immune cells, genotoxic stress, and cellular metabolites influence the DSB repair in the cell.

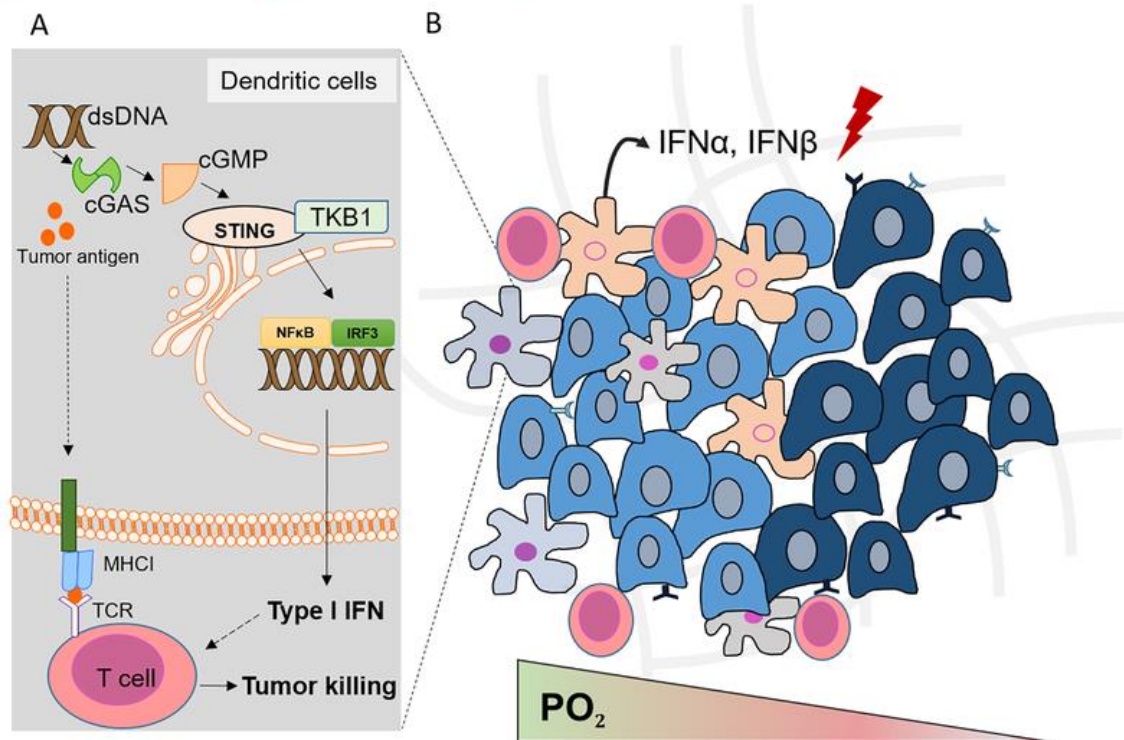
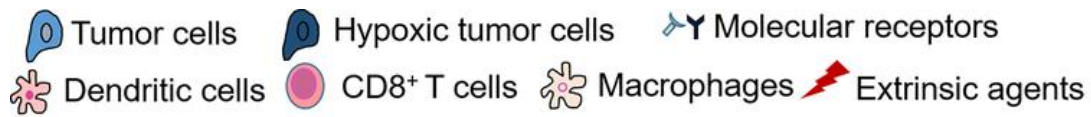


Figure 3. The solid tumor microenvironment comprising hypoxia, inflammation, and immune cells impact DSB repair pathways in cancer cells. The diagrams were drawn using motifolio drawing toolkits (www.motifolio.com). **A.** In DCs, the presence of dsDNA activates the cGAS-STING pathway and leads to activation of IRF-3 and NF-kB enhancing the pro-inflammatory immune response. **B.** DSB-mediated expression of cellular cytokines, chemokines, and crosstalk between stromal cells in the solid tumor microenvironment serves important function in immune cell homing and migration.

DSB Repair Proteins	DSB Repair Pathway	Inhibitors	References
PARP	Alt-NHEJ	Olaparib, Niraparib, Ruvaparib, Veliparib (ABT-888), Talazoparib (BMN-673)	PMID: 28003236
ATM	Signaling (Kinase targets: CHK2, H2AX, NFkB, AKT, p53, IGF-1R)	KU5593, KU60019, CP466722, AZ32, AZD8055, NU7026, VE-821	PMID: 31299316, 22079189
CHK2	Effectors	Prexasertib (LY2606368), Chk2 Inhibitor II (BML-277)	PMID: 27308506
MRE11	Damage Sensors, Resection	Mirin	PMID: 29523233
DNA-PKcs	NHEJ (Kinase targets: CHK2, H2AX, p53, Artemis, Ligase IV)	NU7441 (KU-57788), NU7026, LTURM34, CC-115	PMID: 28820390
Rad51	HR	RI-1, RS-1, B02	PMID: 24856061
Ligase IV	NHEJ	SCR7	PMID: 23260137

Table 1. Different DSB repair pathway proteins and their associated inhibitors.

NCT Number	Conditions	Interventions	Target	Phases	Enrollment
NCT03522246	Epithelial Ovarian Cancer	Rucaparib, Nivolumab	PARP, anti-PD-1	III	1012
NCT03602859	Ovarian Cancer	Niraparib, TSR-042	PARP, anti-PD-1	III	912
NCT03330847	Metastatic Triple Negative Breast Cancer	Olaparib, AZD6738, AZD1775	PARP, ATR, WEE1	II	450
NCT02975934	Metastatic Castration Resistant Prostate Cancer	Rucaparib vs Abiraterone acetate or Enzalutamide or Docetaxel	PARP	III	400
NCT02952534	Metastatic Castration Resistant Prostate Cancer	Rucaparib	PARP	II	360
NCT02854436	Prostatic Neoplasms	Niraparib	PARP	II	301
NCT03414047	Ovarian Cancer	Prexasertib	CHK1, CHK2	II	173
NCT03307785	Advanced Non-Small Cell Lung Cancer	Niraparib, TSR-042, TSR-022, Bevacizumab	PARP, anti-PD-1, anti-TIM-3, VEGF	I	168
NCT02124148	Colorectal and Breast Cancer	Prexasertib and Combination	CHK1, CHK2	I	167
NCT02203513	Ovarian, Breast, and Prostate Cancer	LY2606368	CHK1, CHK2	II	153
NCT03637491	Pancreatic and Non-Small Cell Lung Cancer	Avelumab, Binimetinib and/or Talazoparib	anti-PD-L1, MEK, PARP	II	127

Table 2. Current clinical trials targeting DNA DSB repair pathway proteins as mono- and combination therapy agents. Note: Currently active or recruiting 11 clinical trials are arranged according to the number of enrollment of participants (n>100) in the US, clinicaltrials.gov last accessed on Sep 26, 2019.

HEDGEHOG SIGNALING ENABLES REPAIR OF RIBOSOMAL DNA DOUBLE-
STRAND BREAKS

by

TSSHERING D LAMA-SHERPA, VICTOR T G LIN, BRANDON J METGE,
SHANNON E WEEKS, DONGQUAN CHEN, RAJEEV S SAMANT,
LALITA A SHEVDE

Nucleic Acids Research. 2020 Oct 9;48(18):10342-10352.

Copyright
2020

By Oxford University Press

Used by permission

Format adapted for dissertation

Abstract

Ribosomal DNA (rDNA) consists of highly repeated sequences that are prone to incurring damage. Delays or failure of rDNA double-strand break (DSB) repair are deleterious, and can lead to rDNA transcriptional arrest, chromosomal translocations, genomic losses, and cell death. Here we show that the zinc-finger transcription factor GLI1, a terminal effector of the Hedgehog (Hh) pathway, is required for the repair of rDNA DSBs. We found that GLI1 is activated in triple-negative breast cancer cells in response to ionizing radiation (IR) and localizes to rDNA sequences in response to both global DSBs generated by IR and site-specific DSBs in rDNA. Inhibiting GLI1 interferes with rDNA DSB repair and impacts RNA polymerase I activity and cell viability. Our findings tie Hh signaling to rDNA repair and this heretofore unknown function may be critically important in proliferating cancer cells.

Keywords: Cancer, Hedgehog signaling, ribosomal DNA, Double-Strand breaks repair, Non-homologous End Joining

Introduction

Ribosomal DNA (rDNA) comprises repeated sequences encoding the 45S and 5S ribosomal RNAs (rRNAs) that form the basis of ribosome structure and function (1). These regions of chromatin are open and highly transcribed in actively proliferating cells in order to match their extensive metabolic demands, making them prone to incurring damage (2-4). Genome-wide mapping of DSBs shows a predilection for rDNA that leads to genomic rearrangements (2). Thus, chromosomal translocations in rDNA are among the most common genomic alterations in adult solid tumors (4). Delayed, erroneous, or incomplete repair of double-strand breaks (DSBs) in these loci can lead to deleterious chromosomal translocations, genomic instability, aneuploidy, and ultimately mitotic catastrophe and cell death (5-7).

Cells have two major repair mechanisms in place to resolve DSBs: homologous recombination (HR) and non-homologous end joining (NHEJ). HR is cell cycle-dependent and results in high-fidelity repair of DSBs, whereas NHEJ is cell cycle-independent and comprises blunt end-joining that is more immediate but more error-prone (8). NHEJ is the preferred repair pathway for rDNA DSBs (9), though they may also be resolved by HR machinery independent of the cell cycle as a contingency (10). Errors in repair can lead to loss of repeats and chromosomal translocations involving 45S rDNA loci, which are found on five different chromosomes (4). Delays in the resolution of rDNA DSBs result in the arrest of rDNA transcription by RNA polymerase I (Pol I) via an ATM-dependent mechanism (9). Unrepaired rDNA damage, especially of 45S rDNA, is deleterious (5). Thus, rDNA repair is an attractive target for novel cancer therapeutics.

We sought to investigate the role of Hedgehog (Hh) signaling in DNA repair. Previous work in our laboratory connected GLI1, a zinc-finger transcription factor that is a terminal effector of the Hh pathway, to the DNA single-strand break (SSB) repair via the nucleotide and base excision repair pathways (NER and BER). We showed that GLI1 upregulates expression of NER and BER genes in response to SSBs to facilitate their repair (11). Hh inhibition is also known to sensitize cancer cells to agents that induce DSBs, but the mechanisms by which Hh influences DSB repair are poorly understood (12,13). We hypothesized that induction of DSBs by ionizing radiation (IR) would result in cis-tromic changes in GLI1 in order to orchestrate the activation of DNA repair programs. Unexpectedly, we found that GLI1 occupancy of rDNA loci is markedly enriched in response to IR and that GLI1 is required for timely repair of rDNA DSBs.

Materials and methods

Cell culture

SUM1315 cells were cultured in DMEM/F12 (Gibco) containing 5% heat-inactivated FBS (Gibco), 10 µg/mL insulin (Sigma), and 25 ng/mL EGF (Sigma). MDA-MB-468 cells were cultured in DMEM/F12 containing 10% FBS. SUM159 cells were cultured in DMEM/F12 containing 5% FBS, 10 µg/mL insulin, and 1 µg/mL hydrocortisone (Sigma). Culture media were all free of antibiotics and antimycotics unless otherwise stated. Cells were maintained at 37°C in a humidified environment containing 5% CO₂.

Hh/GLI1 inhibition

Cells were treated with 10 μ M vismodegib (SelleckChem) or 10 μ M GANT61 (Tocris) solubilized in DMSO (Fisher) as stated in each figure. Unless otherwise noted, cells were treated with an inhibitor or vehicle control for 24 hours prior to irradiation. Where noted, SUM1315 cells were stably transfected with either a non-targeted plasmid or shRNA directed against GLI1 as previously described (14) and maintained in selection with 300 μ g/mL G418 (Gibco).

Ionizing radiation

Cells were irradiated with the indicated doses using the X-RAD 320 (Precision) X-ray irradiator with exposures quantified using the UNIDOS E dosimeter (PTW).

Chromatin immunoprecipitation and next-generation sequencing.

SUM1315 cells were plated on 100 mm dishes (Corning). At approximately 90% confluence, they were either mock irradiated or irradiated with 4 Gy and crosslinked with 1% formaldehyde (Fisher) at room temperature at the indicated times after irradiation. Where indicated, cells were pre-treated with DMSO or 10 μ M GANT61 beginning 24 hours prior to irradiation. After crosslinking, cells were harvested for chromatin immunoprecipitation (ChIP) using the SimpleChIP Plus Kit with Magnetic Beads (Cell Signaling) according to manufacturer's protocol. Sonication was done with six 10-second pulses at 50% power using a FB-120 sonic dismembrator (Fisher), with 60-second rests on ice in between each pulse. After confirmation of shearing quality using agarose gel electrophoresis, 10 μ g of crosslinked, sheared chromatin was used for each immunoprecipitation reaction, with 2% input controls saved for comparison.

GLI1 ChIP was performed using 3 μ g of C-1 antibody (Santa Cruz). For standard ChIP analysis, equal volumes of eluted DNA were used for quantitative PCR and normalized to C_T values of the corresponding 2% input control with the following formula: Percent Input = $2\% \times 2^{(C_T \text{ 2\% Input Sample} - C_T \text{ IP Sample})}$. Nonspecific signals calculated from beads only controls were subtracted from each corresponding IP. Primers used are tabulated in Supplementary Table S1. For ChIP-Seq, 2% input controls and eluted DNA from ChIP reactions done in duplicate were submitted to an external vendor (GENEWIZ) for next-generation sequencing. ChIP-Seq data was aligned to the hg19 genome using BWA Aligner (15). Peak calling was done using MACS2 (16) (<https://github.com/taoliu/MACS/tree/master/MACS2>) and filtered for peaks of interest between -5000 and +2000 of transcriptional start sites. ChIP-Seq peaks were visualized using the Integrative Genomics Viewer (17).

Immunoblotting

Cells were lysed in RIPA buffer (Millipore) containing HALT protease and phosphatase inhibitor cocktail (ThermoScientific) and sonicated to complete lysis. Lysates were clarified by centrifugation before protein concentrations were assayed using the Precision Red assay (Cytoskeleton). Equal masses were electrophoresed by SDS-PAGE and wet transferred to PVDF membranes (BioRad). When probing for proteins with molecular weights over 200 kDa, precast gradient gels were used (Invitrogen and BioRad) and wet transfers were done at 30 V for 16 hours. Primary antibodies against γ -H2AX (Cell Signaling, 9718S), GLI1 (Cell Signaling, 2643S), fibrillarin (Cell Signaling, 2639S), I-SceI (Abcam, ab216263), 53BP1 (Cell Signaling, 4937S), phospho-

53BP1 S1778 (Cell Signaling, 2675S), ATM (Cell Signaling, 2873S), phospho-ATM S1981 (Cell Signaling, 5883S), NBS1 (Cell Signaling, 3002S), phospho-NBS1 S343 (Cell Signaling, 3001S), and β -actin (Sigma) were used, as well as secondary HRP-conjugated antibodies against mouse and rabbit IgG (GE) when appropriate. Chemiluminescence images were captured using the Imager 600 (Amersham). Densitometry was calculated using ImageJ software (NIH).

Immunocytochemistry

Cells were plated on poly-L-lysine coated coverslips (Corning) in 35 mm dishes (Corning) at a seeding density of 300,000 cells per dish and were fixed with 4% paraformaldehyde (Sigma) for 30 minutes followed with two washes with ice-cold PBS (Corning). The fixed cells were permeabilized in 0.1% Triton X-100 (Fisher) in PBS (PBST) for 15 minutes followed by blocking in 5% BSA (Fisher) in PBST for 1 hour. Cells were incubated overnight at 4°C with 1:200 GLI1 (Cell Signaling, 2553S), 1:400 γ -H2AX (Cell Signaling, 9718S), 1:400 fibrillarin (Cell Signaling, 2639S), and 1:200 phospho-53BP1 S1778 (Cell Signaling, 2675S) primary antibodies in 5% BSA. Following three 10-minute washes with PBS, cells were incubated in the dark with 1:100 secondary anti-mouse and anti-rabbit IgG antibodies conjugated to Alexa Fluor 488 and 594 (Invitrogen) in 5% BSA, followed by three 10-minute washes in PBS before mounting with DAPI using VECTASHIELD (Vector Laboratories). Slides were visualized using an Eclipse TE2000-U microscope (Nikon) and representative images for γ -H2AX or phospho-53BP1 foci were captured at 100X magnification. Cells from 10 random fields were counted for analysis of γ -H2AX or phospho-53BP1 foci at 30X magnification. Cells were considered positive for γ -H2AX or phospho-53BP1 foci if 10

or more foci were identified. Intensity of GLI1-Fibrillarin co-localization was determined using the manufacturer's protocol for calculating binary intersection mean intensity in NIS-Elements (Nikon) software from five random 100X fields of similar cell density (approximately 10 cells per field).

Confocal microscopy

SUM1315 cells incubated for 1 hour at room temperature with 1:200 GLI1 (Cell Signaling, 2553S) and 1:200 phospho-53BP1 S1778 (Cell Signaling, 2675S) primary antibodies in 5% BSA. After washing, cells were incubated in 1:100 secondary anti-mouse and anti-rabbit IgG antibodies conjugated to Alexa Fluor 488 and 594 (Invitrogen) in 5% BSA, followed by three washes in PBS before incubation for 1 hour with 1:50 UBF Antibody (F-9) conjugated to Alexa Fluor 647 (Santa Cruz, sc-13125 AF647). The cells were stained with DAPI (Fisher) and mounted with VECTASHIELD (Vector Laboratories) and analyzed using a Nikon AIR Confocal Microscope at 60X. Intensity of phospho-53BP1-GLI1-UBF1 co-localization was determined using the manufacturer's protocol for calculating binary intersection mean intensity in NIS-Elements (Nikon) software from five random confocal images.

Nucleolar isolation

Nucleoli were purified using a published protocol (18) with minor adaptation. Cells were plated onto 100 mm tissue culture dishes in complete media. After reaching 90% confluence, they were washed three times with cold PBS at pH 7.4 and were collected in a minimal volume of PBS using cell scraper. Pooled cells from at least 10 dishes were centrifuged at 500 g for 5 minutes. The Reference Volume (RV) was then

determined by visually estimating the volume of the cell pellet. Cell pellets were resuspended in 15 RV of Nucleoli Standard Buffer (NSB) (10 mM Tris-HCl, pH 7.4, 10 mM NaCl, 1 mM MgCl₂, and HALT protease and phosphatase inhibitor cocktail) and incubated on ice for 30 minutes. NP-40 (Roche) was then added to a final concentration of 0.3%. The cells were homogenized using a 7 mL Dounce homogenizer (Wheaton). The homogenate was centrifuged at 1200 x g for 10 min. The supernatant containing the cytoplasmic fraction was removed and the pellet was resuspended in 10 RV of 250 mM sucrose containing 10 mM MgCl₂. Nuclei were then purified from the homogenate by centrifugation at 1200 g for 10 minutes through an 880 mM sucrose cushion containing 5 mM MgCl₂. Purified nuclei were resuspended in 10 RV of 340 mM sucrose containing 5 mM MgCl₂ and sonicated using several 10-second pulses with 60-second rests on ice between pulses. Membrane disruption was confirmed with phase contrast microscopy to ensure the absence of intact cells and that the nucleoli were devoid of their surrounding nuclei. Nucleoli were then purified from the homogenate by centrifugation at 2000 g for 20 minutes at 4°C through an 880 mM sucrose cushion containing 5mM MgCl₂. Purified nucleoli were resuspended in 340 mM sucrose containing the HALT inhibitor cocktail and stored at -80°C for later analysis.

Luciferase reporter assay

Cells were counted by hemocytometer and plated at 25,000 cells per well in a 96-well plate (Corning). After 24 hours, each well was transfected with 50 ng of 8XGli-BS-Luc reporter plasmid (19) using FuGENE 6 (Promega). Twenty-four hours after transfection, they were irradiated with 4 Gy as noted. The experiment was terminated 6

hours later for measuring luciferase activity using the Luciferase Assay System (Promega) and a GloMax 20/20 Luminometer (Promega) according to manufacturer's protocol. Experiments were performed in triplicate and normalized to total protein content as measured by Precision Red assay.

Endogenous protein co-immunoprecipitation

SUM1315 cells were raised to confluence and treated as indicated. At the listed times, cells were washed in ice cold PBS and lysed in RIPA buffer containing HALT protease and phosphatase inhibitor cocktail. Lysates were kept on ice for 1 hour before being syringe-passed 15 times through a 21G needle and clarified by centrifugation at 10,000 RPM for 10 minutes at 4°C. Protein concentration was measured by Precision Red and equal amounts of lysate (750 µg) were used for each immunoprecipitation and corresponding non-specific binding control, with 30 µg of whole cell lysate set aside as an input loading control. Lysates were incubated and rotated with or without α-GLI1 (Cell Signaling, 2643S) for 16 hours at 4°C before being added to 30 µL slurry of Protein A/G PLUS-Agarose beads (Santa Cruz, sc-2003) washed in PBS prior to use. After 4 hours of rotation at 4°C, beads were isolated by centrifugation and washed in RIPA buffer 3 times before immunoprecipitated protein was released by adding denaturing sample buffer containing fresh β-mercaptoethanol and boiled at 95°C for 5 minutes. Immunoblotting for GLI1 in this experiment was done with an antibody from a different source animal (Cell Signaling, 2553S) to avoid detection of potentially confounding IgG peptides.

RNA isolation

Cells were washed in ice cold PBS before RNA was harvested using the PureLink RNA Mini Kit (Ambion) according to manufacturer instructions. Quality of RNA was confirmed by A260:280 ratio and quantitated using the NanoDrop Lite spectrophotometer (Thermo Fisher).

Quantitative PCR

When appropriate, cDNA was reverse transcribed from equal amounts (1 μ g) of isolated RNA using the High Capacity Reverse Transcription Kit (Applied Biosystems). Quantitative PCR was done using the Step ONE Plus Real Time PCR System (Applied Biosystems) with either TaqMan Fast Advanced Master Mix (Applied Biosystems) or Maxima SYBR Green/ROX qPCR Master Mix (Thermo Scientific). TaqMan primers (LifeTech) used were GLI1 (Hs01110766_m1) and ACTB (Hs99999903_m1). Primers used for SYBR Green reactions are tabulated in Supplementary Table S1. For RNA polymerase I activity assays, cDNA was diluted 1:50 prior to use. All reactions were done in triplicate and expression relative to stated controls was calculated using the $\Delta\Delta C_T$ method unless otherwise noted.

Neutral comet assay

Neutral comet assays were done using the CometAssay Kit (Trevigen) according to manufacturer's protocol. Following staining with SYBR Gold (Invitrogen), 50 cells per slide well were analyzed using Comet Assay IV software (Instem).

GFP-based NHEJ repair assay

The reporter plasmid and assay have been previously described (20). SUM1315 and MDA-MB-468 cells were transfected with the pimeJ5-GFP reporter plasmid using Lipofectamine 2000 (Invitrogen) according to manufacturer's protocol and maintained in selection with 2 µg/mL puromycin (Sigma) for 4 weeks before resistant colonies were isolated and further expanded. 80,000 stably transfected cells were then seeded per well in a 12-well plate (Corning) in triplicate. After 24 hours, each well was transfected with 2 µg of I-SceI plasmid using FuGENE 6 according to manufacturer's protocol. Parallel transfection of GFP was done to estimate transfection efficiency. Media was replaced with the appropriate complete media containing either DMSO or 10 µM GANT61. Prior to harvest, cells were stained with 7-aminoactinomycin D (Invitrogen) as a viability control. Flow cytometry was done to quantify the percentage of GFP-expressing cells 72 hours after transfection, with 100,000 events collected per sample. Data were analyzed using FlowJo (Tree Star).

Luciferase-based NHEJ reporter assay

The reporter assay has been previously described (20,21). pGL3-Control (Promega) plasmid was digested with HindIII (Thermo Scientific) to create a double-strand break between the promoter and firefly luciferase coding sequence. Digested plasmid was then treated with calf intestinal phosphatase (Thermo Scientific) to mitigate spontaneous re-ligation. Linearized plasmid was confirmed by electrophoresis and isolated using the Monarch DNA Gel Extraction Kit (New England Biolabs). Cells were plated at a density of 25,000 per well in a 96-well plate. After 24 hours, each well was

transfected with 50 ng of either linearized or uncut plasmid as well as 10 pg of Renilla luciferase vector as a transfection efficiency control using FuGENE 6. Luciferase activity was measured 24 hours after transfection using the Dual Luciferase Reporter Assay System (Promega) and normalized to the Renilla luciferase signal. Data are reported as a percentage of the normalized firefly luciferase activity from cells transfected with uncut pGL3-Control plasmid. All assays were done in triplicate.

RNA polymerase (Pol) I activity assay

The activity assay has been previously described (22). RNA Pol I activity was determined by using quantitative PCR to measure expression of two amplicons within the short-lived 5' external transcribed spacer (ETS) region of the 47S pre-rRNA (Supplementary Table S1). RNA was isolated and used to generate cDNA as described above. cDNA was diluted 1:50 prior to quantitative PCR as described above.

I-PpoI cleavage assay

Cells were transfected with pBABE-HA-ER-IPpoI (23) using FuGENE6 according to manufacturer's protocol. Sixteen hours after transfection, cells were plated in 35 mm dishes and subsequently treated with 1 μ M tamoxifen (Sigma) or ethanol vehicle control as noted. Sixteen hours after initiating treatment, tamoxifen-containing media was replaced with complete media. Genomic DNA was isolated at the indicated time-points after tamoxifen withdrawal using the QIAamp DNA Mini Kit (Qiagen) and assessed for I-PpoI induced damage at 45S rDNA loci using quantitative PCR to measure an amplicon spanning the restriction site (Supplementary Table S1), such that unrepaired

breaks would reduce expression. 5 ng of genomic DNA was used for each reaction, which were done in triplicate and normalized to β -actin expression.

Three-dimensional (3D) culture

SUM1315 and MDA-MB-468 cells were pre-treated with GANT61 for 24 hours and irradiated with 4 Gy. 200 μ L of Cultrex 3D Culture Matrix Reduced Growth Factor Basement Membrane Extract (RGF BME) was added to a sterile 8 well chamber (Millipore) and allowed to solidify at 37°C for 30 minutes. Cells were trypsinized, counted by hemocytometer, and diluted in assay medium before seeding to a final density of 5,000 cells per well containing the 3D matrix. Assay medium was replaced every 4 days. Cell growth was captured and analyzed on day 8 and day 16 for SUM1315 and MDA-MB-468 cells, respectively. A Nikon Eclipse TE2000-U microscope was used to visualize cells at 30X magnification. ImageJ software was used to measure spheroids.

Colony formation assays

SUM1315 cells were treated for 24 hours with either DMSO or 20 μ M GANT61. Cells were then mock irradiated or irradiated with 4 Gy as indicated. Four hours after irradiation, plates were washed with PBS and cells were trypsinized for counting by hemocytometer. Cells were seeded in triplicate in 6-well plates (Corning) at a density of 1,500 cells per well in either DMSO- or GANT61-containing medium. Twenty-four hours after seeding, media was gently aspirated and replaced with complete medium without drug. Alternatively, SUM1315 cells stably transfected with non-targeting shRNA or shGLI1 were irradiated and seeded as noted in complete medium containing G418

without replacement of media after plating. Ten days after seeding, plates were washed with PBS and cells were fixed using 4% PFA before staining with 0.1% crystal violet (Sigma) in 10% ethanol (Pharmco) for counting.

I-PpoI Colony Formation Assay

SUM1315 non-targeting (NT) or shGLI1 were transfected with pICE-HA-NLS-I-PpoI or empty vector using Fugene 6 as per manufacturer protocol. Briefly, cells were transfected in 60mm dishes, and 48 hours post transfection cells were seeded at low density in six well plates. Colonies were allowed to form 7-10 days post seeding. Foci were stained with 0.1% crystal violet and were counted using Image J analysis software. All experiments were done in triplicate and represented as percent change of I-PpoI versus vector control. Statistical analysis was performed using a One-Way ANOVA and p values are indicated. pICE-HA-NLS-I-PpoI was a gift from Steve Jackson (Addgene plasmid # 46963; <http://n2t.net/addgene:46963> ;RRID:Addgene_46963).

MTS assay

SUM1315 cells stably transfected with non-targeting (NT) shRNA or shGLI1 were seeded in a 96-well plate at a density of 5000 cells per well in either plain media or (0.1, 0.5, 1, 2.5, 5,7.5,10) μ M doxorubicin-containing media for 48 hours. Plates were replenished with medium containing MTS reagent (Promega), incubated for 1hr, and absorbance was recorded at 490nm for colorimetric determination of viable cells.

Statistics

Prism 8 (GraphPad) was used for data visualization and statistical analyses. Results shown are representative examples from at least three independent replicates. All error bars shown represent the standard error of the mean. Statistical significance was defined as $p < 0.05$. Details about specific tests applied are in the respective legends. Unless otherwise noted below, statistics were calculated from $n = 3$ technical replicates from an individual experiment. For neutral comet assays, $n = 50$ cells were counted per condition. For γ -H2AX foci and phospho-53BP1 foci, n was dependent on the number of cells counted in 10 random 30X fields. For 3D cultures, $n = 50$ spheroids per condition were counted.

Results

GLI1 localizes to 45S rDNA repeats in response to IR

To explore the hypothesis that DNA damage induces cis-tromic changes in GLI1, we undertook an unbiased screening approach in SUM1315 triple-negative breast cancer (TNBC) cells known to have aberrant activation of Hh signaling reflected by high endogenous levels of GLI1. GLI1-associated chromatin was immunoprecipitated from cells four hours after 4 Gy IR or mock irradiation (Supplementary Figure S1A) and evaluated by next-generation sequencing (ChIP-Seq). We found that GLI1 associates with a novel motif (Figure 1A and Supplementary Figure S1B) that is distinct from the previously reported core sequence (5'-GACCACCCA-3') (24). We identified ChIP-Seq peaks that were specific to the irradiated and nonirradiated samples (Supplementary Tables S2 and S3). Surprisingly, unique peaks specific to irradiated cells were markedly

enriched for rDNA loci, with approximately a third of the hits associated with RNA5S1-17, RNA45SN1-5, RNA18SN1-5, RNA28SN1-5, and RNA5-8SN1-5 (Figure 1B). We manually searched the 45S rDNA coding sequence for putative GLI1 interacting sequences based either on the previously reported core sequence or the motif calculated from our ChIP-Seq data. Using the Integrated Genomics Viewer (17) to visualize peaks at these potential sites, we focused on five putative GLI1 binding sites with associated peaks that were enhanced after irradiation, ruling out candidates where no peak was seen (Figure 1C). Site A is based on the previously reported consensus and is located in the 5' external transcribed spacer (ETS). Sites B-E are based on our novel predicted binding sequence and cluster in the 28S region. To validate results of the ChIP-Seq screen, we performed quantitative PCR of immunoprecipitated chromatin and discovered that GLI1 association with these five sites was induced as early as 1 hour following 4 Gy IR (Figure 1D). Because the 45S rDNA repeats comprise the nucleolar organizer regions (NORs), we enriched nucleoli through a sucrose cushion and found that the nucleolar fraction of GLI1 is increased in response to IR (Supplementary Figure S1C). Using immunocytochemistry, we were able to visualize nucleolar GLI1 in irradiated cells. The incidence (Figure 1E) and intensity (Figure 1F) of nucleolar GLI1 as evidenced by its colocalization with fibrillarin was significantly elevated in SUM1315 cells following IR compared to non-irradiated controls.

Hh activity is induced by IR and facilitates resolution of DSBs

We observed a significant increase in GLI1 reporter activity in response to IR as evidenced in three different TNBC cell lines (Figure 2A), suggesting an increase

in Hh activity. Concordantly, we registered a significant increase in transcript (Figure 2B) and a concurrent qualitative rise in protein levels (Figure 2C) of GLI1 in irradiated SUM1315 and MDA-MB-468 cells. This is also evident when cells are irradiated with low-dose IR (Supplementary Figure 2A, 2B). Abrogating GLI1 expression (shGLI1) did not induce appreciable dsDNA damage (Supplementary Figure 2A). Furthermore, even when low dose IR is used to induce DNA damage, cells silenced for GLI1 sustained significantly increased dsDNA damage (Supplementary Figure 2A, 2B). To better understand the relevance of IR-induced Hh activation, we inhibited the activity of GLI using GANT61, a direct GLI1/2 inhibitor (Figure 2D, E). This resulted in persistence of IR-induced γ -H2AX expression, suggesting delays in DNA repair (Figure 2E). Complementing the outcomes of SUM1315 cells, MDA-MB-468 cells inhibited for Hh/GLI signaling also demonstrated persistence of IR-induced γ -H2AX expression, although the kinetics between these two cell systems was markedly distinct. (Figure 2E and Supplementary Figure S2C). Hh inhibition using the SMO inhibitor vismodegib (Supplementary Figures S2D and S2E) or stable transfection of GLI1-targeting shRNA (shGLI1) yielded similar findings (Supplementary Figure S2F). This corresponded with statistically significant delays in resolution of IR-induced γ -H2AX foci visualized using immunocytochemistry (Figure 2F). To more specifically examine DSBs, we used neutral comet assays to measure average tail moments in SUM1315 and MDA-MB-468 cells pretreated with GANT61 and then exposed to 4 Gy IR (Figure 2G). As anticipated, the average tail moment increased in irradiated cells with evidence of resolution over time in vehicle-treated cells. However, GANT61-pretreated cells were unable to recover. Hh inhibition using stable transfection of shGLI1

yielded similar results compared to non-targeting shRNA control (Supplementary Figure S2G). Collectively, these findings suggest that inhibiting Hh signaling delays IR-induced DSB repair.

Hh signaling is required for efficient NHEJ

Recalling our initial finding that GLI1 is enriched at rDNA loci following IR, we conjectured that GLI1 promotes rDNA repair, which preferentially utilizes NHEJ (9). SUM1315 and MDA-MB-468 cells were stably transfected with the pimeEJ5-GFP reporter plasmid, a construct used to assay NHEJ activity. After site-specific DSBs were induced by the restriction enzyme I-SceI (Supplementary Figure S3A), GFP-expressing cells that had undergone successful NHEJ-mediated repair were quantified by flow cytometry. Hh inhibition by GANT61 significantly impaired NHEJ in both cell lines (Figure 3A). In an independent verification, we linearized pGL3-Control with the restriction enzyme HindIII, disconnecting the promoter from the firefly luciferase coding sequence. Cells transfected with HindIII-cut pGL3-Control will only express firefly luciferase if NHEJ has resolved the break. Again, GANT61 significantly reduced NHEJ-mediated repair (Figure 3B). We also assessed the possible role of HR in IR-induced dsDNA damage using the DR-GFP luciferase reporter construct. While BRCA1-mutated SUM1315 cells demonstrated a smaller magnitude of HR activity, this was unchanged in presence of GANT61. In MDA-MB-468 cells, GANT61 reduced HR-mediated repair, albeit the overall magnitude of HR activity was very small (Supplementary Figures 3 B-C).

Prior work has suggested that GLI1 may interact with the DSB-sensing proteins MRE11 and RAD50 (25). Using endogenous protein co-immunoprecipitation, we found that GLI1 interacts with 53BP1, a protein critical for dictating repair pathway choice towards NHEJ (26) (Figure 3C). The interaction of endogenous GLI1 with 53BP1 is accompanied by active P-53BP1 foci at DSB sites (Figure 3D, 3E). This suggests that the interaction between GLI1 and 53BP1 is likely important for the rapid NHEJ repair response and P-53BP1 foci formation at DSB sites. Furthermore, IR-induced expression of P-53BP1 and abundance of P-53BP1 foci were reduced when Hh was inhibited by either GANT61 (Figure 3D) or GLI1 knockdown (Figure 3E, Supplementary Figures 3D, 3E).

Hh signaling is required for resolution of site-specific rDNA DSBs

Because these assays address global DNA repair, we sought to assess how rDNA repair specifically is affected by Hhinhibition. To do so, we transfected cells with tamoxifen-inducible I-PpoI (pBABe-HA-ER-IPpoI), a restriction enzyme with limited recognition sites in the human genome, including one in the 45S rDNA sequence (Supplementary Figure S3F). Due to the sheer number of 45S rDNA repeats found throughout the human genome, I-PpoI-induced DNA breaks can be considered a surrogate for rDNA-specific damage (23). We first confirmed that tamoxifen treatment of cells transfected with pBABe-HA-ER-IPpoI reduced abundance of an amplicon spanning the I-PpoI cleavage site in the 45S rDNA sequence by qPCR, indicating breakage (Supplementary Figure S3G). Concomitant with this, we also registered phosphorylation of NBS1 and ATM, which are previously reported indicators of I-PpoI-mediated damage

(Supplementary Figure S3H) (23). Using ChIP, we found that GLI1 localizes to the sites of I-PpoI-mediated breaks in 45S rDNA (Figure 3F). To evaluate the role of GLI1 in the resolution of these breaks, we withdrew tamoxifen after overnight treatment to allow for repair. The abundance of an amplicon spanning the I-PpoI restriction site was reduced by tamoxifen treatment, indicating the presence of breaks that the polymerase was unable to read through (Figure 3G). After tamoxifen was withdrawn for four hours, the magnitude of amplicon abundance increased again in control (NT) cells, implying repair of the cleavage site. We found that GLI1 knockdown (shGLI1) significantly hampered the recovery of amplicon expression after tamoxifen withdrawal, suggesting that GLI1 is required for the efficient repair of site-specific rDNA DSBs. Resolution of rDNA breaks requires the recruitment of repair machinery to sites of damage. Using confocal microscopy, we observed the colocalization of GLI1 and P-53BP1 in the nucleolus in response to IR (Figure 3H and Supplementary Figure S3I). We quantified the intersection of GLI1, P-53BP1, and the nucleolar marker UBF1 at one-hour post-irradiation and noted a substantial increase in their association per cell and per nucleolus (Figure 3H).

Combining Hh inhibition with IR compromises Pol I activity and cell viability

rDNA DSBs temporarily arrest transcription until repair is complete. To assess how Hh inhibition affects 45S rDNA transcription by Pol I in response to damage, we used qPCR to quantify expression of two different sites in the 5' ETS. Because these regions are removed post-transcriptionally during rRNA processing, they have a short half-life and are ideal surrogates for Pol I activity over time (22). As anticipated, in

control cells treated with vehicle, Pol I activity was reduced early in response to IR and recovered at later time points (Figures 4A and 4B), consistent with the kinetics of repair determined by our earlier experiments. When Hh activity was inhibited by GANT61, Pol I activity is reduced by IR as expected, but does not recover. Hh inhibition by stable GLI1 knockdown yielded similar results (Supplementary Figures S4A and S4B). Interestingly, the delay in Pol I recovery that we observed with GLI1 inhibition mirrors prior findings when NHEJ was directly inhibited instead (9). We then explored whether Hh pathway inhibition would lead to sensitivity due to its role in rDNA repair. In order to specifically induce rDNA breaks, we transfected SUM1315 cells with I-PpoI plasmid (or an empty vector control). In order to specifically address the role of Hh/GLI activity, we queried SUM1315 cells stably silenced for GLI1. We assessed the effect on cell survival using a colony formation assay. Introducing I-PpoI (relative to control plasmid) caused an appreciable decrease in the number of colonies (Supplementary Figure 4 C-D). Interestingly, GLI1-silenced cells transfected with I-PpoI showed a striking decrease in the number of colonies formed, suggesting that Hh inhibition further reduces survival of cells inflicted with rDNA breaks with I-PpoI. These findings support that Hh inhibition augments rDNA damage and consequently poses finite lethality to TNBC cells independent of global effects on DSB repair.

To assess the overall outcome of IR-induced DNA damage in the context of Hh inhibition, we generated spheroids in three-dimensional culture from cells pre-treated with either vehicle control or GANT61 (Figures 4C and 4D). GANT61 alone had a modest effect on non-irradiated cells, but dramatically impaired spheroid growth when

combined with irradiation in both SUM1315 and MDA-MB-468 cells. Similar findings were noted with GLI1 knockdown (Supplementary Figure S4E). Similarly, colony formation, following irradiation, was significantly compromised in cells deficient for Hh/GLI activity (Supplementary Figures 4F and 4G). Next, we examined whether Hh activity also impacts survival of breast tumor cells when they are inflicted with DNA damage with a chemotherapeutic cytotoxic drug, doxorubicin (anthracycline class of molecules clinically used to treat TNBC). We scored cell survival with a colony formation assay using doxorubicin in lieu of IR, and saw that doxorubicin (used at 0.1 μ M) significantly compromised the abundance of colonies formed by GLI1-deficient SUM1315 cells compared to NT shRNA controls as represented and quantified in Supplementary Figures 4H and 4I. We also scored cell viability using the MTS assay and registered a significant decrease in cell viability in doxorubicin-treated SUM1315 shGLI1 cells relative to NT cells ($p < 0.01$) (Supplementary Figure 4J). As such, the data cumulatively indicates that Hh inhibition sensitizes TNBC cells to IR and doxorubicin - a clinically-relevant chemotherapeutic agent used to treat TNBC.

Discussion

Hh signaling is a classical developmental pathway that is aberrantly activated in various cancers (27) and has been linked to tumor initiation, progression, and metastasis in breast cancer. In TNBC patients, high expression of Hh pathway proteins correlates to poor survival (28,29). Treatment of TNBC relies on DNA-damaging agents, including conventional chemotherapy and IR (30). Though inhibiting Hh has been shown to sensitize cancer cells to genotoxic therapies, the underlying mechanisms to this

point have remained vague (12,13). Our study has uncovered an unexpected role for Hh signaling in the repair of damaged rDNA that helps to explain this phenomenon.

Though we found that GLI1 is required for efficient NHEJ-mediated repair of nonspecific DSBs, we demonstrated a marked enrichment of GLI1 at rDNA loci in response to IR using an unbiased ChIP-Seq screen and confirmed this relative to nonspecific binding controls with standard ChIP. Importantly, the precise degree of enrichment at rDNA loci relative to standard genes is unclear. rDNA coding sequences are known to be arranged in tandem arrays of tens to hundreds of repeats, but only 17 5S rDNA sequences and five 45S rDNA sequences are mapped to the current build of the human genome. This was recently identified as a critical unmet need in the rDNA field (31). For this reason, we focused on the defined coding sequences and not the poorly defined intergenic spacers between repeats. Though we found more hits were associated with 5S rDNA repeats, we elected to study the 45S rDNA both because of the availability of tools to study its gene expression (qPCR of the 5'-ETS) and site-specific DSBs (I-PpoI) and because 45S rDNA breaks have been previously shown to be more consequential than those in 5S rDNA (5). Even accounting for the likelihood that pulled-down fragments mapped to multiple repeats, our findings may underestimate the degree of GLI1 interaction with rDNA given the vast number of repeats known to exist in the human genome.

Notably, we did not observe similar enrichment of GLI1 at genes associated with NHEJ, including *XRCC5*, *XRCC6*, *PRKDC*, *LIG4*, and *TP53BP1*, which encode for Ku70, Ku80, DNA-PKcs, DNA ligase IV, and 53BP1, respectively. This suggests that the effect of GLI1 on NHEJ is not related to its transcription factor activity, despite our

finding that GLI1 expression and activity are increased in response to IR. Whether the enrichment of GLI1 at rDNA loci is influenced by upregulated GLI1 protein expression or shifts in subcellular localization that we observed in response to IR remains an open question.

Accordingly, we hypothesized that GLI1 instead recruits NHEJ-associated proteins to the sites of rDNA DSBs. In line with this conjecture, we found that GLI1 interacts with the NHEJ protein 53BP1. Furthermore, we observed using confocal microscopy that GLI1 association with both P-53BP1 and the rDNA marker UBF1 is triggered by IR. Inhibition of GLI1 mutes the accumulation of P-53BP1, interferes with repair of site-specific rDNA DSBs, and delays recovery of Pol I activity, an indicator of unrepaired rDNA DSBs, in response to IR. To our knowledge, this is the first example of a developmental signaling pathway being directly tied to rDNA repair. Given that Hh signaling is intimately involved in orchestrating normal ontogeny and cancer, it is likely that dysregulated Hh activity may craft intersecting and shared programs that enable cells to survive erroneous and possibly lethal impediments.

Interestingly, inhibiting Hh did not impair baseline Pol I activity on its own. Instead, its effect is secondary to compromised rDNA repair. Thus, GLI1 does not appear to directly promote rRNA transcription, but rather helps to maintain the genomic integrity of rDNA loci. These sites may be particularly vulnerable in proliferative and metabolically active states where Hh is activated, such as in normal development and cancer. In this context, protecting rDNA loci from insults such as replication stress and DNA-damaging agents may be a critical new function of Hh signaling with potential

implications for therapeutic resistance in cancer. Our findings suggest that further evaluation of Hh inhibitors as potential radiosensitizers or chemosensitizers is warranted.

Data availability

The datasets used and/or analyzed during the current study have been deposited at the Gene Expression Omnibus (GEO) under the accession number GSE146237.

Supplementary data

Supplementary Data (Table 2 and 3) are available at NAR online.

Acknowledgements

We thank the UAB Animal Resources Program for the use of irradiator facilities; the UAB Comprehensive Flow Cytometry Core for the use of flow cytometry facilities; the UAB High Resolution Imaging Facility and Dr. R. Grabski for technical assistance; J.M. Stark for providing the pimeJ5-GFP construct via AddGene; M.B. Kastan for providing the pBAbE-HA-ER-IPpoI construct via AddGene; J.A. Bonner for the use of comet analysis facilities and H.Q. Trummell for related technical assistance and guidance; and E.S. Yang for providing the I-SceI construct and technical expertise.

FUNDING NCI/NIH [CA183926 to V.T.G.L.]; Merit Review Award [I01 BX003374] from the U.S. Department of Veterans Affairs BLRD service BX003374; NCI/NIH [CA194048 to R.S.S., CA169202 to L.A.S.]; United States Department of Defense [W81XWH-18-1-0036 to L.A.S.]; University of Alabama at Birmingham [AMC21 to

L.A.S.]; Breast Cancer Research Foundation of Alabama [to L.A.S.]. Funding for open access charge: Institutional start-up funds.

Conflict of interest statement. None declared.

References

1. Pelletier, J., Thomas, G. and Volarevic, S. (2018) Ribosome biogenesis in cancer: new players and therapeutic avenues. *Nature reviews. Cancer*, **18**, 51-63.
2. Tchurikov, N.A., Fedoseeva, D.M., Sosin, D.V., Snezhkina, A.V., Melnikova, N.V., Kudryavtseva, A.V., Kravatsky, Y.V. and Kretova, O.V. (2015) Hot spots of DNA double-strand breaks and genomic contacts of human rDNA units are involved in epigenetic regulation. *J Mol Cell Biol*, **7**, 366-382.
3. Tchurikov, N.A., Yudkin, D.V., Gorbacheva, M.A., Kulemzina, A.I., Grischenko, I.V., Fedoseeva, D.M., Sosin, D.V., Kravatsky, Y.V. and Kretova, O.V. (2016) Hot spots of DNA double-strand breaks in human rDNA units are produced in vivo. *Scientific reports*, **6**, 25866.
4. Stults, D.M., Killen, M.W., Williamson, E.P., Hourigan, J.S., Vargas, H.D., Arnold, S.M., Moscow, J.A. and Pierce, A.J. (2009) Human rRNA gene clusters are recombinational hotspots in cancer. *Cancer research*, **69**, 9096-9104.
5. Warmerdam, D.O., van den Berg, J. and Medema, R.H. (2016) Breaks in the 45S rDNA Lead to Recombination-Mediated Loss of Repeats. *Cell Rep*, **14**, 2519-2527.
6. Roukos, V. and Misteli, T. (2014) The biogenesis of chromosome translocations. *Nature cell biology*, **16**, 293-300.
7. Ceccaldi, R., Rondinelli, B. and D'Andrea, A.D. (2016) Repair Pathway Choices and Consequences at the Double-Strand Break. *Trends in cell biology*, **26**, 52-64.
8. Scully, R., Panday, A., Elango, R. and Willis, N.A. (2019) DNA double-strand break repair-pathway choice in somatic mammalian cells. *Nature reviews. Molecular cell biology*.
9. Harding, S.M., Boiarsky, J.A. and Greenberg, R.A. (2015) ATM Dependent Silencing Links Nucleolar Chromatin Reorganization to DNA Damage Recognition. *Cell Rep*, **13**, 251-259.
10. van Sluis, M. and McStay, B. (2015) A localized nucleolar DNA damage response facilitates recruitment of the homology-directed repair machinery independent of cell cycle stage. *Genes & development*, **29**, 1151-1163.
11. Kudo, K., Gavin, E., Das, S., Amable, L., Shevde, L.A. and Reed, E. (2012) Inhibition of Gli1 results in altered c-Jun activation, inhibition of cisplatin-induced upregulation of ERCC1, XPD and XRCC1, and inhibition of platinum-DNA adduct repair. *Oncogene*, **31**, 4718-4724.
12. Mazumdar, T., Devecchio, J., Agyeman, A., Shi, T. and Houghton, J.A. (2011) Blocking Hedgehog survival signaling at the level of the GLI genes induces DNA

damage and extensive cell death in human colon carcinoma cells. *Cancer research*, **71**, 5904-5914.

13. Teichman, J., Dodbiba, L., Thai, H., Fleet, A., Morey, T., Liu, L., McGregor, M., Cheng, D., Chen, Z., Darling, G. *et al.* (2018) Hedgehog inhibition mediates radiation sensitivity in mouse xenograft models of human esophageal adenocarcinoma. *PLoS One*, **13**, e0194809.

14. Das, S., Harris, L.G., Metge, B.J., Liu, S., Riker, A.I., Samant, R.S. and Shevde, L.A. (2009) The hedgehog pathway transcription factor GLI1 promotes malignant behavior of cancer cells by up-regulating osteopontin. *The Journal of biological chemistry*, **284**, 22888-22897.

15. Li, H. and Durbin, R. (2009) Fast and accurate short read alignment with Burrows-Wheeler transform. *Bioinformatics*, **25**, 1754-1760.

16. Zhang, Y., Liu, T., Meyer, C.A., Eeckhoute, J., Johnson, D.S., Bernstein, B.E., Nusbaum, C., Myers, R.M., Brown, M., Li, W. *et al.* (2008) Model-based analysis of ChIP-Seq (MACS). *Genome Biol*, **9**, R137.

17. Robinson, J.T., Thorvaldsdottir, H., Winckler, W., Guttman, M., Lander, E.S., Getz, G. and Mesirov, J.P. (2011) Integrative genomics viewer. *Nat Biotechnol*, **29**, 24-26.

18. Hacot, S., Coute, Y., Belin, S., Albaret, M.A., Mertani, H.C., Sanchez, J.C., Rosa-Calatrava, M. and Diaz, J.J. (2010) Isolation of nucleoli. *Curr Protoc Cell Biol*, **47**, 3.36.31-33.36.10.

19. Sasaki, H., Hui, C., Nakafuku, M. and Kondoh, H. (1997) A binding site for Gli proteins is essential for HNF-3beta floor plate enhancer activity in transgenics and can respond to Shh in vitro. *Development (Cambridge, England)*, **124**, 1313-1322.

20. Zhuang, J., Zhang, J., Willers, H., Wang, H., Chung, J.H., van Gent, D.C., Hallahan, D.E., Powell, S.N. and Xia, F. (2006) Checkpoint kinase 2-mediated phosphorylation of BRCA1 regulates the fidelity of nonhomologous end-joining. *Cancer research*, **66**, 1401-1408.

21. Sulkowski, P.L., Corso, C.D., Robinson, N.D., Scanlon, S.E., Purshouse, K.R., Bai, H., Liu, Y., Sundaram, R.K., Hegan, D.C., Fons, N.R. *et al.* (2017) 2-Hydroxyglutarate produced by neomorphic IDH mutations suppresses homologous recombination and induces PARP inhibitor sensitivity. *Sci Transl Med*, **9**, eaal2463.

22. Peltonen, K., Colis, L., Liu, H., Trivedi, R., Moubarek, M.S., Moore, H.M., Bai, B., Rudek, M.A., Bieberich, C.J. and Laiho, M. (2014) A targeting modality for destruction of RNA polymerase I that possesses anticancer activity. *Cancer cell*, **25**, 77-90.

23. Berkovich, E., Monnat, R.J., Jr. and Kastan, M.B. (2007) Roles of ATM and NBS1 in chromatin structure modulation and DNA double-strand break repair. *Nature cell biology*, **9**, 683-690.
24. Kinzler, K.W. and Vogelstein, B. (1990) The GLI gene encodes a nuclear protein which binds specific sequences in the human genome. *Mol Cell Biol*, **10**, 634-642.
25. Li, X., Wang, W., Wang, J., Malovannaya, A., Xi, Y., Li, W., Guerra, R., Hawke, D.H., Qin, J. and Chen, J. (2015) Proteomic analyses reveal distinct chromatin-associated and soluble transcription factor complexes. *Mol Syst Biol*, **11**, 775.
26. Panier, S. and Boulton, S.J. (2014) Double-strand break repair: 53BP1 comes into focus. *Nature reviews. Molecular cell biology*, **15**, 7-18.
27. Amakye, D., Jagani, Z. and Dorsch, M. (2013) Unraveling the therapeutic potential of the Hedgehog pathway in cancer. *Nature medicine*, **19**, 1410-1422.
28. Habib, J.G. and O'Shaughnessy, J.A. (2016) The hedgehog pathway in triple-negative breast cancer. *Cancer Med*, **5**, 2989-3006.
29. Noman, A.S., Uddin, M., Rahman, M.Z., Nayeem, M.J., Alam, S.S., Khatun, Z., Wahiduzzaman, M., Sultana, A., Rahman, M.L., Ali, M.Y. *et al.* (2016) Overexpression of sonic hedgehog in the triple negative breast cancer: clinicopathological characteristics of high burden breast cancer patients from Bangladesh. *Scientific reports*, **6**, 18830.
30. Liedtke, C., Mazouni, C., Hess, K.R., Andre, F., Tordai, A., Mejia, J.A., Symmans, W.F., Gonzalez-Angulo, A.M., Hennessy, B., Green, M. *et al.* (2008) Response to neoadjuvant therapy and long-term survival in patients with triple-negative breast cancer. *Journal of clinical oncology : official journal of the American Society of Clinical Oncology*, **26**, 1275-1281.
31. Baserga, S.J., DiMario, P.J. and Duncan, F.E. (2020) Emerging Roles for the Nucleolus 2019. *Journal of Biological Chemistry*, **295**, 5535-5537.

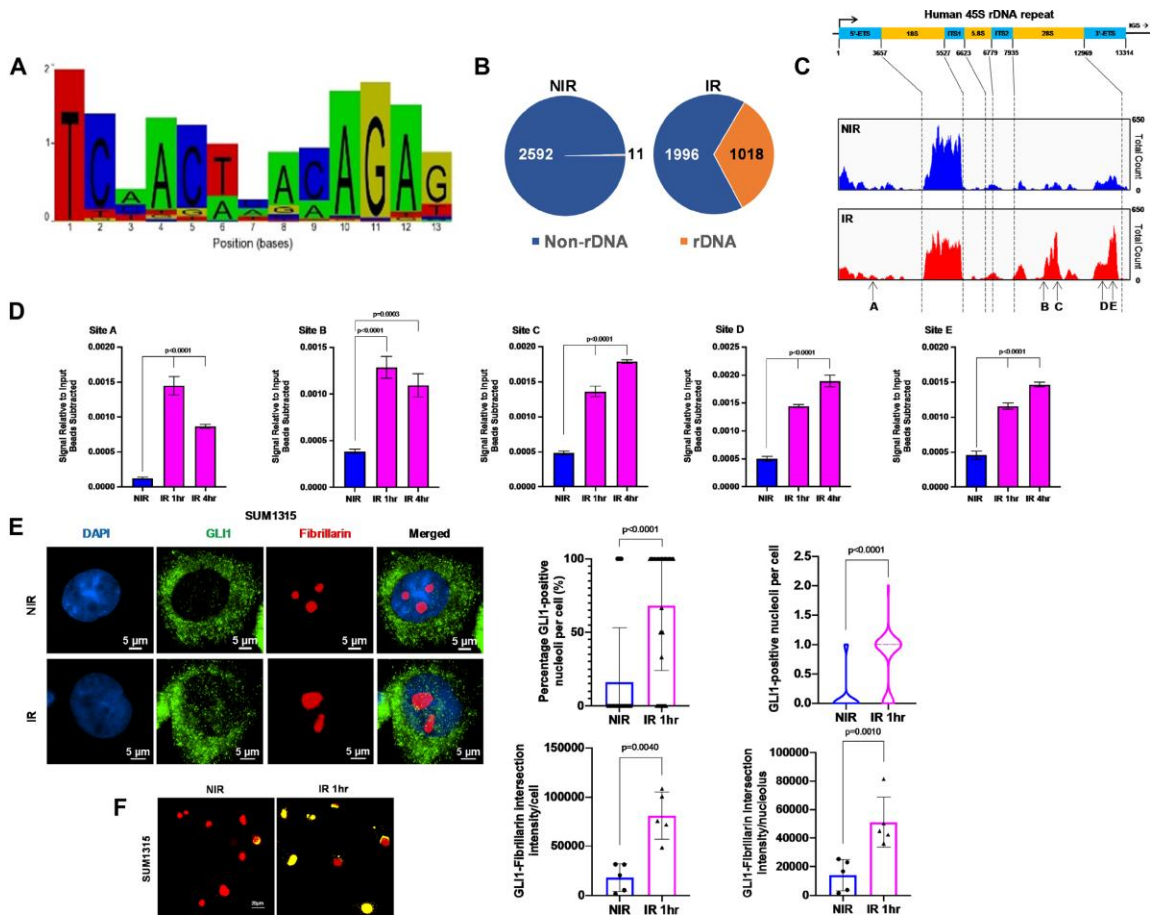


Figure 1. Ionizing radiation induces GLI1 binding to novel sequences in rDNA. (A) ChIP-Seq data was used to predict a novel GLI1-associated sequence after IR. (B) Unique ChIP-Seq peaks following IR were enriched in rDNA loci compared to NIR. (C) GLI1 association was increased in the 28S region of 45S rDNA after IR at sites A-E. (D) Five putative GLI1 binding sites (A–E) show increase in GLI1 occupancy after IR and were validated with ChIPqPCR. Statistical significance was determined with a one-way ANOVA and Dunnett’s multiple comparison test, comparisons between NIR- and IR-treated cells are shown. (E) Immunocytochemistry demonstrates higher GLI1 presence in the fibrillarin-positive nucleoli 1hr after IR, quantitated as a percentage of nucleoli per cell or absolute number of nucleoli. (F) Fibrillarin and GLI1 co-localization, depicted in yellow, increases after IR, normalized either to the total number of cells or nucleoli using NIS binary intersection mean intensity (n = 5). Significance was determined by using t-test. All error bars depict the SEM.

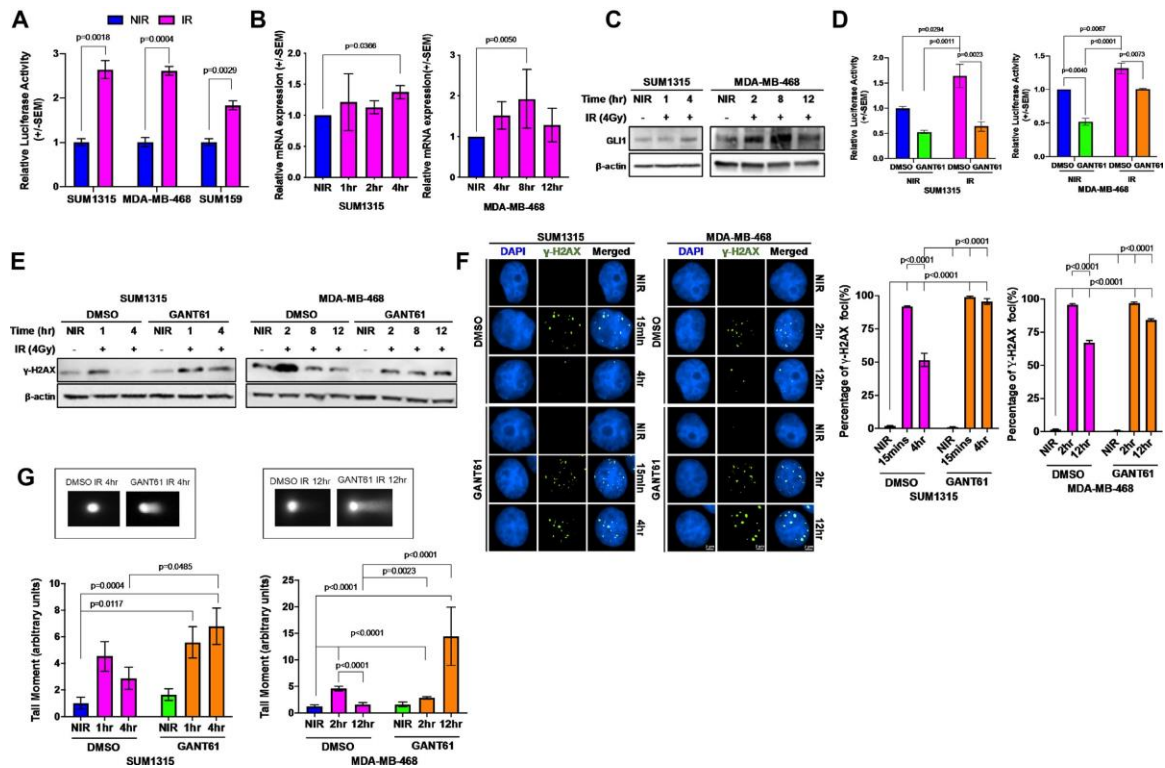


Figure 2. Inhibition of Hh/GLI signaling delays ionizing radiation-induced DSB repair in TNBC cells. (A) 8X-GBS-luciferase reporter assays show Hh activation in multiple TNBC cell lines after IR, confirmed by GLI1 (B) mRNA and (C) protein expression using qPCR and immunoblotting, respectively in SUM1315 and MDA-MB-468 cell lines. Statistical significance was determined with a multiple t test and a one-way ANOVA with Dunnett's multiple comparison test. For one-way ANOVA, comparisons between NIR- and IR-treated cells are shown. (D) GANT61 suppresses IR-induced Hh activation. Statistical significance represents the results of a two-way ANOVA and Tukey multiple comparison test. (E) GANT61 leads to delayed resolution of IR-induced γ -H2AX after IR shown by immunoblot compared to vehicle control. (F) IR-induced γ -H2AX foci shown by immunocytochemistry show similar delay in foci resolution. (G) Neutral comet assays show impaired DSB repair in GANT61-treated cells. Statistical significance was determined with a two-way ANOVA and Tukey's multiple comparison test. Comparisons for DMSO treated NIR and DMSO treated IR-4 h for SUM1315 and IR-12 h for MDA-MB468 are shown. All error bars depict the SEM.

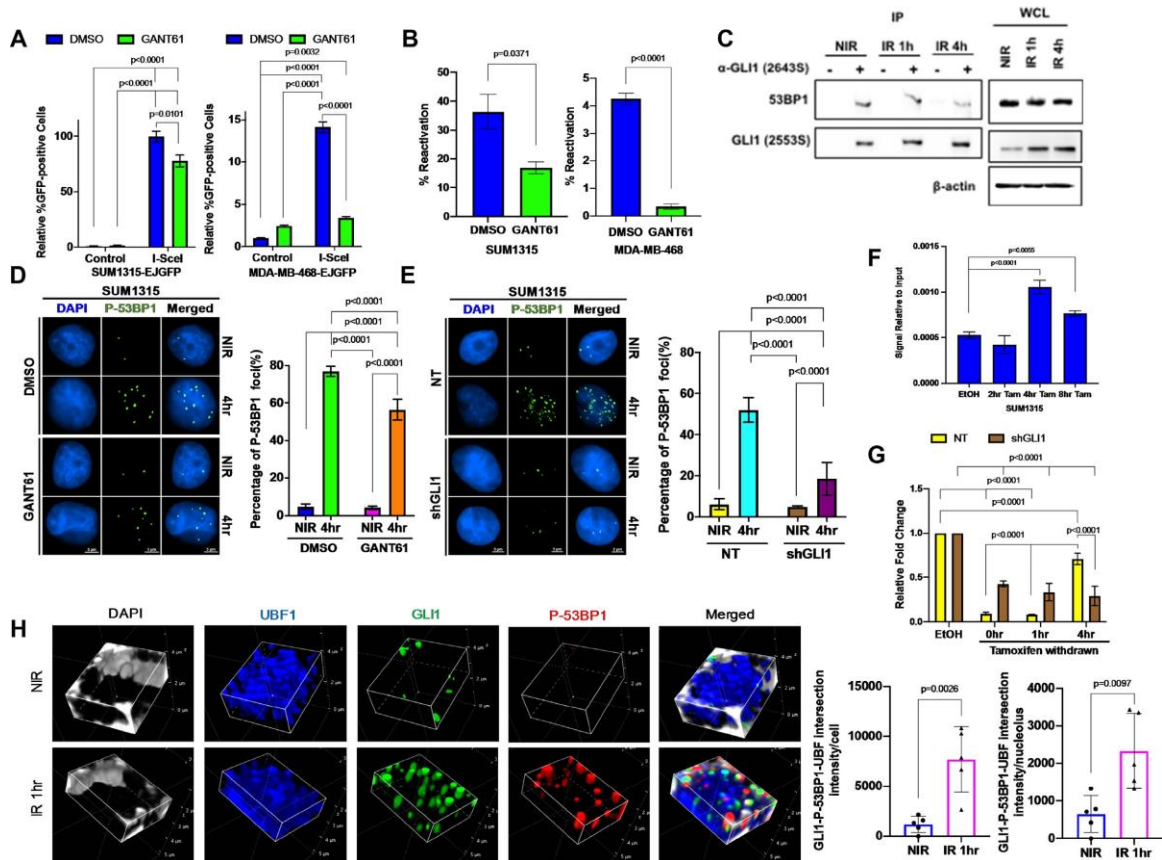


Figure 3. Hh inhibition impairs NHEJ and delays repair of rDNA DSBs. (A) Hh inhibition compromises repair of I-SceI-induced breaks by NHEJ in cells stably expressing the pimeJ5-GFP reporter. Statistical analysis was performed with a two-way ANOVA and Tukey's multiple comparison test, p values are indicated. (B) Impaired NHEJ in Hh-inhibited cells is also evident by diminished reactivation of linearized firefly luciferase plasmid. Statistical analysis was determined with a t-test. (C) Endogenous protein co-immunoprecipitation of SUM1315 lysates shows that 53BP1 interacts with GLI1. Whole cell lysate (WCL) input controls are shown to the right. (D, E) P-53BP1 foci are reduced by (D) GANT61 and (E) stable knockdown of GLI1 compared to controls in SUM1315 cell line at 4 h post-IR. Statistical analysis was performed with a two-way ANOVA and Tukey's multiple comparison test, p values are indicated. (F) GLI1 localizes to I-PpoI-induced rDNA breaks as evidenced by greater occupancy at the I-PpoI break-site following tamoxifen treatment shown by ChIP-qPCR. Statistical significance was determined with a one-way ANOVA and Dunnett's multiple comparison test, comparisons between ethanol treated and tamoxifen withdrawn cells are shown. (G) Tamoxifen treatment induces breaks in SUM1315 NT and shGLI1 cells as measured by reduction in magnitude of amplicon spanning the I-PpoI restriction site. 4 hr post tamoxifen withdrawal, amplicon levels in NT cells increase but stable knockdown of GLI1 remains unchanged indicating efficient repair of these sites of damage in NT compared to shGLI1. Statistical significance was determined with a two-way ANOVA and Tukey's multiple comparison test for treatment at respective time points.

Comparisons for ethanol-treated and tamoxifen withdrawn cells and comparison at 4 h after tamoxifen withdrawal between NT and shGLI1 cells are shown. (H) 3D confocal images of NIR (top) and IR (bottom) SUM1315 cells labeled with GLI1 (green), P-53BP1 (red), UBF (blue), and DAPI (gray) depict increased nucleolar localization and interaction of GLI1 and P-53BP1 1 h post IR in the nucleolar compartment. GLI1 and P-53BP1 interaction in the nucleolus was quantified from five NIR and IR cells and normalized either to the number of cells or nucleoli per field using NIS binary intersection mean intensity ($n = 5$). All error bars depict the SEM.

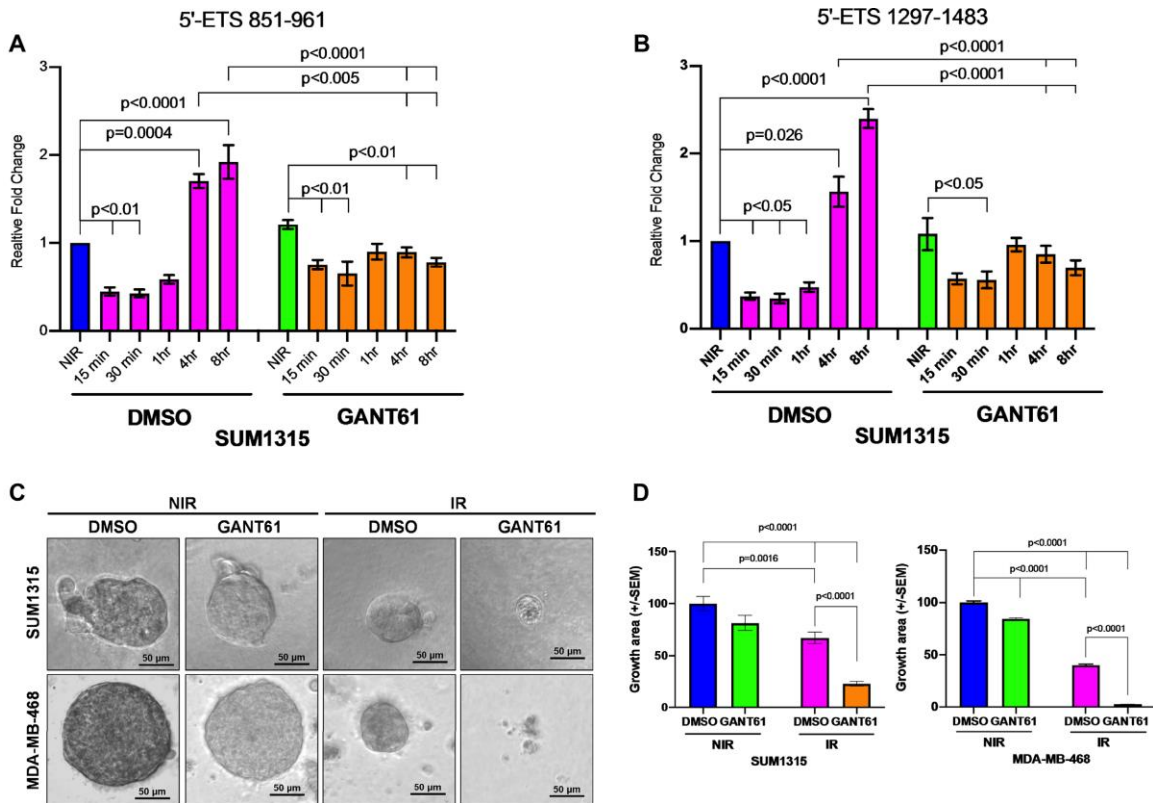
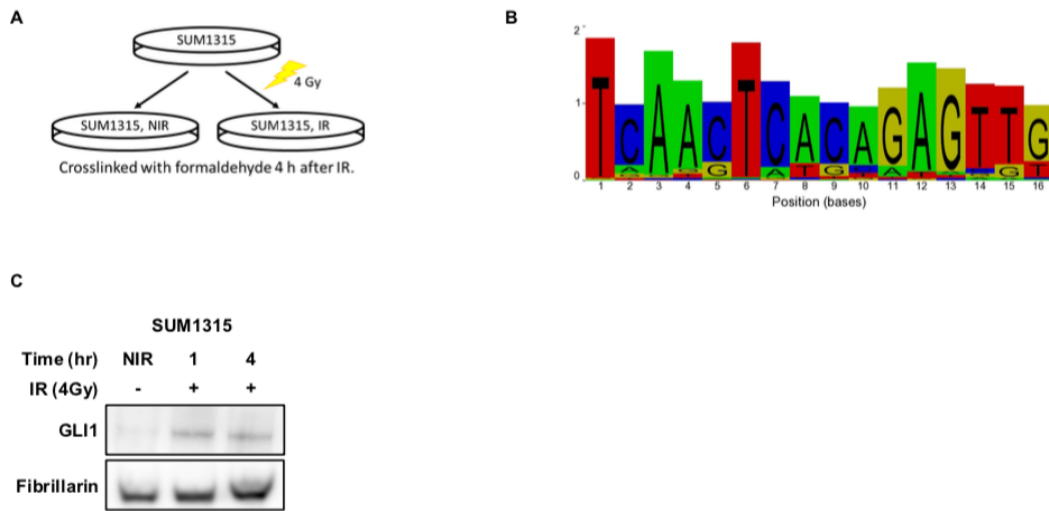


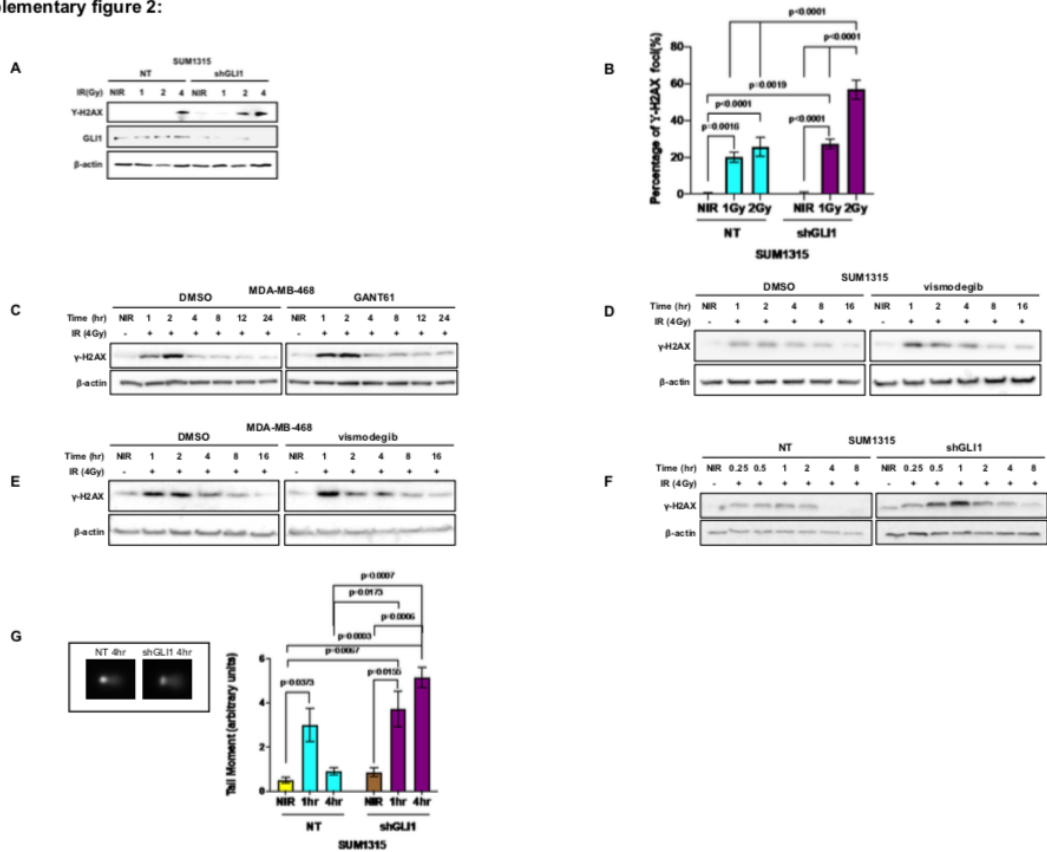
Figure 4. Inhibiting Hh/GLI signaling impairs re-activation of Pol I activity following irradiation-induced DSBs. (A, B) Pol I activity, as quantitated by qPCR of two different amplicons in the 5' ETS of 45S rDNA, is reduced by IR and recovers following repair in cells treated with vehicle control compared to GANT61-treated cells. Statistical significance was determined with a two-way ANOVA and Tukey's multiple comparison test. Comparisons for DMSO- and GANT61- NIR group with cells collected at different time points post IR and DMSO- and GANT61-treated cells at 4 and 8 h are shown. (C, D) Hh inhibition with GANT61 combined with IR almost completely abrogates spheroid growth, compared to more modest reductions with either modality alone. Growth area was quantified using ImageJ software per 10 \times field. Statistical significance was determined with a two-way ANOVA and Tukey's multiple comparison test for each condition. All error bars depict the SEM.

Supplementary figure 1:



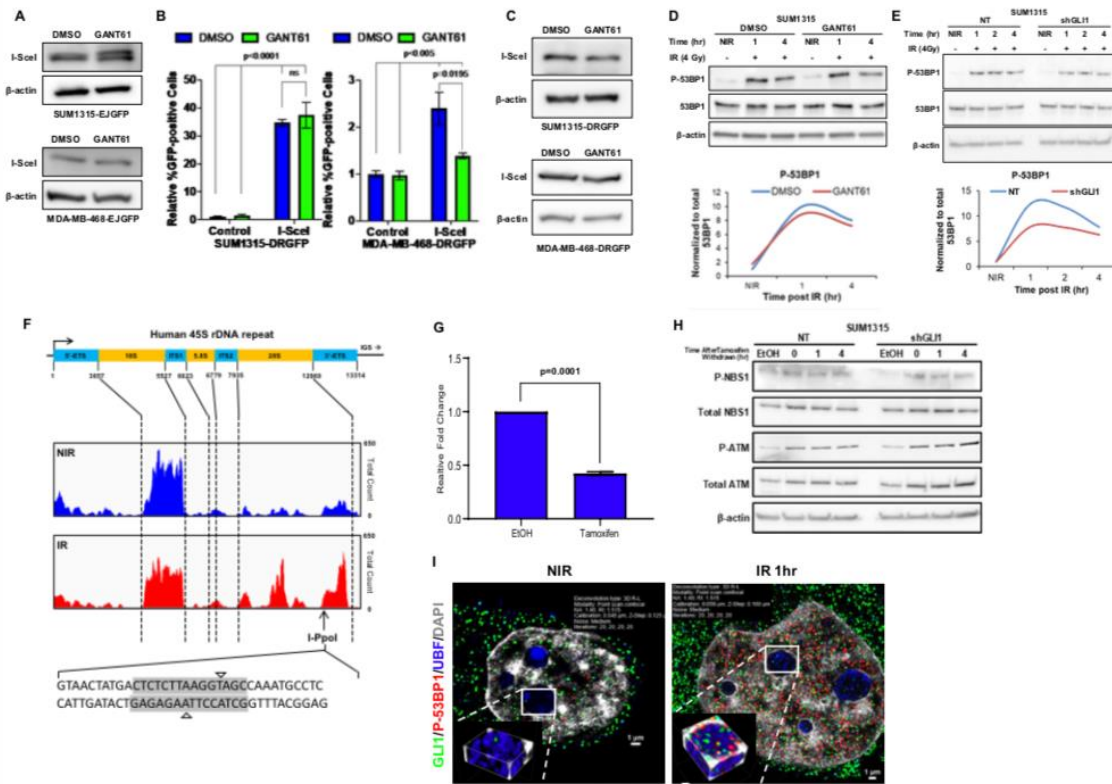
Supplementary Figure S1. Ionizing radiation induces GLI1 binding to novel sequences in rDNA. (A) ChIP-Seq experiment schema. (B) GLI1-associated sequence predicted using ChIP-Seq data from non-irradiated SUM1315 cells. (C) Nucleolar isolation demonstrates increased nucleolar GLI1 following IR by immunoblotting. Fibrillarin is shown as a loading and fractionation control.

Supplementary figure 2:



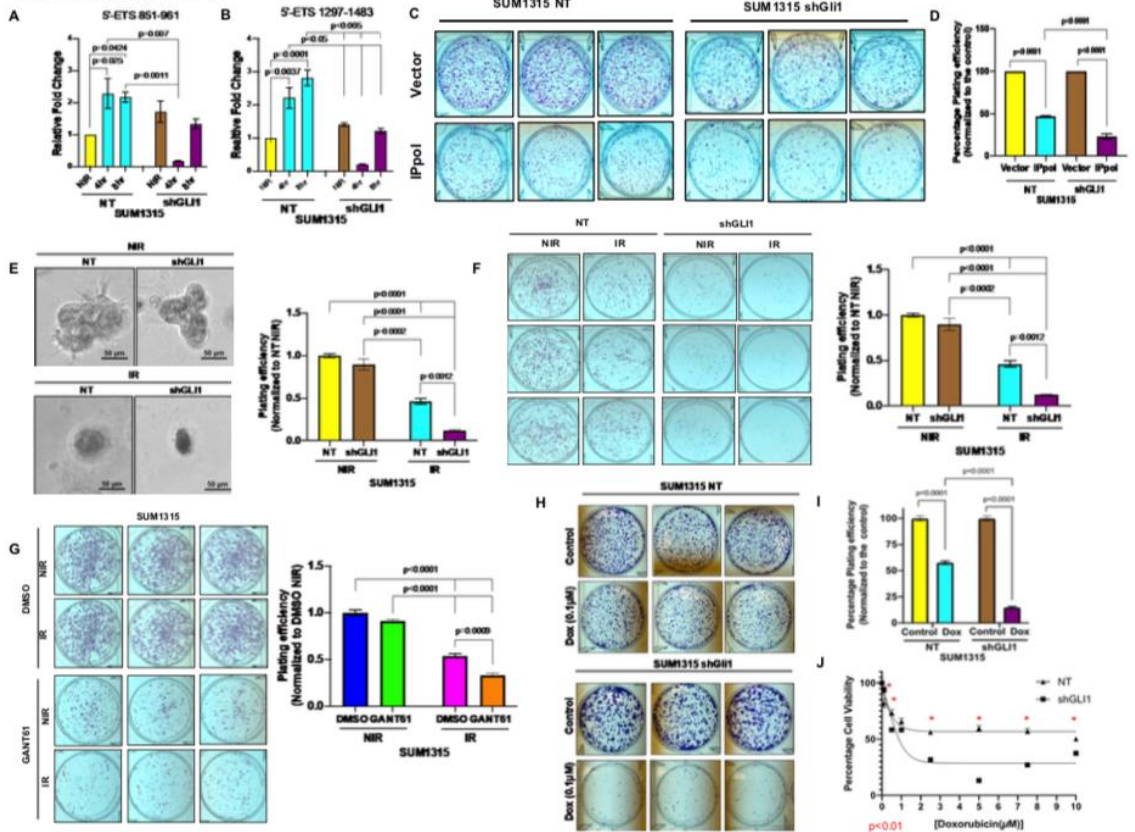
Supplementary Figure S2. Inhibition of Hh/GLI signaling delays ionizing radiation-induced DSB repair in TNBC cells. (A) SUM1315 cells abrogated for GLI1 (shGLI1) demonstrate DSB damage (evident by γ -H2AX western blot) consistent with a dose-dependent manner, with the greatest DNA damage at 4Gy relative to lower intensity IR. (B) IR-induced γ -H2AX foci, scored by immunocytochemistry, indicate dose-dependent increase in DNA damage, consistent with the immunoblot. Statistical significance was determined with a two-way ANOVA and multiple comparison test for each condition using Tukey test. (C) A longer time-course in MDA-MB-468 cells demonstrates prolonged γ -H2AX expression to at least 24h following IR in GANT61-treated cells. (D-E) Vismodegib prolongs IR-induced γ -H2AX signal in SUM1315 (D) and MDA-MB-468 (E) cells compared to vehicle-treated cells. (F) Stable knockdown of GLI1 prolongs γ -H2AX signal after IR compared to non-targeting shRNA controls. (G) Neutral comet assays demonstrate delayed resolution of DSBs in shGLI1 cells over time compared to non-targeting controls. All error bars depict the SEM. Statistical analysis was performed using a two-way ANOVA and multiple comparison Tukey test, p values are indicated.

Supplementary figure 3:



Supplementary Figure S3. Hh inhibition impairs NHEJ and delays repair of rDNA DSBs. (A) I-SceI expression in SUM1315-EJGFP and MDA-MB-468-EJGFP transfected cells. (B-C) Hh inhibition does not impair repair of I-SceI-induced breaks by HR in SUM1315 cells but decreased repair in MDA-MB-468 stably expressing the DR-GFP reporter, albeit at a much lesser magnitude. (C) I-SceI expression in SUM1315-DRGFP and MDA-MB-468-DRGFP transfected cells. Statistical analysis was performed using a two-way ANOVA and multiple comparison test using Tukey test, p values are indicated. (D-E) P-53BP1 levels are reduced by (D) GANT61 treatment and (E) stable knockdown of GLI1 compared to controls. (F) Schematic illustrating the position of the I-PpoI restriction site in the 28S region of the 45S rDNA repeat sequence, 5' to site D in Fig. 1C. The I-PpoI recognition sequence is depicted in grey. (G) SUM1315 cells were transfected with pBABE-HA-ER-I-PpoI and treated with either ethanol (EtOH) as a vehicle control or tamoxifen. Genomic DNA was isolated and qPCR was used to quantify an amplicon spanning the I-PpoI restriction site. Reduced abundance of the amplicon is indicative of I-PpoI-induced rDNA breaks. Statistical analysis was performed with a one-way ANOVA and Dunnett's multiple comparison test. (H) Protein lysates from Fig. 3G demonstrated induction of phospho-NBS1 and phospho-ATM after tamoxifen treatment in NT and shGLI1, confirming DNA damage resulting from tamoxifen-induced I-PpoI double-strand break. (I) Representative confocal images of NIR (left) and IR (right) SUM1315 cells. Magnified 3D images (bottom left) depict increased GLI1 and P-53BP1 localization in the nucleolus marked by UBF and DAPI post-IR. All error bars depict the SEM.

Supplementary figure 4:



Supplementary Figure S4. Inhibiting Hh/GLI signaling impairs re-activation of Pol I activity following irradiation-induced DSBs. (A-B) Induction of Pol I activity following repair of IR- induced rDNA damage, as quantitated by qPCR of two different amplicons in the 5' ETS of 45S rDNA, occurs in non-targeting controls, but not in shGLI1 cells, consistent with delayed repair. Statistical significance was determined with a two-way ANOVA and Tukey multiple comparison test. Comparisons for NT- and shGLI1- NIR group with cells collected after different time points post IR and NT and shGLI1- NIR group with cells collected after different time points post IR are shown. (C-D) Introducing I-PpoI expression plasmid (relative to control plasmid) caused an appreciable decrease in the number of colonies. (C) GLI1-silenced cells transfected with I-PpoI showed a striking decrease in the number of colonies formed relative to NT cells. This is indicated by representative images of colony formation in SUM1315 NT and shGLI1 cells. (D) Percent change in the number of colonies formed I-PpoI- transfected *versus* empty vector-transfected SUM1315 NT and shGLI1 cells indicates that shGLI1 cells are higher sensitivity in shGLI1 cells compared to control upon rDNA damage. Stable silencing of GLI1 compromises (E) spheroid growth and (F) colony formation following IR. (G) GANT61 also reduces colony formation in irradiated SUM1315 cells. Statistical analysis was performed using a two-way ANOVA and multiple comparison Tukey test, p values are indicated. (H-I) Colony formation was scored with SUM1315 cells treated with doxorubicin. Doxorubicin (0.1µM) significantly compromised colony formation of GLI1-deficient SUM1315 cells compared to non-targeting (NT) shRNA controls as represented in (H) and quantified in

(I). (J) Cell viability scored by MTS assay was also significantly decreased in doxorubicin-treated SUM1315 shGLI1 cells compared to NT cells ($p < 0.01$). All error bars depict the SEM. Statistical analysis was performed using a multiple comparison two-way ANOVA followed by Tukey's comparison test, p values are indicated.

Target Site	Primer Pair
ChIP Site A	F: 5'-CAGGTGTTTCCTCGTACCG-3' R: 5'-CAAGGCACGCCTCTCAGAT-3'
ChIP Site B	F: 5'-CGACGTCGGCTACCCACC-3' R: 5'-GACTGGAGAGGCCTCGGG-3'
ChIP Site C	F: 5'-GGTTGATATAGACAGCAGGAC-3' R: 5'-CTCCCGTCCACTCTCGAC-3'
ChIP Site D	F: 5'-CTATGACTCTCTTAAGGTAGC-3' R: 5'-CAGACTAGAGTCAAGCTCAAC-3'
ChIP Site E	F: 5'-TGGTGGGATTGGTCTCTCTC-3' R: 5'-CAGCCTGCGTACTGTGAAAA-3'
45S rRNA 5'-ETS 851-961	F: 5'-GAACGGTGGTGTGTCGTT-3' R: 5'-GCGTCTCGTCTCGTCTCA-3'
45S rRNA 5'-ETS 1297-1483	F: 5'-CAGGTGTTTCCTCGTACCG-3' R: 5'-GCTACCATAACGGAGGCAGA-3'
I-PpoI Flanking	F: 5'-CCAGTGCTCTGAATGTCAAAG-3' R: 5'-GGACAGTGGGAATCTCGTTC-3'

Supplementary Table S1. Sequences of primer pairs used in this study. F and R designate the forward and reverse primers, respectively.

QUANTITATIVE IMAGING AND MOLECULAR ANALYSIS OFFER INSIGHTS
INTO THE ROLE OF HEDGEHOG SIGNALING IN AUGMENTING TUMOR
HYPOXIA

by

TSSHERING D LAMA-SHERPA, SHAMIK DAS, DOMINIQUE C HINSHAW,
SARAH C KAMMERUD, PATRICK N SONG, HEBAALLAH M ALSHEIKH, ANNA
G SORACE, RAJEEV S. SAMANT, AND LALITA A. SHEVDE

In preparation for Cancer Research

Format adapted for dissertation

Abstract

Metastases account for the majority of mortalities related to breast cancer. The onset and sustained presence of hypoxia strongly correlates with increased incidence of metastasis and unfavorable prognosis in breast cancer patients. The Hedgehog (Hh) signaling pathway is dysregulated in breast cancer and its abnormal activity enables tumor progression and metastasis. We hypothesized that Hh activity crafts a hypoxic tumor microenvironment and enables adaptation of breast cancer cells to hypoxia. In this study, using radiolabeled tracer [¹⁸F]-fluoromisonidazole (FMISO) positron emission tomography (PET) imaging we show that pharmacological inhibition of Hh signaling in a syngeneic mammary tumor model mitigates tumor hypoxia. Mechanistically, we see that in hypoxia, Hh activity is robustly activated and institutes increased HIF signaling in a VHL-dependent manner. The collective findings establish a novel perspective on Hh activity in crafting a hypoxic tumor and molecularly navigating the tumor cells to engage adaptation to hypoxic conditions. Importantly, we present a strategy of utilizing longitudinal hypoxia imaging to measure the efficacy of Vismodegib (GDC-0449) in a preclinical model of TNBC.

Keywords: Hypoxia, Hedgehog pathway, Breast Cancer, Metastasis

Introduction

Breast cancer is one of the commonly occurring cancer in women worldwide. Hypoxic conditions within breast cancer have been identified as an adverse indicator for patient prognosis (1). Hypoxia is created by the rapid increase in cellular density and concomitantly decreased apoptosis. The need for higher oxygen consumption paired with remoteness from the nearest blood vessel reduces oxygen availability and consequently drives hypoxia. Hypoxia leads to the formation of structurally and functionally abnormal blood vasculature within the solid tumor, aiding in tumor progression (2). From an extensive study, it has been shown that the mean partial pressure of oxygen (PO₂) in breast tumors ranges from 2.5 to 28 mm of mercury (Hg), with a median value of 10 mm Hg, as compared with 65 mm Hg in normal human breast tissue (3). Intratumoral hypoxia profoundly modulates gene expression, cellular communication, and reconfigures the tumor microenvironment (structurally and compositionally); therefore, it is critical to decipher the mechanisms underlying the development of a hypoxic environment and the cellular adaptation of cancer cells to hypoxia.

The transcription factor HIF-1 α is accountable for the vast responses during hypoxia. HIF-1 α dimerizes with HIF-1 β and transactivates numerous genes through binding to hypoxia response elements (HREs) in promoters or enhancers, leading to activated expression of several genes that impinge upon angiogenesis, metabolic reprogramming, survival, and metastatic dissemination (3,4). HIF-1 α transcription factor is regulated in an oxygen-dependent manner through prolyl hydroxylation by proline hydroxylase (PHD), ubiquitination by an E3 ligase called Von Hippel Lindau protein (VHL), and proteasomal degradation by the 26S proteasome (5). Recent studies have

shown that growth factor signaling pathways like phosphatidylinositol-3-kinase (PI3K), mouse double minute 2 homolog (Mdm2), and heat shock protein 90 (HSP90) can activate the HIF-1 α mediated hypoxic response (6).

The Hedgehog (Hh) signaling pathway is aberrantly activated in breast cancer (7). We and others have reported that aberrant Hh activity enables and enhances tumor malignancy and metastatic potential (8-10). Hh signaling is much appreciated for its indispensable involvement in tissue development, patterning, differentiation, epithelial mesenchymal transition (EMT), and stem cell maintenance (7). The canonical mammalian Hh signaling pathway can be initiated by any of its three ligands, Desert hedgehog (DHH), Indian hedgehog (IHH), or Sonic hedgehog (SHH). Once ligand binding occurs, the 12-pass transmembrane protein receptors, Patched1 (PTCH1), relieve their inhibitory action on Smoothed (SMO), a 7-pass transmembrane G-protein coupled signal transduction molecule. SMO then activates a signaling cascade resulting in the translocation of the glioma associated oncogene homolog (GLI) transcription factors to the nucleus. Of the three GLI transcription factors, GLI1 exclusively acts as a transcription activator, whereas GLI2 and GLI3 can act either as repressors or activators in a context-dependent manner (7). However, besides the classical pathway, multiple tumor microenvironment (TME) non-classical mechanisms have been identified in eliciting GLI protein activity in the absence of Hh ligands, that include TGF β , OPN, and EGF (11). As such, the TME significantly influences the behavior of cancer cells and ultimately their response to therapy. Recent studies have implicated a possible role of Hh signaling in the hypoxic TME (12-15). However, the functional and mechanistic role of

the Hh pathway in crafting a hypoxic niche and influencing cancer cell adaptation to the hypoxic microenvironment remains unexplored.

[¹⁸F]-FMISO PET imaging is widely used to detect intracellular hypoxia within the tumor in breast cancer patients and in preclinical models of breast cancer (16-18). [¹⁸F]-FMISO is a radiolabeled tracer that non-invasively diffuses into cells under normal oxygen concentration. However, under hypoxic conditions, the nitroimidazole group of [¹⁸F]-FMISO is reduced and retained in PO₂ less than or equal to 10mmHg. [¹⁸F]-FMISO covalently binds to cellular molecules at rates that are inversely proportional to oxygen concentration. [¹⁸F]-FMISO has a half-life of 110 minutes and significant uptake is seen in the liver, kidney, and bladder (19). [¹⁸F]-FMISO PET imaging has been assessed as a predictive prognostic factor in patients with pancreatic and breast cancer (16,20). [¹⁸F]-FMISO retention at higher rates has been correlated with shorter progression-free survival in renal and head-and-neck cancer (21).

We used a preclinical syngeneic mammary tumor model to investigate the role of Hh signaling in sculpting tumor hypoxia. We quantified hypoxia using [¹⁸F]-FMISO PET imaging and also undertook mechanistic investigations to unravel the role of Hh activity in programming tumor cells to adapt to hypoxia. Our findings provide novel insight into the role of Hh pathway in modulating temporal changes in tumor hypoxia. We also show that hypoxia exacerbates Hh/GLI transcriptional activity that in turn, enables robust HIF-signaling. Our findings implicate that Hh signaling-associated hypoxia adaptation presents as a targetable vulnerability of breast cancer.

Materials and Methods

Cell Culture

SUM1315 and SUM159 breast cancer cells acquired from Asterand, Inc were cultured in DMEM/F12 (Thermo Fisher, Waltham, MA) supplemented with 5% heat-inactivated fetal bovine serum (Thermo Fisher), 5 mg/ml insulin (Sigma-Aldrich, St. Louis, MO) and either 10 ng/ml EGF (Sigma-Aldrich) or 1 μ g/ml hydrocortisone (Sigma-Aldrich) respectively, without antibiotics or antimycotics (15). PLEASE ADD DETAILS ABOUT THE 4T1 CELLS. All cells were maintained in a humidified 5% CO₂ environment.

Hypoxia Treatment conditions

For hypoxic culture conditions, cells were incubated at 37°C in a humidified hypoxic chamber (Billups Rothenberg Inc., Del Mar, CA) infused with 1% O₂, 5% CO₂ and 94% N₂. Cells were incubated for 24hrs unless mentioned otherwise.

Hedgehog Pathway Inhibition

Breast cancer cells were treated with various inhibitors. Unless otherwise mentioned, cells were pretreated for 24 hours with the inhibitors, followed by other treatments. The inhibitors include GANT61 (Tocris, Avonmouth, Bristol, UK), BMS-833923 (Selleck Chemicals, Houston, TX), and Vismodegib (Selleck Chemicals). SUM1315 and SUM159 were stably transfected with non-targeting plasmid control (NT) or GLI1 shRNA (shGLI1) and selected on G418 (Invitrogen, Carlsbad, CA) as previously described (22).

Western Blotting Analysis

Whole cell lysates were prepared by lysing cells with 2X Laemmli buffer with β -mercaptoethanol, followed by boiling at 95°C for 5 minutes. For cytoplasmic and nuclear isolation, the proteins were collected using NE-PER kit (Pierce Rockford, IL) following the manufacturer's protocol. Thirty micrograms of protein was resolved by SDS-PAGE and transferred to polyvinylidene difluoride membranes. Membranes were incubated overnight at 4°C with primary antibodies. Immunoblotting was done with GLI1 (2553, Cell Signaling Danvers, MA), HDAC1 (2062, Cell Signaling), Histone H3 (4499, Cell Signaling), GLI2 (PA-1941, BosterBio, Pleasanton, CA). β -actin (A3854, Sigma-Aldrich) was used to confirm equal loading for whole cell lysates. β -tubulin (2146, Cell Signaling) or HDAC1 antibodies were used to determine cytosolic and nuclear fraction purity, respectively. Anti-rabbit or anti-mouse HRP-conjugated secondary antibody (GE Healthcare, Chicago, IL) were used for detection, and blots were developed with either ECL or Super Signal substrate (Pierce, Rockford, IL) and imaged using an Amersham Imager 600.

Luciferase Assays

Cells were seeded at 25,000 per well of a 96-well plate and the following day transiently transfected with 50ng/well of HRE-luc or 8X-GLI-luc reporter DNA using Fugene6 (Promega, Madison, WI). Twenty-four hours later, the transfection mix was removed and replaced with regular growth media containing DMSO or 10 μ M GANT61 or 2.5 μ M BMS-833923 or 0-100 μ M acriflavine. The cells were placed in hypoxia in

media containing inhibitor for another 24 hours. The data represented is the relative light units normalized to total protein, performed in triplicate.

Drug/Inhibitor Treatments

Twenty-four hours after seeding, cells were pre-treated with 150 μ M VH298 (Sigma-Aldrich) or 10 μ M clasto-Lactacystin β -Lactone (Sigma-Aldrich) for 2 hours. The media was replaced with media without inhibitors and put in hypoxia chamber for 24 hours. Lysates were collected with 2X Laemmli buffer.

Quantitative RT-PCR (qRT-PCR)

RNA was collected from SUM1315 and SUM159 cells using QIAGEN RNAeasy Mini Kit (Hilden, Germany). cDNA was synthesized using High Capacity Reverse Transcriptase Kit (Applied Biosystems, Foster City, CA), and qRT-PCR was performed using StepOnePlus Real-Time PCR System (Applied Biosystems). TaqMan Fast Advanced Master mix (Applied Biosystems) was used for gene expression assays. TaqMan primers (Life Technologies, Carlsbad, CA) used were GLI1 (Hs01110766_m1), GLI2 (Hs00257977_m1), PTCH1 (Hs00181117_m1), SMO (Hs01090242_m1), PDK1 (Hs01561850_m1), CA9 (Hs00154208_m1), VEGFA (Hs00900055_m1), BNIP3 (Hs00969291_m1), and ACTB (Hs99999903_m1). Transcript expression levels were calculated using the change in the C_T method and normalized to β -actin as previously described (23).

In vivo FMISO/PET Imaging and Analysis

The animal studies were conducted under an IACUC-approved protocol. Eight week old female Balb/c mice were injected with 4T1 luciferase-expressing cells into the third mammary fat pad at a concentration of 500,000/100uL in HBSS buffer. Tumor growth was documented once per week by bioluminescent imaging (BLI) using the IVIS Imaging System (Xenogen Corp., Alameda, CA) and thrice weekly by caliper measurement. The mice were randomized based on the BLI average radiance when the average tumor diameter reached approximately 3mm (12 days post injection). Mice were orally administered 100uL of Vismodegib or DMSO vehicle control (2mg/mouse) thrice weekly following randomization for a total of 7 doses. Mice were imaged with [¹⁸F]-FMISO-PET at baseline (day 13 post injection) and on days 20 and 27. Approximately 150 μCi of [¹⁸F]-FMISO was injected retro-orbitally into each mouse, and 80 minutes later, mice were anesthetized with isoflurane for PET/CT image acquisition. SOFIE GNEXT PET/CT scanner (SOFIE, Culver City, CA) was used to acquire the PET/CT images. The PET/CT image analysis was done using MATLAB software by drawing three-dimensional (3D) regions of interest (ROIs) around the tumor volume using CT images to confirm tumor location. The mean standardized uptake values (SUV) were measured in the ROI and normalized to the body weight of the mice and the injected dose. Normal muscle [¹⁸F]-FMISO uptake was measured as a control, and tumor-to-muscle ratio was obtained for each mouse. SUV_{mean} of tumors at baseline and post-Vismodegib treatment were compared to the vehicle control.

Immunohistochemistry

Primary tumors were collected for immunohistochemical processing. Paraffin-embedded slides were cut into 5µm sections and stained with CA9 (Novus Biologicals, Centennial CO) at 1:400 dilution overnight. Tumor sections (5µm) from mice treated with either vehicle control or Vismodegib were also stained with isoleucin B4 (Vector Laboratories, Burlingame, CA) using the Vectastain Elite ABC-HRP kit (Vector Laboratories). Briefly, after deparaffinization and rehydration, citrate antigen retrieval and peroxidase blocking was performed. Samples were incubated overnight in primary antibody in binding buffer (10mM HEPES, 250mM NaCl, 0.1mM Ca⁺, 0.1% BSA), then washed with PBS + 0.05% Tween-20. Samples were incubated in ABC reagent, washed, and developed with DAB solution before being counterstained with Harris hematoxylin, dehydrated, cleared, and mounted. Isolectin B4-stained slides were used to evaluate micro-vessel density by quantitating total micro-vessels per field. Collagen fibers in the tumor tissue were stained using picosirius red staining kit (Polysciences, Inc., Warrington, PA) as per manufacturer's instructions. Brightfield images were captured using a Nikon Eclipse E200 (Nikon, Tokyo, Japan). Polarized light images were captured using a Nikon Eclipse Ti-U. Collagen content was measured using Image J by converting collagen staining to mean gray intensity.

Ex-vivo lung imaging

Mice were injected intraperitoneally with D-luciferin at 150 mg/kg. 10 minutes later, mice were put under anesthesia using isoflurane gas and euthanized. Immediately after necropsy, lungs were individually resected and placed into black paper tray. 3 drops of luciferin at 150 mg/kg were added and lungs imaged at 3 and 5 mins, 10bin, level B.

Assays for glucose consumption and lactate production

Conditioned medium from cells cultured in normoxic or hypoxic conditions was collected, cleared by centrifugation, and assayed for glucose and lactate levels using the Amplex Red Glucose/Glucose Oxidase Assay Kit (Invitrogen) and Lactate Colorimetric/Fluorometric Assay Kit (BioVision, Milpitas, CA), respectively.

Statistical Analysis

Statistical analysis were assessed by using multiple comparison test per experimental design. The graphs were plotted using GraphPad Prism 8 software (La Jolla, CA) and are representative of three independent replicates. Statistical significance was determined if the analysis reached 95% confidence and for $p < 0.05$. The statistical tests used are listed in the corresponding figure legends. When appropriate, error bars represent the standard error of the mean.

Results

Vismodegib decreases tumor hypoxia in the 4T1-Balb/c preclinical model

To test the hypothesis that Hh activity influences the hypoxic TME, we adopted [^{18}F]-FMISO-PET imaging and histological analysis of the tumor, in response to a Hh inhibitor. [^{18}F]-FMISO-PET imaging is a quantitative tool that can be used to evaluate temporal changes in hypoxia (24). We conducted a longitudinal study using [^{18}F]-FMISO-PET imaging in a 4T1 syngeneic mouse triple-negative mammary tumor model and administered Vismodegib, an FDA-approved, orally available, Hh pathway inhibitor. Female BALB/c mice bearing orthotopic mammary 4T1 tumors were randomized into

Vismodegib and control groups when the tumor diameter averaged ~3-4mm. Mice were orally administered either Vismodegib or vehicle control thrice weekly for 2 weeks. [¹⁸F]-FMISO-PET imaging on day13 was used as a baseline before administration of Vismodegib. [¹⁸F]-FMISO-PET imaging after one and two weeks of DMSO or Vismodegib administration was evaluated on days 20 and 27 respectively (Figure 1A). At baseline, both groups started out with comparable average tumor size and tumor hypoxia (as determined by average tumor radiance and tumor standard uptake value (SUV) respectively). [¹⁸F]-FMISO retention longitudinally increased in tumors of mice from the control group, while in the Vismodegib-treated mice FMISO uptake remained steady (Figure 1B). On day 20 and day 27, relative to mice administered vehicle control, hypoxia within the tumor is significantly reduced in the Vismodegib-treated group as evident by lower values of tumor SUV and tumor to muscle SUV ratio (Figure 1C, Supplementary Figure 1A). Primary tumor growth was comparable in Vismodegib and vehicle control-treated mice as indicated by the bioluminescence (BLI) readings of the tumor, caliper measurements, and tumor weight (Figure 1D, Supplementary Figure 1B, and Supplementary Figure 1C). In order to complement temporal changes in hypoxia, we sought to further analyze the tumors histologically at the end of treatment. Qualitative CA9 immunohistochemical analysis informs about the extent of hypoxia in the tissue (Please cite 1-2 references here). While the tumors from vehicle control group show evidence of robust hypoxia, the tumors from the Vismodegib-treated group have characteristically weaker staining for CA9 staining (Figure 1E). These findings are in agreement with the [¹⁸F]-FMISO retention data. Collectively, these findings suggest that

Hh inhibition with Vismodegib reduces the longitudinal progression of tumor hypoxia *in vivo*.

Vismodegib remodels the extracellular matrix and decreases pulmonary metastasis

Hypoxic tumors are characterized by abnormal vasculature due to temporal changes in oxygenation status, leading to the formation of disorganized and leaky blood vessels during tumor progression (25). Our previous research showed that Hh signaling enhances pro-angiogenic signaling (26). We examined these 4T1 tumors for their vascularity by staining for isolectin B4. Vehicle control tumors show large diameter blood vessels and significantly higher microvessel density compared to the Vismodegib-treated tumors (Figure 2A). In addition to enabling angiogenesis, hypoxia also alters the organization of collagen in the TME, facilitating tumor invasion and metastasis (27,28). Since the Vismodegib-treated mice showed decreased metastases, we queried whether this could be attributed to collagen deposition alterations within the primary tumors. Interestingly, we found that Vismodegib-treated tumors had broken and misaligned collagen fibers compared to straight and continuously aligned fibers in control. This indicates Vismodegib reduces crosslinked collagen within the extracellular matrix of the tumor as determined by picrosirius red staining of the primary tumors (Figure 2C, Supplementary Figure 2A). Aligned with these results, BLI of the lungs shows significantly decreased lung metastasis in the Vismodegib-treated mice (Figure 2B). Overall, our data indicates that Vismodegib remarkably remodels the TME and decreases metastasis to the lungs.

Hypoxia activates Hh signaling in tumor cells

Building upon the leads presented thus far, we sought to evaluate the relevance of Hh activity in enabling adaptation to hypoxia. We first scored the effect of hypoxia on Hh transcriptional activity. We transiently transfected SUM1315, SUM159, MDA-MB-231, MDA-MB-436, and MDA-MB-468 cell lines with an 8X-GLI reporter construct and incubated the cells in hypoxia for 24 hrs. We see that hypoxia supports a significant increase in 8X-GLI reporter activity relative to cells in normoxia (Figure 3A). In agreement with this, GLI1, the terminal effector protein of the Hh pathway demonstrates nuclear accumulation in hypoxic conditions (Figure 3B). In order to query the direct effect of HIF-1 α in navigating this increase in Hh activity, we treated cells with acriflavine, which prevents dimerization of HIF-1 α . Acriflavine caused a significant decrease in 8X GLI activity in hypoxic conditions suggesting that HIF-mediated signaling impacts Hh activation (Figure 3C). Concordant with these observations, we see that transcript levels of *bonafide* Hh pathway target genes GLI1, GLI2, and PTCH1 are upregulated in hypoxia. To appreciate the relevance of hypoxia-induced elevated Hh activity, we treated cells with GANT61, a direct inhibitor of GLI1/2. GANT61 antagonized hypoxia-induced upregulation of steady state transcript levels of GLI1, GLI2, and PTCH1 (Figure 3D) underscoring the role of hypoxia in elevating Hh activity. Taken together, the data suggest that hypoxia exacerbates Hh signaling in TNBC cells.

Hh activity reinforces hypoxic response in TNBC cell lines

Elevated Hh activity in hypoxic culture conditions suggests that the pathway likely plays an essential role in sustenance of the cancer cells in a harsh

microenvironment. To interrogate the significance of hypoxia-induced upregulation of Hh activity, we stably silenced GLI1 in SUM1315 and SUM159 cells and evaluated the transcription activity of HIF-1 α using the HRE-luc reporter in hypoxic conditions (29). Abrogating GLI1 expression led to significant decrease in HRE-luc activity (Figure 4A). We also assessed the expression of hypoxia gene targets BNIP3, CA9, and VEGFA. While all of these are upregulated in hypoxia, abrogating GLI1 significantly decreased their steady-state transcript levels in SUM1315 and SUM159 cells (Figure 4B). HIF-1 α navigates a shift of cancer cell metabolism by increasing reliance on anaerobic glycolysis (30). Glucose consumption and lactate production are key features of this cellular metabolic alteration (31). We see that silencing GLI1 led to a significant decrease in cellular glucose consumption (Figure 4C) and lactate production compared to the non-target control cells in hypoxic culture conditions, (Figure 4D), indicating that Hh/GLI activity perpetuates a robust hypoxia response in breast cancer cells.

Hh signaling pathway increases HIF- α transcription factor stability in VHL-dependent mechanism

HIF-1 α protein stability underlies an effective adaptive response in hypoxic cells (4). In order to evaluate the effect of Hh/GLI activity on HIF-1 α , we inhibited Hh/GLI using two inhibitors that act at non-overlapping nodes in the Hh pathway. While GANT61 inhibits binding of GLI to the DNA (32), (BMS) 833923 targets the Smoothed regulatory molecule (33). HIF-1 α protein is stably expressed in hypoxic conditions; however, inhibition of Hh leads to decreased cellular accumulation of HIF-1 α in SUM1315, SUM159, and 4T1 cells (Figure 5A, Supplementary Figure 3A). Building

upon this lead, we enquired the cellular levels of VHL, a well-known regulator of HIF-1 α protein stability. We found that inhibiting Hh activity using GANT61 led to increased VHL protein expression in a concentration-dependent manner in SUM1315 and SUM159 (Figure 5B). Silencing GLI1 led to increased VHL expression in normoxic and hypoxic conditions (Figure 5C, Supplementary Figure 3B). Hh inhibition did not alter VHL transcript levels (Figure 5D). To evaluate if Hh-mediated HIF-1 α protein stability is VHL-dependent, we used VH298, a VHL inhibitor that covalently binds to VHL (cite references here). We found that HIF-1 α protein stability in GLI1 silenced cells recovered after VHL was inhibited by VH298 (Figure 5E). Additionally, to verify that Hh-mediated HIF-1 α protein stability is dependent on VHL mediated proteasomal degradation, we used lactacystin, a 26S proteasomal inhibitor. We uncovered that HIF-1 α protein stability in GLI1 silenced cells recovers following proteasome inhibition (Figure 5F). Taken together, we established that Hh-mediated HIF-1 α stability is dependent on inhibition of VHL regulation.

Discussion

The ability of tumor cells to adapt to hypoxia determines their ability to survive the formidable hypoxic microenvironment. HIFs play a critical role in the survival of cancer cells by regulating genes that enable angiogenesis, metabolic reprogramming, drug resistance, and survival (34). Breast cancer can metastasize to the lungs, bone, brain, and liver (35). The presentation of metastasis drastically reduces survival in breast cancer patients. In breast cancer, hypoxia is known to promote metastasis (36,37). Given that Hh signaling is abnormally activated in breast cancer, we investigated its role in influencing the hypoxic TME and mechanistically enhancing adaptation to hypoxia. In

this study, we used [¹⁸F]-FMISO-PET imaging to quantitate longitudinal changes in tumor hypoxia. In order to specifically query the role of Hh activity in shaping the hypoxic TME, we administered Vismodegib in a pre-clinical mammary tumor model. To our knowledge, this is the first study to establish that Hh pathway inhibition antagonizes the progressive hypoxic TME, and interferes with VHL-mediated HIF-1 α accumulation in the tumor cells.

Previous studies with inhibition of HIF activity by RNA interference or digoxin found a decrease in both, primary tumor growth and lung metastasis, in mice bearing MDA-MB-231 xenografts (36). However, in our immune competent preclinical model, Vismodegib mitigated tumor hypoxia without an appreciable difference in tumor size. We have previously reported that Vismodegib alters the tumor immune portfolio from an immunosuppressive to an immune reactive type (38). Since a critical step to metastasis is immune evasion, Vismodegib might support this process by mitigating tumor hypoxia, consequently affecting immune cell function.

We determined that Hh inhibition compromises HIF-1 α protein stability in a VHL-dependent manner. In hypoxia, VHL is moderated by a negative feedback loop through HIF binding at the HRE site in the VHL promoter (39). In the current study, we found no significant changes in VHL mRNA expression with Hh inhibition, although, we registered an increase in VHL protein levels in hypoxic conditions in breast cancer cells. Previous studies by Cho et al., showed that VHL inhibits GLI1 nuclear localization and colocalizes with GLI1 by GST pull down assay implicating a role for VHL-mediated regulation of Hh (40). Our data indicates that Hh activity post-translationally regulates

VHL, although whether Hh plays a role in post-translational modification of VHL remains unexplored.

Hypoxic TME presents as a barrier for effectiveness of common cancer treatments. Hypoxic cancer cells are resistant to radiation therapy, immunotherapy, and chemotherapy (41,42). Therefore, altering TME by mitigating hypoxia might make the tumor more susceptible to these therapies. Hypoxia is a known indicator of adverse outcomes in breast cancer patients (43). Our data indicates that Vismodegib moderates hypoxia in a pre-clinical mammary cancer model, providing a supporting rationale to use Vismodegib, which is already in clinic for acute myeloid leukemia and advanced basal cell carcinoma (44), for breast cancer patients that present with elevated tumor hypoxia. As such, the use of Vismodegib to target hypoxic tumors presents as an opportunity to decrease metastasis in breast cancer. Furthermore, using a clinically relevant imaging method for hypoxia, such as [^{18}F]-FMISO-PET imaging, lends us the possibility to longitudinally monitor patients receiving cancer treatment.

Conclusion

Solid tumors are often challenged with a hypoxic microenvironment due to increased demand for oxygen in the proliferating cells. Moreover, the proportions of hypoxic tumor cells in the primary tumor strongly correlate with the incidence of metastasis, treatment resistance, and poor prognosis. Overall, our study revealed that inhibiting Hh signaling ameliorated the tumor hypoxic landscape with a concomitant decrease in metastasis. Molecularly, we determined that Hh blockade significantly mitigated the ability of tumor cells to adapt to hypoxia. Thus, the collective findings

establish a novel perspective on the benefit of Hh inhibitors in impeding hypoxia-mediated tumor progression and metastasis. Using clinically relevant FMISO-PET imaging presents the opportunity to translate this modality to monitor response to Vismodegib therapy.

References

1. Vaupel P. Prognostic potential of the pre-therapeutic tumor oxygenation status. *Advances in experimental medicine and biology* **2009**;645:241-6 doi 10.1007/978-0-387-85998-9_36.
2. Vaupel P, Mayer A, Höckel M. Tumor Hypoxia and Malignant Progression. *Methods in Enzymology*. Volume 381: Academic Press; 2004. p 335-54.
3. Semenza GL. The hypoxic tumor microenvironment: A driving force for breast cancer progression. *Biochimica et biophysica acta* **2016**;1863(3):382-91 doi 10.1016/j.bbamcr.2015.05.036.
4. Semenza GL. Defining the role of hypoxia-inducible factor 1 in cancer biology and therapeutics. *Oncogene* **2010**;29(5):625-34 doi 10.1038/onc.2009.441.
5. Kaelin WG, Jr., Ratcliffe PJ. Oxygen sensing by metazoans: the central role of the HIF hydroxylase pathway. *Molecular cell* **2008**;30(4):393-402 doi 10.1016/j.molcel.2008.04.009.
6. Masoud GN, Li W. HIF-1 α pathway: role, regulation and intervention for cancer therapy. *Acta pharmaceutica Sinica B* **2015**;5(5):378-89 doi 10.1016/j.apsb.2015.05.007.
7. Riobo-Del Galdo NA, Lara Montero Á, Wertheimer EV. Role of Hedgehog Signaling in Breast Cancer: Pathogenesis and Therapeutics. *Cells* **2019**;8(4) doi 10.3390/cells8040375.
8. Das S, Samant RS, Shevde LA. Hedgehog signaling induced by breast cancer cells promotes osteoclastogenesis and osteolysis. *The Journal of biological chemistry* **2011**;286(11):9612-22 doi 10.1074/jbc.M110.174920.
9. Yao Z, Han L, Chen Y, He F, Sun B, kamar S, *et al.* Hedgehog signalling in the tumourigenesis and metastasis of osteosarcoma, and its potential value in the clinical therapy of osteosarcoma. *Cell Death & Disease* **2018**;9(6):701 doi 10.1038/s41419-018-0647-1.
10. D'Amato C, Rosa R, Marciano R, D'Amato V, Formisano L, Nappi L, *et al.* Inhibition of Hedgehog signalling by NVP-LDE225 (Erismodegib) interferes with growth and invasion of human renal cell carcinoma cells. *British journal of cancer* **2014**;111(6):1168-79 doi 10.1038/bjc.2014.421.
11. Shevde LA, Samant RS. Nonclassical hedgehog-gli signaling and its clinical implications. *International Journal of Cancer* **2014**;135(1):1-6 doi 10.1002/ijc.28424.

12. Onishi H, Kai M, Odate S, Iwasaki H, Morifuji Y, Ogino T, *et al.* Hypoxia activates the hedgehog signaling pathway in a ligand-independent manner by upregulation of Smo transcription in pancreatic cancer. *Cancer science* **2011**;102(6):1144-50 doi 10.1111/j.1349-7006.2011.01912.x.
13. Liao C-W, Zheng C, Wang L. Down-regulation of FOXR2 inhibits hypoxia-driven ROS-induced migration and invasion of thyroid cancer cells via regulation of the hedgehog pathway. *Clinical and Experimental Pharmacology and Physiology* **2020**;47(6):1076-82 doi 10.1111/1440-1681.13286.
14. Bhuria V, Xing J, Scholta T, Bui KC, Nguyen MLT, Malek NP, *et al.* Hypoxia induced Sonic Hedgehog signaling regulates cancer stemness, epithelial-to-mesenchymal transition and invasion in cholangiocarcinoma. *Experimental cell research* **2019**;385(2):111671 doi 10.1016/j.yexcr.2019.111671.
15. Park SH, Jeong S, Kim BR, Jeong YA, Kim JL, Na YJ, *et al.* Activating CCT2 triggers Gli-1 activation during hypoxic condition in colorectal cancer. *Oncogene* **2020**;39(1):136-50 doi 10.1038/s41388-019-0972-6.
16. Asano A, Ueda S, Kuji I, Yamane T, Takeuchi H, Hirokawa E, *et al.* Intracellular hypoxia measured by 18F-fluoromisonidazole positron emission tomography has prognostic impact in patients with estrogen receptor-positive breast cancer. *Breast Cancer Research* **2018**;20(1):78 doi 10.1186/s13058-018-0970-6.
17. Whisenant JG, Peterson TE, Fluckiger JU, Tantawy MN, Ayers GD, Yankeelov TE. Reproducibility of static and dynamic (18)F-FDG, (18)F-FLT, and (18)F-FMISO MicroPET studies in a murine model of HER2+ breast cancer. *Molecular imaging and biology* **2013**;15(1):87-96 doi 10.1007/s11307-012-0564-0.
18. Sorace AG, Syed AK, Barnes SL, Quarles CC, Sanchez V, Kang H, *et al.* Quantitative [(18)F]FMISO PET Imaging Shows Reduction of Hypoxia Following Trastuzumab in a Murine Model of HER2+ Breast Cancer. *Molecular imaging and biology* **2017**;19(1):130-7 doi 10.1007/s11307-016-0994-1.
19. Lee ST, Scott AM. Hypoxia Positron Emission Tomography Imaging With 18F-Fluoromisonidazole. *Seminars in Nuclear Medicine* **2007**;37(6):451-61 doi <https://doi.org/10.1053/j.semnuclmed.2007.07.001>.
20. Yamane T, Aikawa M, Yasuda M, Fukushima K, Seto A, Okamoto K, *et al.* [18F]FMISO PET/CT as a preoperative prognostic factor in patients with pancreatic cancer. *EJNMMI Research* **2019**;9(1):39 doi 10.1186/s13550-019-0507-8.
21. Fleming IN, Manavaki R, Blower PJ, West C, Williams KJ, Harris AL, *et al.* Imaging tumour hypoxia with positron emission tomography. *British journal of cancer* **2015**;112(2):238-50 doi 10.1038/bjc.2014.610.

22. Das S, Harris LG, Metge BJ, Liu S, Riker AI, Samant RS, *et al.* The hedgehog pathway transcription factor GLII promotes malignant behavior of cancer cells by up-regulating osteopontin. *The Journal of biological chemistry* **2009**;284(34):22888-97 doi 10.1074/jbc.M109.021949.
23. Lama-Sherpa TD, Lin VTG, Metge BJ, Weeks SE, Chen D, Samant RS, *et al.* Hedgehog signaling enables repair of ribosomal DNA double-strand breaks. *Nucleic Acids Research* **2020** doi 10.1093/nar/gkaa733.
24. Xu Z, Li XF, Zou H, Sun X, Shen B. (18)F-Fluoromisonidazole in tumor hypoxia imaging. *Oncotarget* **2017**;8(55):94969-79 doi 10.18632/oncotarget.21662.
25. Forster JC, Harriss-Phillips WM, Douglass MJ, Bezak E. A review of the development of tumor vasculature and its effects on the tumor microenvironment. *Hypoxia (Auckland, NZ)* **2017**;5:21-32 doi 10.2147/hp.S133231.
26. Harris LG, Pannell LK, Singh S, Samant RS, Shevde LA. Increased vascularity and spontaneous metastasis of breast cancer by hedgehog signaling mediated upregulation of *cyr61*. *Oncogene* **2012**;31(28):3370-80 doi 10.1038/onc.2011.496.
27. Natarajan S, Foreman KM, Soriano MI, Rossen NS, Shehade H, Fregoso DR, *et al.* Collagen Remodeling in the Hypoxic Tumor-Mesothelial Niche Promotes Ovarian Cancer Metastasis. *Cancer Research* **2019**;79(9):2271 doi 10.1158/0008-5472.CAN-18-2616.
28. Grossman M, Ben-Chetrit N, Zhuravlev A, Afik R, Bassat E, Solomonov I, *et al.* Tumor Cell Invasion Can Be Blocked by Modulators of Collagen Fibril Alignment That Control Assembly of the Extracellular Matrix. *Cancer Research* **2016**;76(14):4249 doi 10.1158/0008-5472.CAN-15-2813.
29. Emerling BM, Weinberg F, Liu JL, Mak TW, Chandel NS. PTEN regulates p300-dependent hypoxia-inducible factor 1 transcriptional activity through Forkhead transcription factor 3a (FOXO3a). *Proceedings of the National Academy of Sciences of the United States of America* **2008**;105(7):2622-7 doi 10.1073/pnas.0706790105.
30. Al Tameemi W, Dale TP, Al-Jumaily RMK, Forsyth NR. Hypoxia-Modified Cancer Cell Metabolism. *Frontiers in Cell and Developmental Biology* **2019**;7(4) doi 10.3389/fcell.2019.00004.
31. Lin X, Xiao Z, Chen T, Liang SH, Guo H. Glucose Metabolism on Tumor Plasticity, Diagnosis, and Treatment. *Frontiers in Oncology* **2020**;10(317) doi 10.3389/fonc.2020.00317.

32. Agyeman A, Jha BK, Mazumdar T, Houghton JA. Mode and specificity of binding of the small molecule GANT61 to GLI determines inhibition of GLI-DNA binding. *Oncotarget* **2014**;5(12):4492-503 doi 10.18632/oncotarget.2046.
33. Gibson MK, Zaidi AH, Davison JM, Sanz AF, Hough B, Komatsu Y, *et al.* Prevention of Barrett Esophagus and Esophageal Adenocarcinoma by Smoothed Inhibitor in a Rat Model of Gastroesophageal Reflux Disease. *Annals of Surgery* **2013**;258(1):82-8 doi 10.1097/SLA.0b013e318270500d.
34. Semenza GL. Molecular mechanisms mediating metastasis of hypoxic breast cancer cells. *Trends in molecular medicine* **2012**;18(9):534-43 doi 10.1016/j.molmed.2012.08.001.
35. Siegel RL, Miller KD, Jemal A. Cancer statistics, 2016. *CA: a cancer journal for clinicians* **2016**;66(1):7-30 doi 10.3322/caac.21332.
36. Zhang H, Wong CCL, Wei H, Gilkes DM, Korangath P, Chaturvedi P, *et al.* HIF-1-dependent expression of angiopoietin-like 4 and L1CAM mediates vascular metastasis of hypoxic breast cancer cells to the lungs. *Oncogene* **2012**;31(14):1757-70 doi 10.1038/onc.2011.365.
37. Gilkes DM, Semenza GL. Role of hypoxia-inducible factors in breast cancer metastasis. *Future oncology (London, England)* **2013**;9(11):1623-36 doi 10.2217/fon.13.92.
38. Hanna A, Metge BJ, Bailey SK, Chen D, Chandrashekar DS, Varambally S, *et al.* Inhibition of Hedgehog signaling reprograms the dysfunctional immune microenvironment in breast cancer. *OncoImmunology* **2019**;8(3):1548241 doi 10.1080/2162402X.2018.1548241.
39. Łuczak MW, Roszak A, Pawlik P, Kędzia H, Lianeri M, Jagodziński PP. Increased expression of HIF-1A and its implication in the hypoxia pathway in primary advanced uterine cervical carcinoma. *Oncology reports* **2011**;26(5):1259-64 doi 10.3892/or.2011.1397.
40. Cho HK, Kim SY, Kim KH, Kim HH, Cheong J. Tumor suppressor protein VHL inhibits Hedgehog-Gli activation through suppression of Gli1 nuclear localization. *FEBS letters* **2013**;587(7):826-32 doi 10.1016/j.febslet.2013.01.050.
41. Graham K, Unger E. Overcoming tumor hypoxia as a barrier to radiotherapy, chemotherapy and immunotherapy in cancer treatment. *International journal of nanomedicine* **2018**;13:6049-58 doi 10.2147/ijn.S140462.
42. Eckert F, Zwirner K, Boeke S, Thorwarth D, Zips D, Huber SM. Rationale for Combining Radiotherapy and Immune Checkpoint Inhibition for Patients With Hypoxic Tumors. *Front Immunol* **2019**;10:407- doi 10.3389/fimmu.2019.00407.

43. Muz B, de la Puente P, Azab F, Azab AK. The role of hypoxia in cancer progression, angiogenesis, metastasis, and resistance to therapy. *Hypoxia (Auckland, NZ)* **2015**;3:83-92 doi 10.2147/hp.S93413.
44. Xie H, Paradise BD, Ma WW, Fernandez-Zapico ME. Recent Advances in the Clinical Targeting of Hedgehog/GLI Signaling in Cancer. *Cells* **2019**;8(5) doi 10.3390/cells8050394.

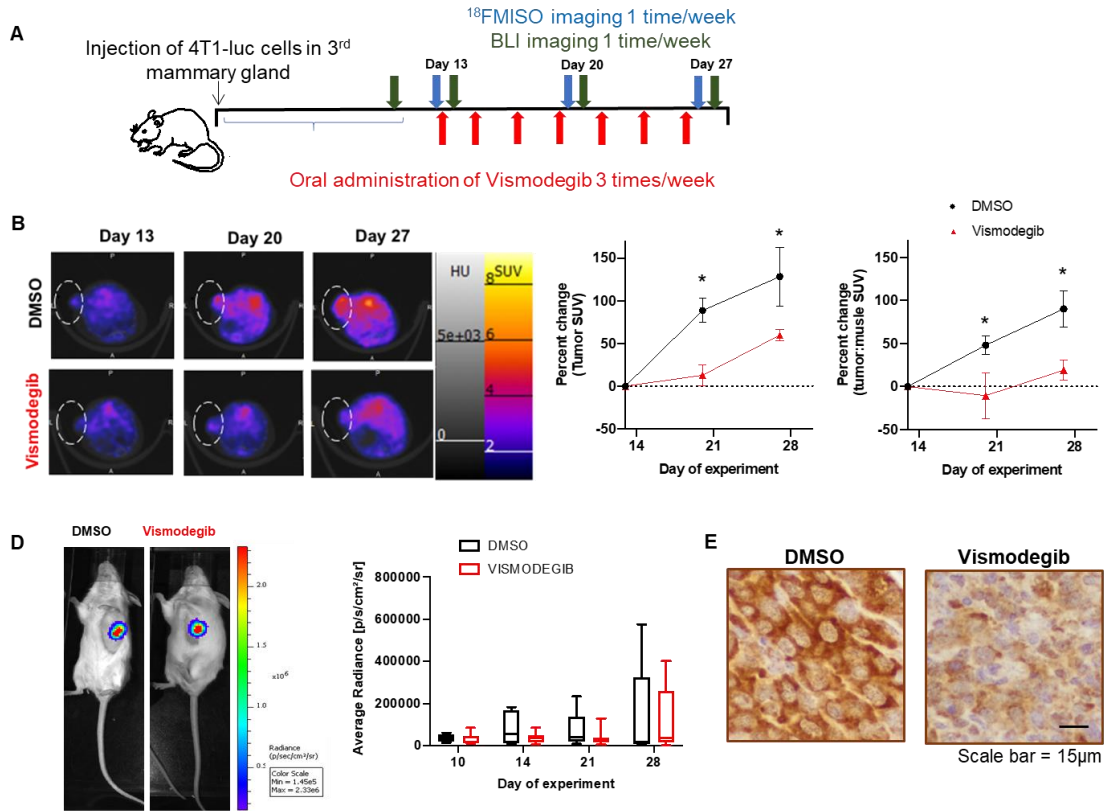


Figure 1. Inhibiting Hh signaling by Vismodegib mitigates tumor hypoxia. (A) Mice experiment schema of tumor implantation, FMISO-PET and BLI imaging, and Vismodegib administration schedule until Day 28. (B) 4T1 syngeneic mouse model showed decreased [¹⁸F]-FMISO uptake in tumor administered with Vismodegib compared to DMSO vehicle control as represented in the central slice images on Day 20 and Day 27. Tumors are indicated by white arrow. (C) Tumor hypoxia, as quantitated by percent change in mean SUV and tumor to muscle ratio shows significantly lower [¹⁸F]-FMISO uptake in second and third week after Vismodegib treatment compared to DMSO control. (n = 5; ANOVA, sidak's multiple comparisons test); *, p < 0.05 (D) Representative images of tumor BLI on Day 28. Average tumor size between the groups is not significantly different as imaged by the BLI. (E) Primary tumor staining for CA9 shows decreases in expression in Vismodegib treated mice compared to DMSO vehicle control. All error bars depict the SEM.

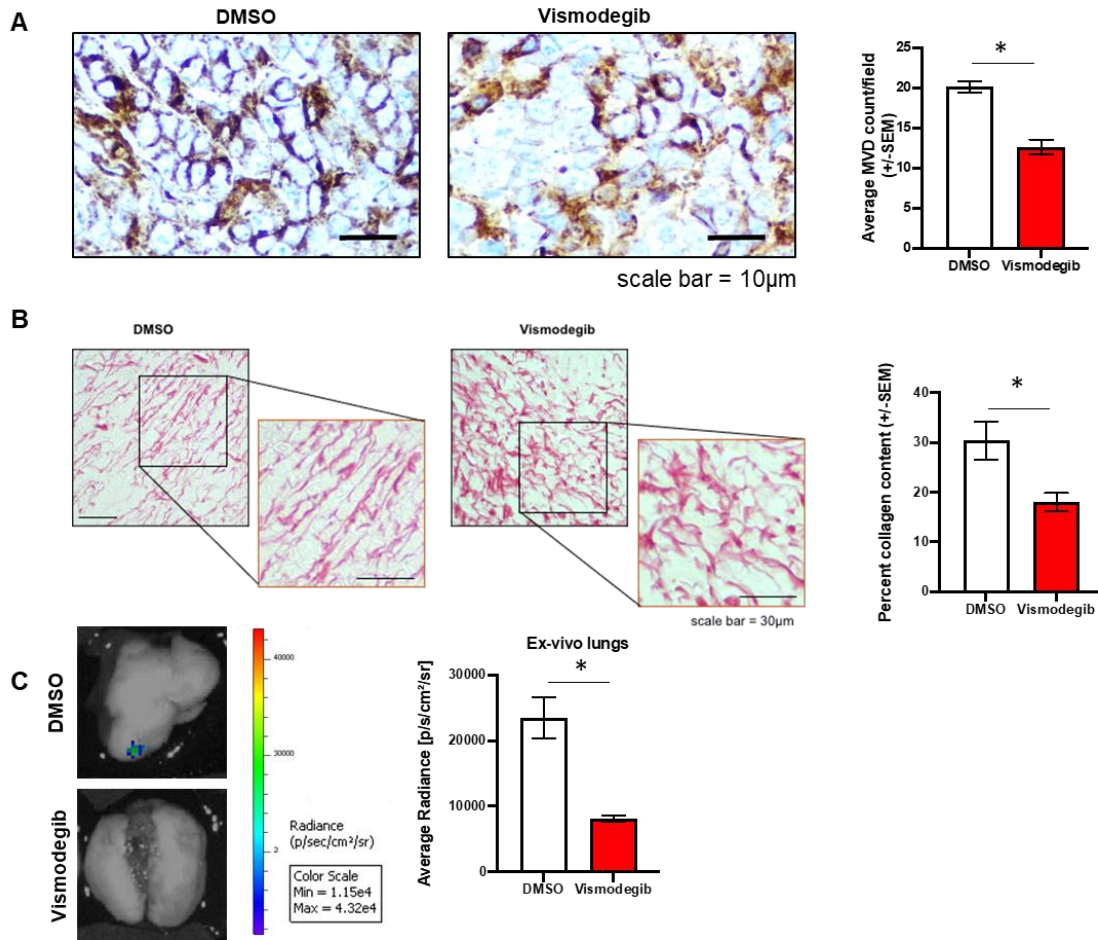


Figure 2. Vismodegib alters the tumor microenvironment and decreases metastasis
(A) Isolectin B4 staining of mice tumors from Vismodegib-treated mice shows decreased angiogenesis as determined by microvessel density per field in comparison to control mice. **(B)** Representative images of ex-vivo lung BLI on Day 34 post injection. Ex-vivo BLI imaging of lungs from Vismodegib-treated mice shows decreased metastasis compared to vehicle control quantified using average radiance. **(C)** Vismodegib alters the collagen fiber alignment quantified by collagen content using picrosirius red staining. All error bars depict the SEM.

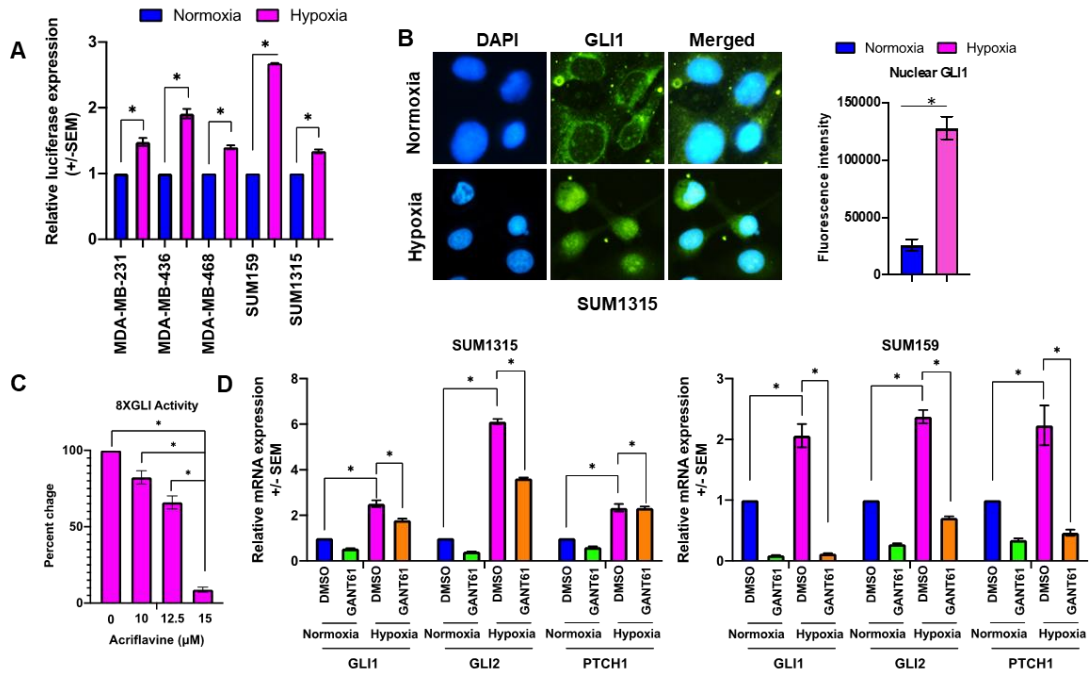


Figure 3. Hypoxia upregulates Hh activity in tumor cells. (A) 8X-GLI-luciferase reporter assay was used to measure Hh pathway activation in normoxia versus hypoxia in MDA-MB-231, MDA-MB-436, MDA-MB-468, SUM159, and SUM1315 cell lines. (B) Hypoxia induces nuclear accumulation of GLI1 (24hrs in hypoxia). GLI1 was visualized by fluorescent immunocytochemistry. (C) Acriflavine decreases 8XGLI reporter activity, in a dose-dependent manner, in SUM1315 cells. (D) The steady state transcript levels of bona fide Hh pathway target genes GLI1, GLI2, and PTCH1 are upregulated in hypoxia compared to normoxia in SUM1315 and SUM159 cells. All error bars depict the SEM.

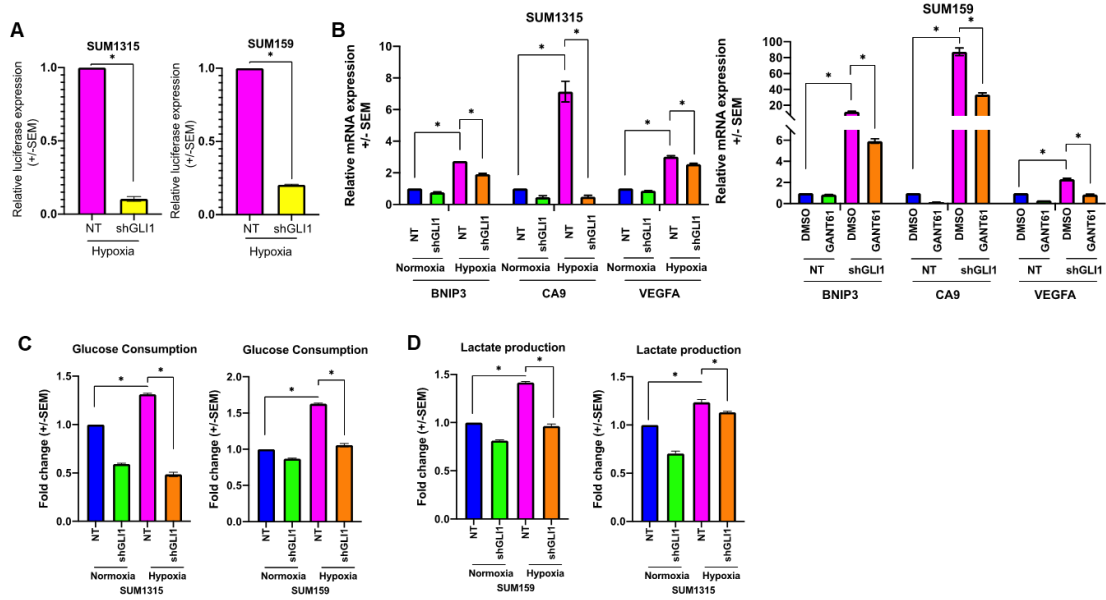


Figure 4. Inhibition of Hh/GLI signaling impairs cellular adaptation in hypoxic conditions. (A) Cells stably abrogated for GLI1 expression support significantly reduced HRE-luciferase reporter activity in SUM1315 and SUM159 cells, in hypoxia. (B) Classical HIF-1 α gene targets are upregulated in hypoxic conditions. GANT61 alleviates this increase. (C) In hypoxia, glucose consumption is significantly elevated. Stable GLI1 silencing abrogates elevated glucose consumption in hypoxia. (D) Elevated lactate production in hypoxia is mitigated by stable GLI1 silencing. N=3; ANOVA, sidak's multiple comparisons test; *, $p < 0.05$. All error bars depict the SEM.

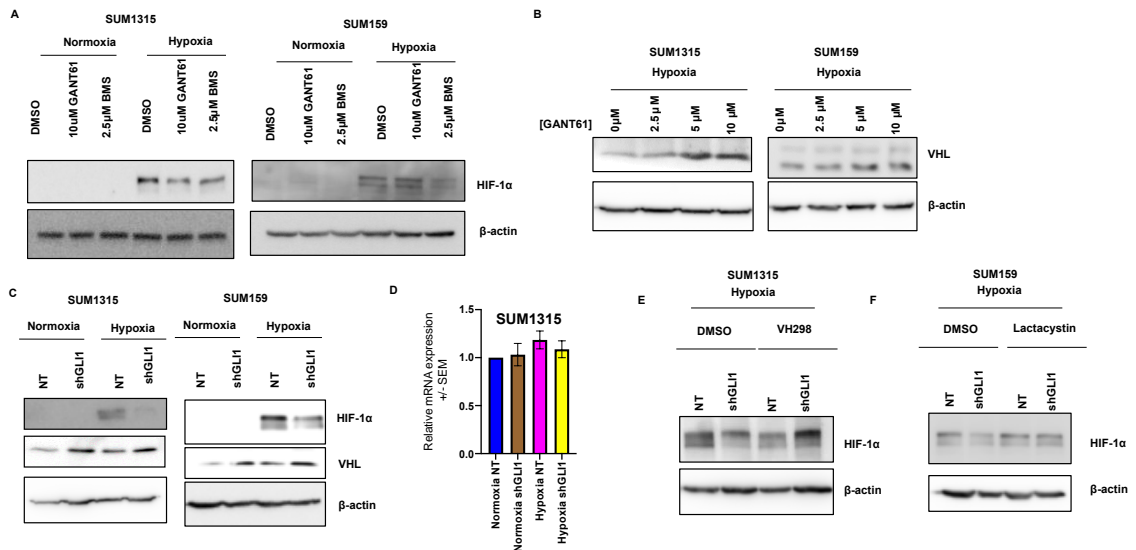
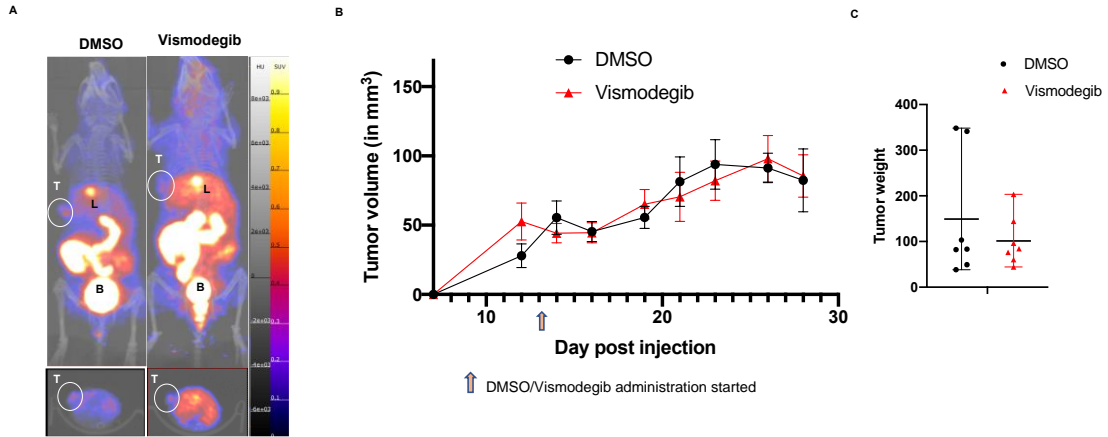
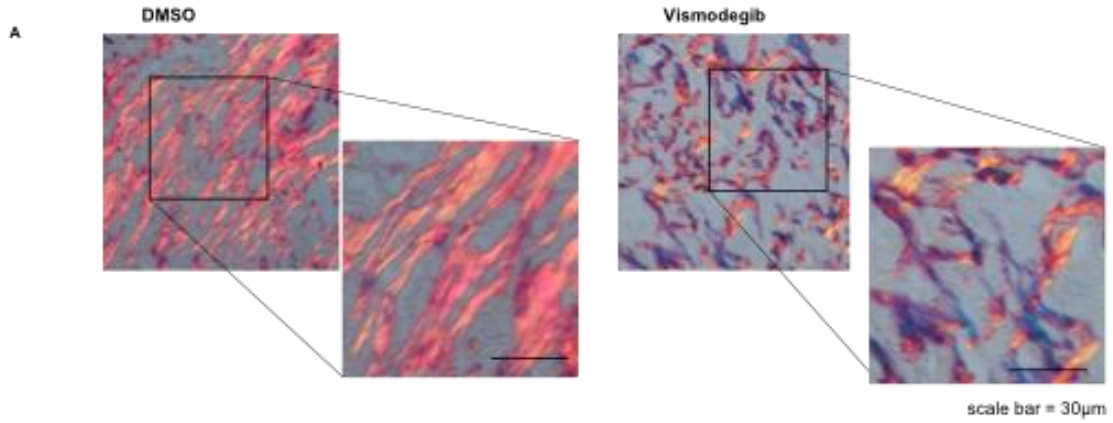


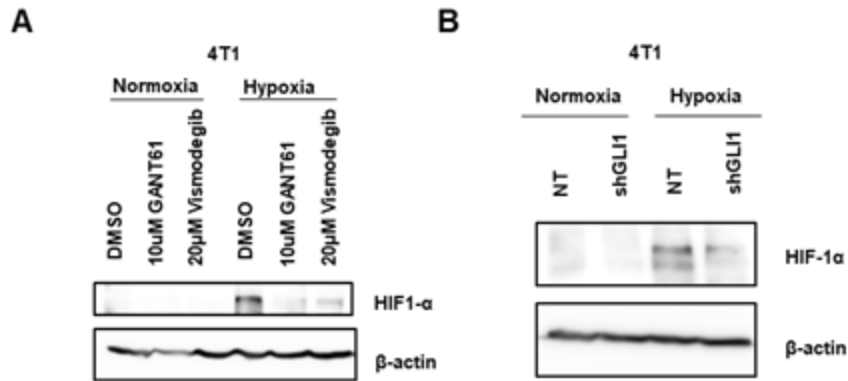
Figure 5. Hh signaling increases HIF-1 α transcription factor stability in a WSB-1-VHL-dependent mechanism (A) Hh pathway inhibition by GANT61 and BMS leads to decrease in accumulation of HIF-1 α protein in SUM1315 and SUM159 cells. **(B)** GANT61 increased expression of VHL protein in hypoxic condition, in a dose-dependent manner. **(C-D)** Hh pathway inhibition in SUM1315 stably knocked-down for GLI1 results in **(C)** decrease in accumulation of HIF-1 α protein in hypoxic condition **(D)** no changes in VHL mRNA expression. **(E)** VH298 led to increased accumulation of HIF-1 α protein in SUM1315 stably knocked-down for GLI1 in hypoxia compared to the control. **(F)** Similar recovery of HIF-1 α protein in SUM159 stably knocked-down for GLI1 in hypoxia following proteasome inhibition by lactacystin. All error bars depict the SEM.



Supplementary Figure 1 Inhibition of Hh signaling decreases tumor hypoxia and lung metastasis. (A) Representative images of 4T1 tumors (tumor denoted by T; liver denoted by L; bladder denoted by B) implanted in third mammary gland show FMISO uptake in the tumor. (B) Caliper measurements show no significant difference in tumor size between DMSO and Vismodegib treated mice (n=6), DMSO/Vismodegib administration started on day 13. (C) Average tumor size between the groups is not significantly different as shown by the tumor weight (n=6). All error bars depict the SEM



Supplementary Figure S2. Inhibition of Hh signaling disrupts collagen fiber alignment (A) Tumors sections from Vismodegib treated groups show morphological changes in the collagen fiber arrangement. Polarized light images were captured using a Nikon Eclipse Ti-U.



Supplementary Figure S3: Inhibition of Hh signaling decreases HIF-1 α transcription factor stability in 4T1 cells (A) 4T1 cells inhibited for Hh signaling with GANT61 and Vismodegib demonstrate a marked decrease in HIF-1 α accumulation in hypoxic condition. (B) 4T1 shGLI1 cells show decreased accumulation of HIF-1 α in hypoxic conditions compared to NT control cells.

DISCUSSION AND FUTURE DIRECTIONS

Thus far, we discovered that Hh signaling is important for (i) DDR through modulation of the DSB repair pathway and (ii) the tumor microenvironment through supporting tumor hypoxia. Our data support the hypothesis that the Hh signaling pathway serves as a critical target in breast cancer progression. Our studies identified the determinative role of Hh signaling in repairing rDNA DSBs following IR in breast cancer cells. Additionally, we uncovered the role of Hh signaling in crafting a hypoxic niche and influencing breast cancer cell adaptation to the hypoxic microenvironment. This study has implications on several other cancer studies like basal cell carcinoma, medulloblastoma, melanoma, prostate, lung, ovarian, colon, and pancreatic cancer where Hh signaling is also observed to be activated (119, 120).

Hh signaling in DSB repair

Previous studies in Hh signaling and DDR have identified the role of Hh in SSB repair via nucleotide, mismatch, and base excision repair pathways (103-107). Additionally, studies show that Hh inhibition sensitizes cancer cells to genotoxic therapies like IR (121-123). However, the molecular mechanisms underlying sensitivity to genotoxic stress in absence of Hh signaling remained unexplored. We for the first time, show that inhibition of Hh signaling led to impairment of the DSB repair process through impinging on the non-homologous end joining (NHEJ) repair pathway. Interestingly, our

unbiased approach to search for GLI cistrome after sensitization of cancer cells to IR located enriched GLI1 binding at the rDNA loci in the nucleolus. Since DSBs in 45S rDNA sites are lethal, this led us to further validate the consequence of GLI inhibition on rDNA DSBs (124). We found that Hh pathway inhibition leads to sensitivity through rDNA breaks inflicted by the I-PpoI restriction enzyme independent of global effects on DSB repair. Our study uncovered a novel link between Hh signaling and rDNA repair, critical for proliferating cells.

Recent studies show that BRCA-deficient TNBC tumors are sensitive to PARP inhibitors due to synthetic lethality (125). However, tumors can acquire resistance to PARP inhibitors and employ resistance mechanisms including upregulation of RAD51 to re-establish HR proficiency (126). Among the TNBC cell lines we utilized in the study, SUM1315 cells are HR-incompetent due to a BRCA1 mutation, whereas MDA-MB-468 cells are wild-type for BRCA1/2. In our study, we show that loss of Hh signaling impairs NHEJ, but the Hh signaling-mediated NHEJ loss could in turn enhance HR by RAD51 upregulation. We used the DR-GFP luciferase reporter construct to assay HR activity in both cell lines and did not register an HR upregulation. We also examined RAD51 expression in the SUM1315 and MDA-MB-468 cells with I-SceI-induced breaks in cells stably expressing the pimEJ5-GFP and DRGFP reporter respectively with or without Hh inhibition (**Figure 1**). We did not find compensatory RAD51 upregulation in these cells.

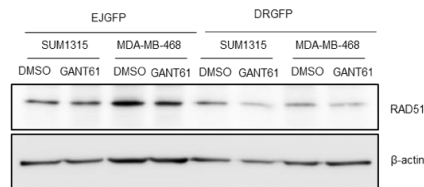


Figure 1. Alteration of RAD51 in I-SceI transfected NHEJ and HR GFP reporter cells. Immunoblot of RAD51 +/- Hh inhibition in SUM1315 and MDA-MB-468 cells.

The nucleolar DNA damage response mechanism is an emerging field of study. Ribosomal DNA (rDNA) are highly repetitive sequences and are actively transcribed by RNA Polymerase I and it accounts for 60% of total cellular transcription in a rapidly growing cell (127). Genotoxic stress can lead to inhibition of RNA polymerase I activity resulting in nucleolar reorganization making rDNA accessible to repair factors in the nucleoli that are normally barred from the nucleolus (128). One such factor that is reported to be recruited in the nucleolus to repair rDNA DSBs is MRE11-RAD50-NBS1 (MRN) complex. MRN complex is recruited by the nucleolar protein TCOF1 in rDNA DSBs and is important for genome integrity and cell survival (124, 129). Prior work distinguishing protein-protein interaction of transcription factors show that GLI1 interact with the DSB-sensing proteins MRE11 and RAD50 (130). Since our study establishes the role of Hh in rDNA DSB repair, it is pertinent to examine the possible association of MRN complex and GLI1 in rDNA DSBs repair.

Although our work contributes to an improved understanding of Hh in the rDNA DSBs repair pathway, we were not able to fully translate our study into a preclinical model for further validation. It has been increasingly important to understand how TME might impact the DSBs repair pathway (131). Our TNBC cell line and spheroid model doesn't capture the TME components that might affect the outcome. One way to assess the preclinical validation of Hh inhibition on tumor growth is to knock-down GLI1 in 4T1 cells, a murine TNBC line, and evaluate the repair proteins involved in DSB and NHEJ. Then assess for overall sensitivity for IR following Hh inhibition in a syngeneic mice tumor model. We found that *in vitro*, 4T1 cells show persistent DNA damage measured by DSB surrogate marker, γ -H2AX in the context of Hh inhibition, at 12 hr

following IR, compared to control (**Figure 2A**). We then assessed the overall outcome of IR-induced DNA damage by generating spheroids in three-dimensional culture from 4T1 cells without treatment or pre-treated with either vehicle control (DMSO) or GANT61 and Vismodegib. GANT61 and Vismodegib alone had a modest effect on non-irradiated cells but dramatically impaired spheroid growth when combined with irradiation (**Figure 2B**).

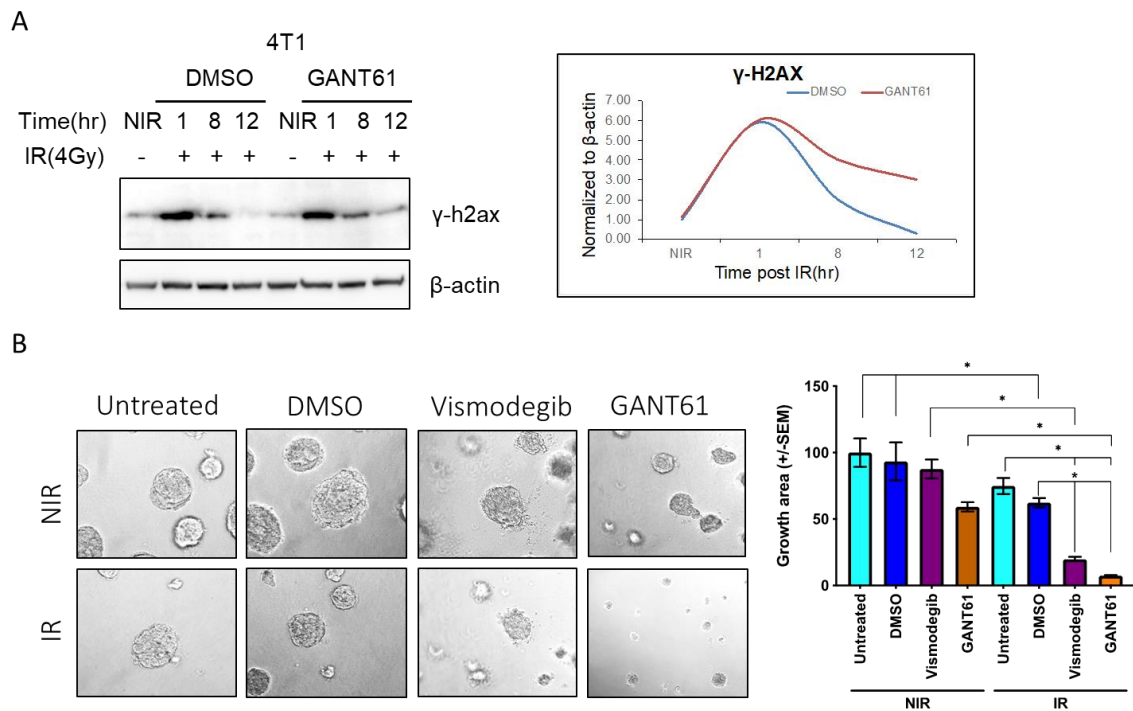


Figure 2. Inhibiting Hh signaling increases sensitivity to IR-induced DSBs in aggressive mammary tumor line 4T1. (A) Hh inhibition with GANT61 combined with IR leads to persistent γ -H2AX expression in 4T1 cells. (B) Inhibition of Hh pathway almost completely abrogates spheroid growth, compared to more modest reductions with either modality alone. The growth area was quantified using ImageJ software per 10 \times field. Statistical significance was determined with a two-way ANOVA and Tukey's multiple comparison test for each condition. Error bars depict the SEM.

Since 4T1 shows sensitivity *in vitro*, we can further examine radio-sensitivity in a syngeneic TNBC mouse model. We can randomize 4T1 tumors, harvest 1hr following IR (2, 4, 6 Gy), and analyze for γ -H2AX (DSB marker) and p-53BP1 foci (NHEJ marker)

using immunocytochemistry on frozen tumors. We expect that Hh inhibition would lead to decreased 53BP1 foci formation and marked increases in γ -H2AX in 4T1 tumors.

Hh signaling in crafting hypoxic microenvironment and adaptation to hypoxia

We investigated the role of Hh signaling in hypoxia by quantitating hypoxic parameters using radiolabeled tracer, [^{18}F]-fluoromisonidazole (FMISO) positron emission tomography (PET) imaging. This is the first study to show that pharmacological inhibition of Hh signaling in a mammary tumor model mitigates tumor hypoxia complemented by mechanistic studies unraveling the role of Hh activity in programming tumor cells to adapt to hypoxia. Our finding provides novel insight into the role of Hh pathway in modulating temporal changes in tumor hypoxia. Corroborating with our previous study(132), we also found that inhibition of Hh signaling leads to decreased metastasis.

Metastasis is the most lethal aspect of breast cancer since it contributes to increased morbidity and mortality. The survival rate for the breast cancer patient is drastically reduced below 25% upon the development of distant metastasis (133). According to the “seed and soil” hypothesis introduced by Stephen Paget in 1889, disseminated tumor cells can survive in circulation and colonize secondary organs that have a compatible microenvironment permitting tumor cell survival and growth (134). Studies show that tumor cell colonization of distant organs is a selective process and not dependent on the anatomic distance from the tumor (135). The metastasis process has distinct hallmarks that include motility and invasion, modulation of microenvironment, plasticity, and colonization of secondary sites (136). Since systemic inhibition of Hh in

the 4T1 model leads to decreased metastasis to the lungs, a rational next step will be to analyze what metastatic processes are impacted by Hh in breast cancer.

Our data indicate that the tumor landscape changes following inhibition of Hh with Vismodegib. One of the first steps in metastasis initiation is the change in tumor motility and invasion through the basement membrane surrounding the primary tumor. Elevated collagen deposition and re-organization collagen fibers by tumor and stromal cells leads to ECM stiffness, and exacerbates tumor cell migration and breast carcinoma malignancy by enhancing integrin signaling dependent mechanotransduction (137). As primary tumors progress, the collagen fibers are realigned to form straight and bundled structures (138). We found that the collagen fibril organization is disorganized and lacks structural integrity in the Hh inhibited tumors indicating the role of Hh in modifying collagen crosslinking. To further validate collagen linearization, we will utilize the second harmonics generation (SHG) imaging and measure collagen fiber anisotropy. To assess the possibility that cross-linking is correlated to amine oxidase crosslinking enzyme LOX, we will examine the expression of LOX in the Hh inhibited mice tumor tissues. Additionally, tumor ECM are typically stiffer than the normal tissue due to accumulation of ECM components such as collagens, glycoproteins, and enzymes, LOX activation, and tumor hypoxia (139-141) . We will assess stiffness of tumor tissue by measuring its elasticity using nanoscale atomic force microscopy (AFM). Hypoxia has also been implicated in altering collagen deposition and promoting invasion and metastasis of breast cancer (142). HIF regulates collagen prolyl 4-hydroxylases that are necessary for collagen biogenesis (142, 143). Given our finding that Hh modulates HIF

levels, it is imperative to examine the role of Hh in collagen biogenesis and/or restructuring.

Tumor hypoxia is associated with adverse patient survival outcomes, albeit there is no accepted method of treatment for hypoxia or hypoxia measurement that is used in the clinic. FMISO utility is extensively investigated in pre-clinical settings and is developed as an imaging agent used to monitor hypoxic within the tumor. Currently, it is the gold standard for hypoxia imaging. However, FMISO is not in routine practice in the clinic due to its slow clearance from normal tissue. Alternative methods to image hypoxia are still in development but have not received FDA approval (144). Our study provides pre-clinical and translational relevance of using the FMISO imaging method in the clinic for predicting outcome in patients, treated with a Hh inhibitor.

Tumor hypoxia is heterogeneous, and it does not always follow a linear path of progress as the tumor size increases. Several factors come into play that can make tumor hypoxia dynamic. Oxygen distribution within the tumor can be affected by the availability of functional blood vessels leading to the creation of acute (minute to hours) and chronic (more than 24 hours) hypoxia. Acute hypoxia can occur as a possible consequence of intermittent opening and closing of blood vessels within a tumor (145, 146). Changes in the blood vasculature can make tumor cells transiently or chronically radio-resistant (146). Current hypoxia studies including our study are done in *in vitro* conditions at around 1% O₂ (considered hypoxia) while the physiological hypoxia can be anywhere between severe (<0.5% O₂) and mild (>0.5%-3% O₂). Similarly, *in vitro* conditions for normoxia are around 21% O₂, while physiological tissue levels of O₂ is around 3-7% O₂ (147). Discrepancies in the study conditions and physiological levels of

O₂ can be a barrier in recognition of the mechanisms of treatment resistance. Hence, in addition to our efforts to elucidate the role of Hh signaling in hypoxia adaptation, it is similarly important to assess how Hh might moderate acute and chronic hypoxia within the tumor.

Interactions between hypoxia and DDR

It is generally accepted that hypoxia within the tumor is a barrier to effective cancer treatment methods such as radiotherapy. O₂ is an important determinant of the DNA lesions incurred during radiation damage. Based on Oxygen Fixation Hypothesis, O₂ is needed in the chemical reaction that leads to the generation of irreversible DNA damage created by ionizing radiation by the fixation of free radicals to the DNA (148). A groundbreaking study by Gray et al., looking at the efficacy of ionizing radiation in cancer at lower oxygen concentrations showed that hypoxic cells experienced reduced radiation-induced damage due to low O₂ (111). Additionally, chemotherapeutic drugs are less effective in hypoxic conditions due to their low efficacy in the absence of oxygen. Hypoxic regions have poor vasculature resulting in reduced distribution of the drug. Additionally, hypoxic cells are non-proliferative, making cytotoxic therapy that targets dividing cells ineffective (112). Subsequent studies in breast cancer have also supported the importance of addressing tumor hypoxia for effective cancer treatment (112). Due to the role of Hh in the regulation of DDR and hypoxic microenvironment, it is plausible that hypoxic tumor cells engage Hh signaling as a defense mechanism to facilitate cell survival against radiation treatment. Building upon our findings that implicate the Hh pathway in promoting DDR and adaptation to hypoxia, the rational next step will be to

examine the possible role of Hh as a key feature that modulates the hypoxic tumor microenvironment.

Altered DDR response in hypoxia. Hypoxia drives genetic instability through the impairment of DSB repair via transcriptional, translational, and epigenetic regulation of several important repair proteins. DNA-PKcs, Ku70/80, BRCA1, and RAD51 are some of the repair proteins that are modulated by hypoxia (reviewed in (147)). Our study presents compelling evidence to study Hh signaling in the regulation of breast cancer radio-resistance mechanisms in tumor hypoxia. Further studies will examine the alteration of rDNA DSB, HR, and NHEJ repair pathway in hypoxia compared to normoxia following genotoxic stress induced by a chemotherapeutic drug such as doxorubicin. Importantly, we will examine how Hh modulates the repair in the presence or absence of hypoxia. This study will be critical to understanding radioresistance in cancer cells.

Altered immune cell function in hypoxia. Hypoxia can alter the tumor microenvironment and the cellular functions of the immune cells within tumor. Macrophages are one of the essential moderators of immune defense but their functions are impacted by the hypoxic microenvironment (149). Tumor-associated Macrophages (TAMs) demonstrate extreme plasticity resulting from the environmental cues they get from the surrounding stromal and cancer cells during tumor progression (150). M1-like macrophages can contribute to an antitumor response, while M2 macrophages are considered to propagate tumor-promoting environment (68). M2 macrophages have

tumor promoting functions leading to tumor growth and metastasis (149). Tumor hypoxia in conjunction with cytokines from the TME is thought to play a critical role in the phenotype shift of TAMs (151, 152).

Macrophages infiltrate both, hypoxic and necrotic regions of the tumor, most likely to clear away dying tumor cells (152, 153). Several chemokines like VEGF, macrophage colony-stimulating factor (M-CSF), CCL2, CCL5, stromal cell-derived factor 1 α (SDF1 α), endothelin, eotaxin, oncostatin M, and Semaphorin 3A (Sema3A) in the TME are implicated in guiding macrophage migration to the hypoxic tumor sites (152, 154-156). These cytokines are expressed by tumor cells, endothelial cells, fibroblasts, and TAMs (152). Once in the hypoxic TME, macrophage mobility is impeded due to diminished CCR2, CCR5, and neuropilin-1 (NRP1) expression in macrophages trapping them in the process (156-158). Casazza et al., showed that inhibiting NRP1 in macrophages obstructed macrophage migration to hypoxic sites and consequently decreased angiogenesis, tumor growth, and metastasis (156).

Macrophages also differentially express MMPs like MMP7 in the hypoxic TME to facilitate tumor migration and invasion (159). Hypoxia-induced endothelin 1 and 2 expression in tumor cells stimulates expression of MMP2 and MMP9 in macrophages leading to higher tumor cell invasion through Matrigel (160, 161). Entrapped macrophages in the hypoxic TME are re-educated to serve tumor growth by aiding in tumor invasion. Interestingly, macrophages that reside in the hypoxic areas of the tumor are low MHC-II expressing and M2-like macrophages (162, 163). Hypoxia itself did not drive the polarization of macrophages but contributed to the fine-tuning of the MHC-II low (M2-like) macrophage by expression of hypoxia-responsive genes that are involved

in angiogenesis, glycolysis, and metastasis (162). Additionally, hypoxia-induced EMT in cancer cells leads to expression of CCL20 cytokine which in turn induces indoleamine 2,3-dioxygenase (IDO), an enzyme required for tryptophan degradation, in monocyte-derived macrophages. IDO induction in macrophages results in suppression of T cell function as determined by lower T cell proliferation and IFN- γ production by T cells (164). Overall, the hypoxic TME re-educates macrophages to allow cancer cell evasion and immunosuppression.

Recently, our lab reported a functional interaction between Hh signaling in breast cancer cells and macrophages in the TME to promote immune suppression (132). Inhibition of Hh signaling led to alteration of several immune profiles including macrophages to an immune-suppressive (M2) phenotype resulting in decreased metastasis to the lungs (132). Hh inhibition led to decrease in the cytokine profile of M2 macrophages hampering their functions. Similarly, Petty et al., found that tumor-derived Hh ligand promotes polarization of macrophages to M2-like resulting in tumor growth in a murine model of hepatocellular carcinoma. Hh-driven M2 macrophages regulate CD8+ T cell by suppressing its migration and infiltration through reduced expression of CXCL9 and CXCL10 (165).

Similar to cancer cells rewiring their metabolic profile and impinging on the anaerobic glycolytic pathway (Warburg effect), M1 and M2 macrophages have a distinct metabolic profile. M1 macrophages increase glucose consumption and lactate release and M2 macrophages mainly engage in oxidative phosphorylation (166). Since metabolic reprogramming is integral to polarization, we assessed the effect of altering Hh signaling in the mitochondrial respiration rate of the in bone marrow-derived murine macrophages

(BMDMs) stimulated by IL-4 and macrophage colony-stimulating factor (M-CSF) to M2 phenotype. We found that inhibition of Hh signaling in M2 macrophages has reduced mitochondrial function reflected in compromised oxygen consumption rate and respiration parameters analyzed by Seahorse extracellular flux (**Figure 3**).

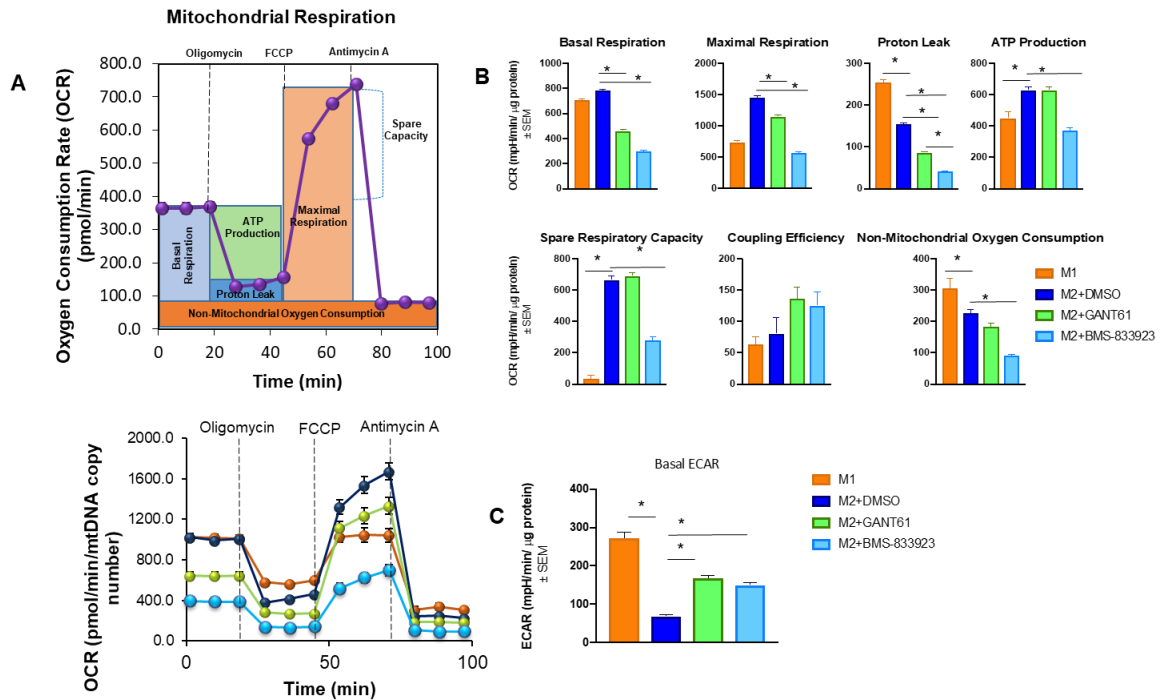


Figure 3. Inhibition of Hh signaling decreases metabolic reliance on OXPHOS with a reciprocal increase in glycolysis in M2 macrophages. (A) Seahorse XFe24 extracellular flux analyzer was used to analyze mitochondrial functions and real-time OCR was determined during sequential treatments with Oligomycin (ATP-synthase inhibitor), FCCP (Uncoupler), and A-antimycin- A/rotenone (ETC inhibitors). BMDMs skewed to M1 or M2, M2 + DMSO, M2 + Hh inhibitors were used for all panels. Hh inhibitors GANT61 and BMS decrease OCR compared to DMSO control. (B) Hh inhibition decreases basal, maximal respiration, proton leak, spare respiratory capacity, non-mitochondrial oxygen consumption, and increases basal extracellular acidification rate (ECAR).

Given, hypoxia prevalence in solid tumors and Hh signaling pathway's role in the macrophage polarization, it is critical to assess whether Hh might be involved in

polarization of macrophages to tumor suppressing M2 phenotype in hypoxic TME. Our data indicate that hypoxia induces Hh activation in breast cancer cells; *in vivo*, these Hh-driven tumor cells can lead to polarization of entrapped macrophages in hypoxic TME. Understanding of the cellular crosstalk driven by Hh between cancer cells and macrophages in the hypoxic TME will be important to understand tumor progression and metastasis. This will help strategize the clinical use of Hh inhibitors like Vismodegib that are already in clinic for patients with hypoxic tumors.

LIST OF REFERENCES

1. Siegel RL, Miller KD, Jemal A. Cancer statistics, 2020. *CA: A Cancer Journal for Clinicians*. 2020;70(1):7-30.
2. Miller KD, Nogueira L, Mariotto AB, Rowland JH, Yabroff KR, Alfano CM, et al. Cancer treatment and survivorship statistics, 2019. *CA: a cancer journal for clinicians*. 2019;69(5):363-85.
3. Haynes B, Sarma A, Nangia-Makker P, Shekhar MP. Breast cancer complexity: implications of intratumoral heterogeneity in clinical management. *Cancer metastasis reviews*. 2017;36(3):547-55.
4. Lawson DA, Kessenbrock K, Davis RT, Pervolarakis N, Werb Z. Tumour heterogeneity and metastasis at single-cell resolution. *Nature Cell Biology*. 2018;20(12):1349-60.
5. Whiteside TL. The tumor microenvironment and its role in promoting tumor growth. *Oncogene*. 2008;27(45):5904-12.
6. Segovia-Mendoza M, Morales-Montor J. Immune Tumor Microenvironment in Breast Cancer and the Participation of Estrogen and Its Receptors in Cancer Physiopathology. *Front Immunol*. 2019;10:348.
7. Place AE, Jin Huh S, Polyak K. The microenvironment in breast cancer progression: biology and implications for treatment. *Breast Cancer Research*. 2011;13(6):227.
8. Hinck L, Näthke I. Changes in cell and tissue organization in cancer of the breast and colon. *Curr Opin Cell Biol*. 2014;26:87-95.
9. Alkabban FM, Ferguson T. Breast Cancer. *StatPearls*. Treasure Island (FL): StatPearls Publishing
Copyright © 2020, StatPearls Publishing LLC.; 2020.
10. Smith RA, Andrews KS, Brooks D, Fedewa SA, Manassaram-Baptiste D, Saslow D, et al. Cancer screening in the United States, 2018: A review of current American Cancer Society guidelines and current issues in cancer screening. *CA: a cancer journal for clinicians*. 2018;68(4):297-316.

11. Pfeiffer RM, Webb-Vargas Y, Wheeler W, Gail MH. Proportion of U.S. Trends in Breast Cancer Incidence Attributable to Long-term Changes in Risk Factor Distributions. *Cancer epidemiology, biomarkers & prevention : a publication of the American Association for Cancer Research, cosponsored by the American Society of Preventive Oncology*. 2018;27(10):1214-22.
12. DeSantis C, Howlander N, Cronin KA, Jemal A. Breast cancer incidence rates in U.S. women are no longer declining. *Cancer epidemiology, biomarkers & prevention : a publication of the American Association for Cancer Research, cosponsored by the American Society of Preventive Oncology*. 2011;20(5):733-9.
13. Coombs NJ, Cronin KA, Taylor RJ, Freedman AN, Boyages J. The impact of changes in hormone therapy on breast cancer incidence in the US population. *Cancer causes & control : CCC*. 2010;21(1):83-90.
14. Harvie M, Howell A, Evans DG. Can diet and lifestyle prevent breast cancer: what is the evidence? *American Society of Clinical Oncology educational book American Society of Clinical Oncology Annual Meeting*. 2015:e66-73.
15. Newman LA. Parsing the Etiology of Breast Cancer Disparities. *Journal of clinical oncology : official journal of the American Society of Clinical Oncology*. 2016;34(9):1013-4.
16. Daly B, Olopade OI. A perfect storm: How tumor biology, genomics, and health care delivery patterns collide to create a racial survival disparity in breast cancer and proposed interventions for change. *CA: a cancer journal for clinicians*. 2015;65(3):221-38.
17. Howlander N, Cronin KA, Kurian AW, Andridge R. Differences in Breast Cancer Survival by Molecular Subtypes in the United States. *Cancer epidemiology, biomarkers & prevention : a publication of the American Association for Cancer Research, cosponsored by the American Society of Preventive Oncology*. 2018;27(6):619-26.
18. Prat A, Adamo B, Cheang MC, Anders CK, Carey LA, Perou CM. Molecular characterization of basal-like and non-basal-like triple-negative breast cancer. *The oncologist*. 2013;18(2):123-33.
19. Toth-Fejel S, Cheek J, Calhoun K, Muller P, Pommier RF. Estrogen and androgen receptors as comediators of breast cancer cell proliferation: providing a new therapeutic tool. *Archives of surgery (Chicago, Ill : 1960)*. 2004;139(1):50-4.
20. Fountzilas G, Giannoulatou E, Alexopoulou Z, Zagouri F, Timotheadou E, Papadopoulou K, et al. TP53 mutations and protein immunopositivity may predict for poor outcome but also for trastuzumab benefit in patients with early breast cancer treated in the adjuvant setting. *Oncotarget*. 2016;7(22):32731-53.
21. Oh D-Y, Bang Y-J. HER2-targeted therapies — a role beyond breast cancer. *Nature Reviews Clinical Oncology*. 2020;17(1):33-48.

22. Sporikova Z, Koudelakova V, Trojanec R, Hajduch M. Genetic Markers in Triple-Negative Breast Cancer. *Clinical breast cancer*. 2018;18(5):e841-e50.
23. Haffty BG, Yang Q, Reiss M, Kearney T, Higgins SA, Weidhaas J, et al. Locoregional relapse and distant metastasis in conservatively managed triple negative early-stage breast cancer. *Journal of clinical oncology : official journal of the American Society of Clinical Oncology*. 2006;24(36):5652-7.
24. Morris GJ, Naidu S, Topham AK, Guiles F, Xu Y, McCue P, et al. Differences in breast carcinoma characteristics in newly diagnosed African-American and Caucasian patients. *Cancer*. 2007;110(4):876-84.
25. Dent R, Trudeau M, Pritchard KI, Hanna WM, Kahn HK, Sawka CA, et al. Triple-negative breast cancer: clinical features and patterns of recurrence. *Clinical cancer research : an official journal of the American Association for Cancer Research*. 2007;13(15 Pt 1):4429-34.
26. Lehmann BD, Bauer JA, Chen X, Sanders ME, Chakravarthy AB, Shyr Y, et al. Identification of human triple-negative breast cancer subtypes and preclinical models for selection of targeted therapies. *The Journal of clinical investigation*. 2011;121(7):2750-67.
27. Adams S, Gray RJ, Demaria S, Goldstein L, Perez EA, Shulman LN, et al. Prognostic value of tumor-infiltrating lymphocytes in triple-negative breast cancers from two phase III randomized adjuvant breast cancer trials: ECOG 2197 and ECOG 1199. *Journal of clinical oncology : official journal of the American Society of Clinical Oncology*. 2014;32(27):2959-66.
28. Wong YC, Xie B. The role of androgens in mammary carcinogenesis. *Italian journal of anatomy and embryology = Archivio italiano di anatomia ed embriologia*. 2001;106(2 Suppl 1):111-25.
29. Coleman RE, Gregory W, Marshall H, Wilson C, Holen I. The metastatic microenvironment of breast cancer: clinical implications. *Breast (Edinburgh, Scotland)*. 2013;22 Suppl 2:S50-6.
30. Soysal SD, Tzankov A, Muenst SE. Role of the Tumor Microenvironment in Breast Cancer. *Pathobiology : journal of immunopathology, molecular and cellular biology*. 2015;82(3-4):142-52.
31. Hu M, Polyak K. Microenvironmental regulation of cancer development. *Current opinion in genetics & development*. 2008;18(1):27-34.
32. Polyak K. Breast cancer: origins and evolution. *The Journal of clinical investigation*. 2007;117(11):3155-63.

33. Dvorak HF. Tumors: wounds that do not heal-redux. *Cancer immunology research*. 2015;3(1):1-11.
34. Li B, Wang JHC. Fibroblasts and myofibroblasts in wound healing: Force generation and measurement. *Journal of Tissue Viability*. 2011;20(4):108-20.
35. Folgueira MA, Maistro S, Katayama ML, Roela RA, Mundim FG, Nanogaki S, et al. Markers of breast cancer stromal fibroblasts in the primary tumour site associated with lymph node metastasis: a systematic review including our case series. *Bioscience reports*. 2013;33(6).
36. Balkwill FR, Capasso M, Hagemann T. The tumor microenvironment at a glance. *Journal of Cell Science*. 2012;125(23):5591.
37. Orimo A, Gupta PB, SgROI DC, Arenzana-Seisdedos F, Delaunay T, Naeem R, et al. Stromal Fibroblasts Present in Invasive Human Breast Carcinomas Promote Tumor Growth and Angiogenesis through Elevated SDF-1/CXCL12 Secretion. *Cell*. 2005;121(3):335-48.
38. Erez N, Truitt M, Olson P, Hanahan D. Cancer-Associated Fibroblasts Are Activated in Incipient Neoplasia to Orchestrate Tumor-Promoting Inflammation in an NF- κ B-Dependent Manner. *Cancer Cell*. 2010;17(2):135-47.
39. Choi YP, Lee JH, Gao M-Q, Kim BG, Kang S, Kim SH, et al. Cancer-associated fibroblast promote transmigration through endothelial brain cells in three-dimensional in vitro models. *International Journal of Cancer*. 2014;135(9):2024-33.
40. Surowiak P, Murawa D, Materna V, Maciejczyk A, Pudelko M, Ciesla S, et al. Occurrence of stromal myofibroblasts in the invasive ductal breast cancer tissue is an unfavourable prognostic factor. *Anticancer research*. 2007;27(4c):2917-24.
41. Krüger-Genge A, Blocki A, Franke RP, Jung F. Vascular Endothelial Cell Biology: An Update. *International journal of molecular sciences*. 2019;20(18).
42. Carmeliet P, Jain RK. Molecular mechanisms and clinical applications of angiogenesis. *Nature*. 2011;473(7347):298-307.
43. Watnick RS. The role of the tumor microenvironment in regulating angiogenesis. *Cold Spring Harbor perspectives in medicine*. 2012;2(12):a006676.
44. Paku S, Paweletz N. First steps of tumor-related angiogenesis. *Laboratory investigation; a journal of technical methods and pathology*. 1991;65(3):334-46.
45. Niu G, Chen X. Vascular endothelial growth factor as an anti-angiogenic target for cancer therapy. *Current drug targets*. 2010;11(8):1000-17.

46. Bergers G, Song S. The role of pericytes in blood-vessel formation and maintenance. *Neuro-oncology*. 2005;7(4):452-64.
47. Uzzan B, Nicolas P, Cucherat M, Perret G-Y. Microvessel Density as a Prognostic Factor in Women with Breast Cancer. *Cancer Research*. 2004;64(9):2941.
48. Białas M, Dyduch G, Dudała J, Bereza-Buziak M, Hubalewska-Dydejczyk A, Budzyński A, et al. Study of Microvessel Density and the Expression of Vascular Endothelial Growth Factors in Adrenal Gland Pheochromocytomas. *International Journal of Endocrinology*. 2014;2014:104129.
49. Niethammer AG, Xiang R, Becker JC, Wodrich H, Pertl U, Karsten G, et al. A DNA vaccine against VEGF receptor 2 prevents effective angiogenesis and inhibits tumor growth. *Nature Medicine*. 2002;8(12):1369-75.
50. Armulik A, Genové G, Betsholtz C. Pericytes: Developmental, Physiological, and Pathological Perspectives, Problems, and Promises. *Developmental Cell*. 2011;21(2):193-215.
51. Barlow KD, Sanders AM, Soker S, Ergun S, Metheny-Barlow LJ. Pericytes on the Tumor Vasculature: Jekyll or Hyde? *Cancer Microenvironment*. 2013;6(1):1-17.
52. Cooke VG, LeBleu VS, Keskin D, Khan Z, O'Connell JT, Teng Y, et al. Pericyte depletion results in hypoxia-associated epithelial-to-mesenchymal transition and metastasis mediated by met signaling pathway. *Cancer Cell*. 2012;21(1):66-81.
53. Ruan J, Luo M, Wang C, Fan L, Yang SN, Cardenas M, et al. Imatinib disrupts lymphoma angiogenesis by targeting vascular pericytes. *Blood*. 2013;121(26):5192-202.
54. Thompson E, Taube JM, Elwood H, Sharma R, Meeker A, Warzecha HN, et al. The immune microenvironment of breast ductal carcinoma in situ. *Modern pathology : an official journal of the United States and Canadian Academy of Pathology, Inc*. 2016;29(3):249-58.
55. Miyan M, Schmidt-Mende J, Kiessling R, Poschke I, de Boniface J. Differential tumor infiltration by T-cells characterizes intrinsic molecular subtypes in breast cancer. *Journal of translational medicine*. 2016;14(1):227.
56. Ruffell B, DeNardo DG, Affara NI, Coussens LM. Lymphocytes in cancer development: polarization towards pro-tumor immunity. *Cytokine & growth factor reviews*. 2010;21(1):3-10.
57. Fridman WH, Pagès F, Sautès-Fridman C, Galon J. The immune contexture in human tumours: impact on clinical outcome. *Nature reviews Cancer*. 2012;12(4):298-306.
58. Linehan DC, Goedegebuure PS. CD25+ CD4+ regulatory T-cells in cancer. *Immunologic research*. 2005;32(1-3):155-68.

59. Tan W, Zhang W, Strasner A, Grivennikov S, Cheng JQ, Hoffman RM, et al. Tumour-infiltrating regulatory T cells stimulate mammary cancer metastasis through RANKL-RANK signalling. *Nature*. 2011;470(7335):548-53.
60. Mahmoud SM, Paish EC, Powe DG, Macmillan RD, Grainge MJ, Lee AH, et al. Tumor-infiltrating CD8+ lymphocytes predict clinical outcome in breast cancer. *Journal of clinical oncology : official journal of the American Society of Clinical Oncology*. 2011;29(15):1949-55.
61. Jenkins RW, Barbie DA, Flaherty KT. Mechanisms of resistance to immune checkpoint inhibitors. *British journal of cancer*. 2018;118(1):9-16.
62. Darvin P, Toor SM, Sasidharan Nair V, Elkord E. Immune checkpoint inhibitors: recent progress and potential biomarkers. *Experimental & Molecular Medicine*. 2018;50(12):1-11.
63. Patente TA, Pinho MP, Oliveira AA, Evangelista GCM, Bergami-Santos PC, Barbuto JAM. Human Dendritic Cells: Their Heterogeneity and Clinical Application Potential in Cancer Immunotherapy. *Front Immunol*. 2019;9(3176).
64. da Cunha A, Michelin MA, Murta EF. Pattern response of dendritic cells in the tumor microenvironment and breast cancer. *World journal of clinical oncology*. 2014;5(3):495-502.
65. Fainaru O, Almog N, Yung CW, Nakai K, Montoya-Zavala M, Abdollahi A, et al. Tumor growth and angiogenesis are dependent on the presence of immature dendritic cells. *FASEB journal : official publication of the Federation of American Societies for Experimental Biology*. 2010;24(5):1411-8.
66. Obeid E, Nanda R, Fu YX, Olopade OI. The role of tumor-associated macrophages in breast cancer progression (review). *International journal of oncology*. 2013;43(1):5-12.
67. Allen M, Louise Jones J. Jekyll and Hyde: the role of the microenvironment on the progression of cancer. *The Journal of pathology*. 2011;223(2):162-76.
68. Hao NB, Lü MH, Fan YH, Cao YL, Zhang ZR, Yang SM. Macrophages in tumor microenvironments and the progression of tumors. *Clinical & developmental immunology*. 2012;2012:948098.
69. Atri C, Guerfali FZ, Laouini D. Role of Human Macrophage Polarization in Inflammation during Infectious Diseases. *International journal of molecular sciences*. 2018;19(6).
70. Laskin DL. Macrophages and inflammatory mediators in chemical toxicity: a battle of forces. *Chemical research in toxicology*. 2009;22(8):1376-85.

71. Solinas G, Germano G, Mantovani A, Allavena P. Tumor-associated macrophages (TAM) as major players of the cancer-related inflammation. *Journal of Leukocyte Biology*. 2009;86(5):1065-73.
72. Semenza GL. The hypoxic tumor microenvironment: A driving force for breast cancer progression. *Biochimica et biophysica acta*. 2016;1863(3):382-91.
73. Semenza GL. Molecular mechanisms mediating metastasis of hypoxic breast cancer cells. *Trends in molecular medicine*. 2012;18(9):534-43.
74. Semenza GL. Defining the role of hypoxia-inducible factor 1 in cancer biology and therapeutics. *Oncogene*. 2010;29(5):625-34.
75. Zhang H, Wong CCL, Wei H, Gilkes DM, Korangath P, Chaturvedi P, et al. HIF-1-dependent expression of angiopoietin-like 4 and L1CAM mediates vascular metastasis of hypoxic breast cancer cells to the lungs. *Oncogene*. 2012;31(14):1757-70.
76. Vaupel P. Prognostic potential of the pre-therapeutic tumor oxygenation status. *Advances in experimental medicine and biology*. 2009;645:241-6.
77. Meneses AM, Wielockx B. PHD2: from hypoxia regulation to disease progression. *Hypoxia (Auckland, NZ)*. 2016;4:53-67.
78. Mole DR, Maxwell PH, Pugh CW, Ratcliffe PJ. Regulation of HIF by the von Hippel-Lindau tumour suppressor: implications for cellular oxygen sensing. *IUBMB life*. 2001;52(1-2):43-7.
79. Cockman ME, Masson N, Mole DR, Jaakkola P, Chang GW, Clifford SC, et al. Hypoxia inducible factor-alpha binding and ubiquitylation by the von Hippel-Lindau tumor suppressor protein. *The Journal of biological chemistry*. 2000;275(33):25733-41.
80. Siegel RL, Miller KD, Jemal A. Cancer statistics, 2016. *CA: a cancer journal for clinicians*. 2016;66(1):7-30.
81. Runowicz CD, Leach CR, Henry NL, Henry KS, Mackey HT, Cowens-Alvarado RL, et al. American Cancer Society/American Society of Clinical Oncology Breast Cancer Survivorship Care Guideline. *CA: a cancer journal for clinicians*. 2016;66(1):43-73.
82. Anders CK, Carey LA. Biology, metastatic patterns, and treatment of patients with triple-negative breast cancer. *Clinical breast cancer*. 2009;9 Suppl 2(Suppl 2):S73-81.
83. Li CH, Karantza V, Aktan G, Lala M. Current treatment landscape for patients with locally recurrent inoperable or metastatic triple-negative breast cancer: a systematic literature review. *Breast Cancer Research*. 2019;21(1):143.

84. Kim K, Park HJ, Shin KH, Kim JH, Choi DH, Park W, et al. Breast Conservation Therapy Versus Mastectomy in Patients with T1-2N1 Triple-Negative Breast Cancer: Pooled Analysis of KROG 14-18 and 14-23. *Cancer research and treatment : official journal of Korean Cancer Association*. 2018;50(4):1316-23.
85. Golshan M, Loibl S, Wong SM, Houber JB, O'Shaughnessy J, Rugo HS, et al. Breast Conservation After Neoadjuvant Chemotherapy for Triple-Negative Breast Cancer: Surgical Results From the BrightNess Randomized Clinical Trial. *JAMA Surgery*. 2020;155(3):e195410-e.
86. Abdulkarim BS, Cuartero J, Hanson J, Deschênes J, Lesniak D, Sabri S. Increased risk of locoregional recurrence for women with T1-2N0 triple-negative breast cancer treated with modified radical mastectomy without adjuvant radiation therapy compared with breast-conserving therapy. *Journal of clinical oncology : official journal of the American Society of Clinical Oncology*. 2011;29(21):2852-8.
87. Yao Y, Chu Y, Xu B, Hu Q, Song Q. Radiotherapy after surgery has significant survival benefits for patients with triple-negative breast cancer. *Cancer medicine*. 2019;8(2):554-63.
88. Khalifa J, Duprez-Paumier R, Filleron T, Lacroix Triki M, Jouve E, Dalenc F, et al. Outcome of pN0 Triple-Negative Breast Cancer with or without Lymph Node Irradiation: A Single Institution Experience. *The breast journal*. 2016;22(5):510-9.
89. Sato H, Niimi A, Yasuhara T, Permata TBM, Hagiwara Y, Isono M, et al. DNA double-strand break repair pathway regulates PD-L1 expression in cancer cells. *Nat Commun*. 2017;8(1):1751.
90. Twyman-Saint Victor C, Rech AJ, Maity A, Rengan R, Pauken KE, Stelekati E, et al. Radiation and dual checkpoint blockade activate non-redundant immune mechanisms in cancer. *Nature*. 2015;520(7547):373-7.
91. Sherry AD, Newman NB, Chakravarthy AB, Mayer I, Rafat M. Post-Radiotherapy Inflammation Predicts Recurrence and Mortality in Stage I-III Triple-Negative Breast Cancer. *International Journal of Radiation Oncology, Biology, Physics*. 2019;105(1):E33.
92. Hatzis C, Symmans WF, Zhang Y, Gould RE, Moulder SL, Hunt KK, et al. Relationship between Complete Pathologic Response to Neoadjuvant Chemotherapy and Survival in Triple-Negative Breast Cancer. *Clinical cancer research : an official journal of the American Association for Cancer Research*. 2016;22(1):26-33.
93. Jiang T, Shi W, Wali VB, Pongor LS, Li C, Lau R, et al. Predictors of Chemosensitivity in Triple Negative Breast Cancer: An Integrated Genomic Analysis. *PLoS medicine*. 2016;13(12):e1002193.
94. Piccart-Gebhart MJ, Burzykowski T, Buyse M, Sledge G, Carmichael J, Lück HJ, et al. Taxanes alone or in combination with anthracyclines as first-line therapy of patients with metastatic breast cancer. *Journal of clinical oncology : official journal of the American Society of Clinical Oncology*. 2008;26(12):1980-6.

95. Schmid P, Adams S, Rugo HS, Schneeweiss A, Barrios CH, Iwata H, et al. Atezolizumab and Nab-Paclitaxel in Advanced Triple-Negative Breast Cancer. *New England Journal of Medicine*. 2018;379(22):2108-21.
96. Beniey M, Haque T, Hassan S. Translating the role of PARP inhibitors in triple-negative breast cancer. *Oncoscience*. 2019;6(1-2):287-8.
97. Cyprian FS, Akhtar S, Gatalica Z, Vranic S. Targeted immunotherapy with a checkpoint inhibitor in combination with chemotherapy: A new clinical paradigm in the treatment of triple-negative breast cancer. *Bosnian journal of basic medical sciences*. 2019;19(3):227-33.
98. Killock D. AKT inhibition improves OS in TNBC. *Nature Reviews Clinical Oncology*. 2020;17(3):135-.
99. Rangel MC, Bertolette D, Castro NP, Klauzinska M, Cuttitta F, Salomon DS. Developmental signaling pathways regulating mammary stem cells and contributing to the etiology of triple-negative breast cancer. *Breast cancer research and treatment*. 2016;156(2):211-26.
100. Fu N, Lindeman GJ, Visvader JE. Chapter Five - The Mammary Stem Cell Hierarchy. In: Rendl M, editor. *Current Topics in Developmental Biology*. 107: Academic Press; 2014. p. 133-60.
101. Habib JG, O'Shaughnessy JA. The hedgehog pathway in triple-negative breast cancer. *Cancer medicine*. 2016;5(10):2989-3006.
102. Turk AA, Wisinski KB. PARP inhibitors in breast cancer: Bringing synthetic lethality to the bedside. *Cancer*. 2018;124(12):2498-506.
103. Meng E, Hanna A, Samant RS, Shevde LA. The Impact of Hedgehog Signaling Pathway on DNA Repair Mechanisms in Human Cancer. *Cancers*. 2015;7(3):1333-48.
104. Kudo K, Gavin E, Das S, Amable L, Shevde LA, Reed E. Inhibition of Gli1 results in altered c-Jun activation, inhibition of cisplatin-induced upregulation of ERCC1, XPD and XRCC1, and inhibition of platinum-DNA adduct repair. *Oncogene*. 2012;31(44):4718-24.
105. Mazumdar T, DeVecchio J, Agyeman A, Shi T, Houghton JA. The GLI genes as the molecular switch in disrupting Hedgehog signaling in colon cancer. *Oncotarget*. 2011;2(8):638-45.
106. Inaguma S, Riku M, Hashimoto M, Murakami H, Saga S, Ikeda H, et al. GLI1 interferes with the DNA mismatch repair system in pancreatic cancer through BHLHE41-mediated suppression of MLH1. *Cancer Res*. 2013;73(24):7313-23.

107. Agyeman A, Mazumdar T, Houghton JA. Regulation of DNA damage following termination of Hedgehog (HH) survival signaling at the level of the GLI genes in human colon cancer. *Oncotarget*. 2012;3(8):854-68.
108. Zhang R, Wu J, Ferrandon S, Glowacki KJ, Houghton JA. Targeting GLI by GANT61 involves mechanisms dependent on inhibition of both transcription and DNA licensing. *Oncotarget*. 2016;7(49):80190-207.
109. Lama-Sherpa TD, Lin VTG, Metge BJ, Weeks SE, Chen D, Samant RS, et al. Hedgehog signaling enables repair of ribosomal DNA double-strand breaks. *Nucleic Acids Research*. 2020.
110. Overgaard J. Hypoxic radiosensitization: adored and ignored. *Journal of clinical oncology : official journal of the American Society of Clinical Oncology*. 2007;25(26):4066-74.
111. Gray LH, Conger AD, Ebert M, Hornsey S, Scott OC. The concentration of oxygen dissolved in tissues at the time of irradiation as a factor in radiotherapy. *The British journal of radiology*. 1953;26(312):638-48.
112. Graham K, Unger E. Overcoming tumor hypoxia as a barrier to radiotherapy, chemotherapy and immunotherapy in cancer treatment. *International journal of nanomedicine*. 2018;13:6049-58.
113. Bijlsma MF, Groot AP, Oduro JP, Franken RJ, Schoenmakers SH, Peppelenbosch MP, et al. Hypoxia induces a hedgehog response mediated by HIF-1alpha. *Journal of cellular and molecular medicine*. 2009;13(8b):2053-60.
114. Onishi H, Kai M, Odate S, Iwasaki H, Morifuji Y, Ogino T, et al. Hypoxia activates the hedgehog signaling pathway in a ligand-independent manner by upregulation of Smo transcription in pancreatic cancer. *Cancer science*. 2011;102(6):1144-50.
115. Spivak-Kroizman TR, Hostetter G, Posner R, Aziz M, Hu C, Demeure MJ, et al. Hypoxia Triggers Hedgehog-Mediated Tumor–Stromal Interactions in Pancreatic Cancer. *Cancer Research*. 2013;73(11):3235-47.
116. Katagiri T, Kobayashi M, Yoshimura M, Morinibu A, Itasaka S, Hiraoka M, et al. HIF-1 maintains a functional relationship between pancreatic cancer cells and stromal fibroblasts by upregulating expression and secretion of Sonic hedgehog. *Oncotarget*; Vol 9, No 12. 2018.
117. Zhang RY, Qiao ZY, Liu HJ, Ma JW. Sonic hedgehog signaling regulates hypoxia/reoxygenation-induced H9C2 myocardial cell apoptosis. *Exp Ther Med*. 2018;16(5):4193-200.

118. Bhuria V, Xing J, Scholta T, Bui KC, Nguyen MLT, Malek NP, et al. Hypoxia induced Sonic Hedgehog signaling regulates cancer stemness, epithelial-to-mesenchymal transition and invasion in cholangiocarcinoma. *Experimental cell research*. 2019;385(2):111671.
119. di Magliano MP, Hebrok M. Hedgehog signalling in cancer formation and maintenance. *Nature Reviews Cancer*. 2003;3(12):903-11.
120. Gupta S, Takebe N, Lorusso P. Targeting the Hedgehog pathway in cancer. *Therapeutic advances in medical oncology*. 2010;2(4):237-50.
121. Gonnissen A, Isebaert S, McKee CM, Dok R, Haustermans K, Muschel RJ. The hedgehog inhibitor GANT61 sensitizes prostate cancer cells to ionizing radiation both in vitro and in vivo. *Oncotarget*. 2016;7(51):84286-98.
122. Konings K, Vandevoorde C, Belmans N, Vermeesen R, Baselet B, Wallegem MV, et al. The Combination of Particle Irradiation With the Hedgehog Inhibitor GANT61 Differently Modulates the Radiosensitivity and Migration of Cancer Cells Compared to X-Ray Irradiation. *Frontiers in Oncology*. 2019;9(391).
123. Teichman J, Dodbiba L, Thai H, Fleet A, Morey T, Liu L, et al. Hedgehog inhibition mediates radiation sensitivity in mouse xenograft models of human esophageal adenocarcinoma. *PloS one*. 2018;13(5):e0194809.
124. Korsholm LM, Gál Z, Nieto B, Quevedo O, Boukoura S, Lund CC, et al. Recent advances in the nucleolar responses to DNA double-strand breaks. *Nucleic Acids Res*. 2020;48(17):9449-61.
125. Chopra N, Tovey H, Pearson A, Cutts R, Toms C, Proszek P, et al. Homologous recombination DNA repair deficiency and PARP inhibition activity in primary triple negative breast cancer. *Nature Communications*. 2020;11(1):2662.
126. Cruz C, Castroviejo-Bermejo M, Gutiérrez-Enríquez S, Llop-Guevara A, Ibrahim YH, Gris-Oliver A, et al. RAD51 foci as a functional biomarker of homologous recombination repair and PARP inhibitor resistance in germline BRCA-mutated breast cancer. *Annals of oncology : official journal of the European Society for Medical Oncology*. 2018;29(5):1203-10.
127. Warner JR. The economics of ribosome biosynthesis in yeast. *Trends in biochemical sciences*. 1999;24(11):437-40.
128. van Sluis M, McStay B. Nucleolar reorganization in response to rDNA damage. *Current Opinion in Cell Biology*. 2017;46:81-6.
129. Korsholm LM, Gál Z, Lin L, Quevedo O, Ahmad DA, Dulina E, et al. Double-strand breaks in ribosomal RNA genes activate a distinct signaling and chromatin

response to facilitate nucleolar restructuring and repair. *Nucleic Acids Research*. 2019;47(15):8019-35.

130. Li X, Wang W, Wang J, Malovannaya A, Xi Y, Li W, et al. Proteomic analyses reveal distinct chromatin-associated and soluble transcription factor complexes. *Molecular systems biology*. 2015;11(1):775.

131. Lama-Sherpa TD, Shevde LA. An Emerging Regulatory Role for the Tumor Microenvironment in the DNA Damage Response to Double-Strand Breaks. *Molecular Cancer Research*. 2020;18(2):185.

132. Hanna A, Metge BJ, Bailey SK, Chen D, Chandrashekar DS, Varambally S, et al. Inhibition of Hedgehog signaling reprograms the dysfunctional immune microenvironment in breast cancer. *OncoImmunology*. 2019;8(3):1548241.

133. Redig AJ, McAllister SS. Breast cancer as a systemic disease: a view of metastasis. *Journal of internal medicine*. 2013;274(2):113-26.

134. Langley RR, Fidler IJ. The seed and soil hypothesis revisited--the role of tumor-stroma interactions in metastasis to different organs. *International journal of cancer*. 2011;128(11):2527-35.

135. Valastyan S, Weinberg RA. Tumor metastasis: molecular insights and evolving paradigms. *Cell*. 2011;147(2):275-92.

136. Welch DR, Hurst DR. Defining the Hallmarks of Metastasis. *Cancer Research*. 2019;79(12):3011.

137. Levental KR, Yu H, Kass L, Lakins JN, Egeblad M, Erler JT, et al. Matrix crosslinking forces tumor progression by enhancing integrin signaling. *Cell*. 2009;139(5):891-906.

138. Provenzano PP, Eliceiri KW, Campbell JM, Inman DR, White JG, Keely PJ. Collagen reorganization at the tumor-stromal interface facilitates local invasion. *BMC Medicine*. 2006;4(1):38.

139. Nallanthighal S, Heiserman JP, Cheon D-J. The Role of the Extracellular Matrix in Cancer Stemness. *Frontiers in Cell and Developmental Biology*. 2019;7(86).

140. Pang M-F, Siedlik MJ, Han S, Stallings-Mann M, Radisky DC, Nelson CM. Tissue Stiffness and Hypoxia Modulate the Integrin-Linked Kinase ILK to Control Breast Cancer Stem-like Cells. *Cancer Research*. 2016;76(18):5277.

141. Acerbi I, Cassereau L, Dean I, Shi Q, Au A, Park C, et al. Human breast cancer invasion and aggression correlates with ECM stiffening and immune cell infiltration. *Integrative Biology*. 2015;7(10):1120-34.

142. Gilkes DM, Chaturvedi P, Bajpai S, Wong CC, Wei H, Pitcairn S, et al. Collagen prolyl hydroxylases are essential for breast cancer metastasis. *Cancer research*. 2013;73(11):3285-96.
143. Myllyharju J. Prolyl 4-hydroxylases, the key enzymes of collagen biosynthesis. *Matrix biology : journal of the International Society for Matrix Biology*. 2003;22(1):15-24.
144. Quartuccio N, Laudicella R, Mapelli P, Guglielmo P, Pizzuto DA, Boero M, et al. Hypoxia PET imaging beyond 18F-FMISO in patients with high-grade glioma: 18F-FAZA and other hypoxia radiotracers. *Clinical and Translational Imaging*. 2020;8(1):11-20.
145. Brown JM. Evidence for acutely hypoxic cells in mouse tumours, and a possible mechanism of reoxygenation. *The British journal of radiology*. 1979;52(620):650-6.
146. Rockwell S, Dobrucki IT, Kim EY, Marrison ST, Vu VT. Hypoxia and radiation therapy: past history, ongoing research, and future promise. *Current molecular medicine*. 2009;9(4):442-58.
147. Begg K, Tavassoli M. Inside the hypoxic tumour: reprogramming of the DDR and radioresistance. *Cell Death Discovery*. 2020;6(1):77.
148. Dendy PP, Wardman P. Hypoxia in biology and medicine: the legacy of L H Gray. *The British journal of radiology*. 2006;79(943):545-9.
149. Pollard JW. Tumour-educated macrophages promote tumour progression and metastasis. *Nature reviews Cancer*. 2004;4(1):71-8.
150. Sica A, Mantovani A. Macrophage plasticity and polarization: in vivo veritas. *The Journal of clinical investigation*. 2012;122(3):787-95.
151. Henze AT, Mazzone M. The impact of hypoxia on tumor-associated macrophages. *The Journal of clinical investigation*. 2016;126(10):3672-9.
152. Murdoch C, Giannoudis A, Lewis CE. Mechanisms regulating the recruitment of macrophages into hypoxic areas of tumors and other ischemic tissues. *Blood*. 2004;104(8):2224-34.
153. Leek RD, Landers RJ, Harris AL, Lewis CE. Necrosis correlates with high vascular density and focal macrophage infiltration in invasive carcinoma of the breast. *British journal of cancer*. 1999;79(5-6):991-5.
154. Lewis JS, Landers RJ, Underwood JC, Harris AL, Lewis CE. Expression of vascular endothelial growth factor by macrophages is up-regulated in poorly vascularized areas of breast carcinomas. *The Journal of pathology*. 2000;192(2):150-8.

155. Du R, Lu KV, Petritsch C, Liu P, Ganss R, Passegué E, et al. HIF1alpha induces the recruitment of bone marrow-derived vascular modulatory cells to regulate tumor angiogenesis and invasion. *Cancer Cell*. 2008;13(3):206-20.
156. Casazza A, Laoui D, Wenes M, Rizzolio S, Bassani N, Mambretti M, et al. Impeding macrophage entry into hypoxic tumor areas by Sema3A/Nrp1 signaling blockade inhibits angiogenesis and restores antitumor immunity. *Cancer Cell*. 2013;24(6):695-709.
157. Bosco MC, Reffo G, Puppo M, Varesio L. Hypoxia inhibits the expression of the CCR5 chemokine receptor in macrophages. *Cellular immunology*. 2004;228(1):1-7.
158. Sica A, Sacconi A, Bottazzi B, Bernasconi S, Allavena P, Gaetano B, et al. Defective expression of the monocyte chemoattractant protein-1 receptor CCR2 in macrophages associated with human ovarian carcinoma. *Journal of immunology (Baltimore, Md : 1950)*. 2000;164(2):733-8.
159. Burke B, Giannoudis A, Corke KP, Gill D, Wells M, Ziegler-Heitbrock L, et al. Hypoxia-induced gene expression in human macrophages: implications for ischemic tissues and hypoxia-regulated gene therapy. *The American journal of pathology*. 2003;163(4):1233-43.
160. Grimshaw MJ, Hagemann T, Ayhan A, Gillett CE, Binder C, Balkwill FR. A role for endothelin-2 and its receptors in breast tumor cell invasion. *Cancer Res*. 2004;64(7):2461-8.
161. Grimshaw MJ, Naylor S, Balkwill FR. Endothelin-2 is a hypoxia-induced autocrine survival factor for breast tumor cells. *Molecular cancer therapeutics*. 2002;1(14):1273-81.
162. Laoui D, Van Overmeire E, Di Conza G, Aldeni C, Keirsse J, Morias Y, et al. Tumor hypoxia does not drive differentiation of tumor-associated macrophages but rather fine-tunes the M2-like macrophage population. *Cancer Res*. 2014;74(1):24-30.
163. Movahedi K, Laoui D, Gysemans C, Baeten M, Stangé G, Van den Bossche J, et al. Different tumor microenvironments contain functionally distinct subsets of macrophages derived from Ly6C(high) monocytes. *Cancer Res*. 2010;70(14):5728-39.
164. Ye L-Y, Chen W, Bai X-L, Xu X-Y, Zhang Q, Xia X-F, et al. Hypoxia-Induced Epithelial-to-Mesenchymal Transition in Hepatocellular Carcinoma Induces an Immunosuppressive Tumor Microenvironment to Promote Metastasis. *Cancer Research*. 2016;76(4):818.
165. Petty AJ, Li A, Wang X, Dai R, Heyman B, Hsu D, et al. Hedgehog signaling promotes tumor-associated macrophage polarization to suppress intratumoral CD8+ T cell recruitment. *The Journal of clinical investigation*. 2019;129(12):5151-62.

166. Viola A, Munari F, Sánchez-Rodríguez R, Scolaro T, Castegna A. The Metabolic Signature of Macrophage Responses. *Front Immunol.* 2019;10:1462.

APPENDIX: IACUC APPROVAL

MEMORANDUM

DATE: 12-Mar-2020
TO: Samant, Lalita R
FROM: 
Robert A. Kesterson, Ph.D., Chair
Institutional Animal Care and Use Committee (IACUC)
SUBJECT: NOTICE OF APPROVAL

The following application was approved by the University of Alabama at Birmingham Institutional Animal Care and Use Committee (IACUC) on 12-Mar-2020.

Protocol PI: Samant, Lalita R
Title: Sculpting anti-tumor immunity as an approach to treat metastatic breast cancer
Sponsor: DOD - Department of Defense
Animal Project Number (APN): IACUC-21174

This institution has an Animal Welfare Assurance on file with the Office of Laboratory Animal Welfare (OLAW), is registered as a Research Facility with the USDA, and is accredited by the Association for Assessment and Accreditation of Laboratory Animal Care International (AAALAC).

This protocol is due for full review by 23-Apr-2021.

Institutional Animal Care and Use Committee (IACUC)

403 Community Health on 19th | 933 19th Street South

Mailing Address:

CH19-403 | 1720 2nd Ave South | Birmingham AL 35294-2041

phone: 205.934.7692 | fax: 205.934.1188

www.uab.edu/iacuc | iacuc@uab.edu